An update to this article is included at the end

Materials Science & Engineering R 159 (2024) 100805

Contents lists available at ScienceDirect

Materials Science & Engineering R

journal homepage: www.elsevier.com/locate/mser

A comprehensive review on graphene-based materials: From synthesis to contemporary sensor applications

Ramaswamy Sandeep Perala [a,*,1], Narendhar Chandrasekar [a,1], Ramachandran Balaji [b], Pinky Steffi Alexander [c], Nik Zulkarnine Nik Humaidi [a], Michael Taeyoung Hwang [a,*]

[a] Department of BioNanotechnology, Gachon University, 1342 Seongnam-Daero, Sujeong-Gu, Seongnam-si, Gyeonggi-do 13120, Republic of Korea
[b] Department of Electronics and Communication Engineering, Koneru Lakshmaiah Education Foundation, Andhra Pradesh 522302, India
[c] Department of Physics, Bharthiar University, Coimbatore 641046, India

ARTICLE INFO

Keywords:
Graphene
Raman spectroscopy
Electrochemical
FET
Analytes and biosensors

ABSTRACT

Carbon based 2D materials, specifically those of the graphene family, recently gained considerable interest in the study of sensors. It is emerging as a novel and potent material with tunable physicochemical properties such as ballistic conduction, high mechanical strength, a broad spectrum of chemical stability, high surface-area-to-volume ratio, ease of surface functionalization, and the possibility of mass production. This review provides insights into recent advances in graphene-based materials for field-effect transistor-based sensors, electrochemical sensors, and Raman spectroscopy-based sensors. Among the sensing methodologies, those utilizing field-effect transistors demonstrate a high degree of specificity and ultralow sensitivity and are relatively easy to manufacture in large batches with a repeatable sensitivity. Over the last decade, multiple types of sensors based on various graphene-family materials have been researched to detect various types of targets, ranging from biomolecules to heavy metals and chemical pollutants. Owing to their ability to integrate into a portable and rapid test platform, both at the laboratory scale and for point-of-care testing, the graphene family of materials (GFM) is a significantly viable base for sensor fabrication. Electrochemical and Raman spectroscopy-based sensors can provide a robust platform for detection at high-stress environments including fluctuating pH, temperature, and other possible disturbing conditions. The strategies used by researchers to detect specific and ultralow concentrations of analytes in a diverse mixture of targets are elaborated in detail. This review chronologically presents details regarding the GFM ranging from their synthesis to specific application possibilities.

1. Introduction

A sheet of carbon atoms with sp^2 bonds is called graphene, which is ideally organized in a honeycomb lattice, creating a monolayer of carbon atoms that is only one atom thick. This new material has gained significant interest in many disciplines, including nanoelectronics, elevated electronics, energy conversion and storage, field emission displays, and transparent conductors, owing to its remarkable physicochemical and morphological properties. This review focuses on the fabrication and use of graphene for biochemical and physiological sensing. The major driving force behind the creation of new and improved sensors over the last 10 years has been a variety of zero-dimensional (0D) materials, which are also categorized as one dimensional (1D) nanomaterials. These include carbon nanotubes (CNTs), which are 1D cylinders composed of carbon sheets, quantum dots, nanomaterials, nanowires, and nanoscale objects. Since the first free-standing graphene was successfully isolated in 2004, this 2D carbon crystal has been anticipated to introduce novel options for sensor technologies. Considering the recent developments, graphene is significantly promising for several innovative sensors that utilize its extraordinary electrical properties (high carrier mobility and capacity), electrochemical behavior (elevated electron transfer rate), optical characteristics (quenching fluorescence), structural properties (one-atom cross-sectional area and extremely high superficial area towards the volume ratio), or mechanical behavior.

Graphene is unique considering its assortment of properties owing to its defect-free structure; monolayer graphene is another promising material for fabricating highly sensitive devices for sensing and energy

* Corresponding authors.
E-mail addresses: ramaswamysandeep@gmail.com (R.S. Perala), anol81@gachon.ac.kr (M.T. Hwang).
[1] Equally Contributed.

https://doi.org/10.1016/j.mser.2024.100805
Received 31 January 2024; Received in revised form 4 May 2024; Accepted 4 May 2024
Available online 29 May 2024
0927-796X/© 2024 Elsevier B.V. All rights are reserved, including those for text and data mining, AI training, and similar technologies.

storage. Considering another variation of monolayer graphene, crumpled graphene [1,2] (Fig. 1) can be employed to further amplify the sensitivity of graphene-based devices. Crumpling induces variations in the wettability of the devices as the solvents interact differently with the surfaces consisting of corrugations [3]. Consequently, this leads to opportunities for fine-tuning the graphene layers for functionalization, fabrication of the devices, and doping strategies. The interaction of the graphene layer with the substrate over which the device would be fabricated occurs via the π–π interaction, which has been established by Novoselov et al., [4]. Researchers have been evaluating monoaxially- and biaxially-crumpled graphene layers to obtain a better sensitivity from the defect-free graphene monolayers [5].

Graphene has attracted considerable attention as a desirable choice for biosensors owing to its outstanding electrochemical properties, adsorption efficiency, mechanical characteristics, and flexibility. Graphene, which is formed when a carbon atom hybridizes with a sp^2

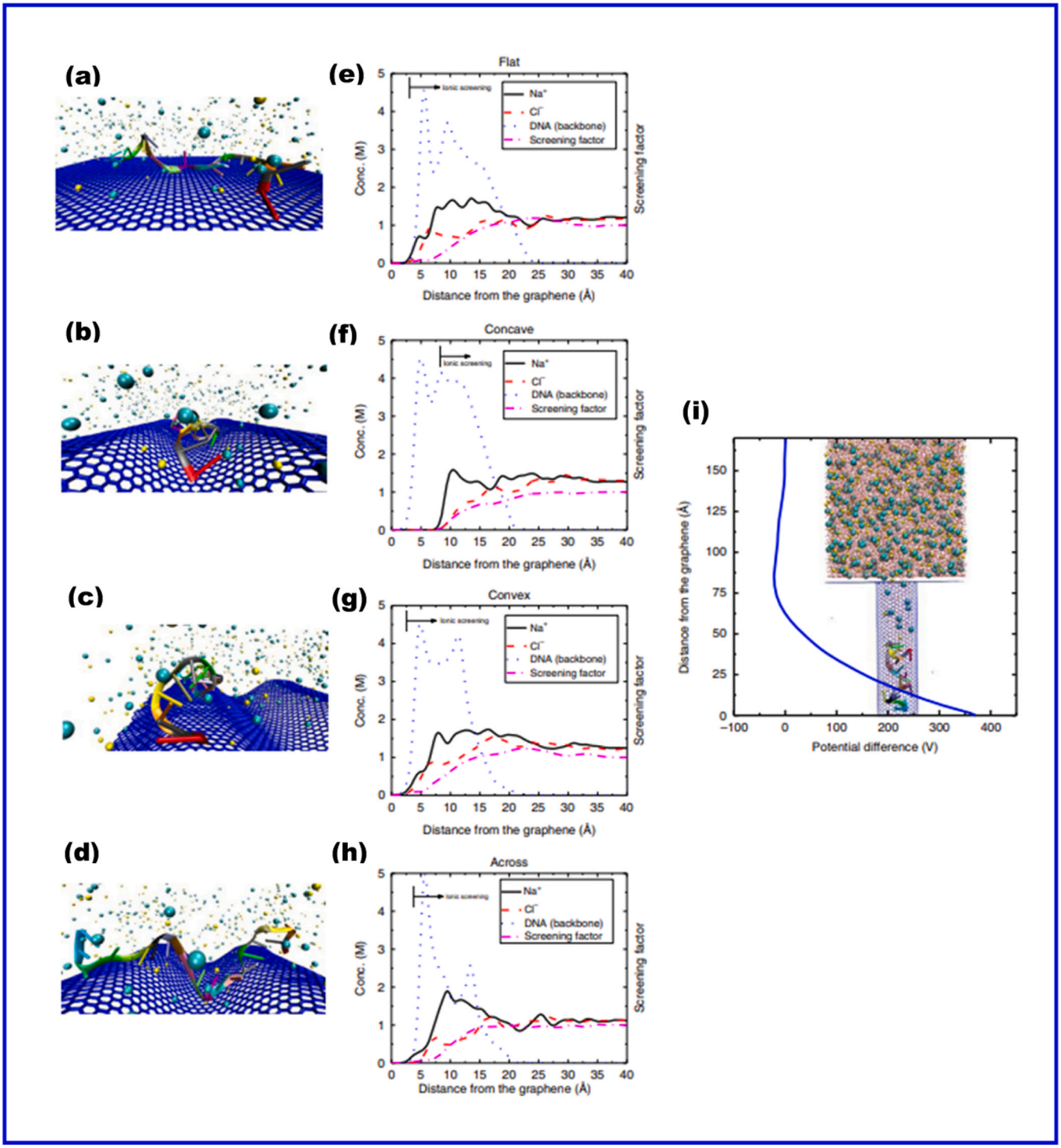


Fig. 1. Representation of the simulation studies by Hwang et al. [1] for compensating DNA on graphene: (a) flat, (b) crumpled concave, (c) crumpled convex, (d) over the crumples. Plot of the molar concentration of ions (sodium and chloride), the backbone of the DNA strand, and screening factor of ions for the following various types of graphene: (e) flat, (f) crumpled concave, (g) crumpled convex, (h) over configurations of DNA. (i) CNT model (2.45 nm diameter) used for a narrow trench in crumpled graphene technique.

electron orbital, is required to build biosensors with a high surface area, good electron transport behavior, and significant mechanical properties. The classification and attributes of graphene are thoroughly described in this review, as well as the application of various graphene family materials (GFM)-based methods with various signal-output strategies to achieve the quantitative detection of various types of biomarkers, including DNA, microRNA, small molecules, and proteins. The recent detection mechanisms, target compounds, detection constraints, and sensing ranges of several graphene-based sensors are discussed and compared. These graphene-based biosensors are expected to be significantly promising for clinical treatment and biological analyses. Thin layers of graphite have been manually exfoliated over silicon oxide pits [6] to create single and layered graphene sheets for nano-electromechanical systems. Interferometry is used to visually recognize vibrations with basic resonant frequencies in the megahertz region that are either electronically or optically triggered. We demonstrate charge responses lower than to 8 ×10"4 electrons per root hertz at an ambient temperature. The narrowest resonator is the limit of two-dimensional nano-electromechanical devices and comprises a hanging sheet of single atoms.

Large-scale graphene sheets created by chemical vapor deposition (CVD) and set up as solution-gated transistors are capable of electronic and label-free sensing of DNA hybridization to a single-base precision. DNA hybridization is detected using a gate voltage that produces the smallest device with a low conductance, which is responsive to the charge transfer between the graphene and DNA molecules. Instead of the electrostatic gating or contaminant screening effects, DNA identification is attributed to n-doping from DNA to graphene [7]. Considering health, ecological, and security issues, the identification of physiologically active compounds is crucial. These monitoring methods include biosensors and bioanalytical methods. A chemical sensor numerically or semi-quantitatively transforms information regarding the existence of a chemical species into a signal that can be used for analysis. The transducer and receiver are the two components of a sensor. Any organic or artificial substance with a particular association with one analyte or a collection of analytes can be a transmitter. A compound serves as a detection component in biosensors. A sensor that transforms molecular information into a quantifiable indication is the second crucial component of a detection device. Bio-analytical methods frequently involve multiple processing steps. In this review, we discuss biosensors and bioanalytical devices that use graphene as a crucial component [8]. The ability of graphene oxide (GO) to detect significantly low levels of organic and biological pollutants makes it a viable material for electrochemical detection, which is reproducible and relatively easier than other methods [9,10].

Other applications of GFM include corrosion prevention [11,12], batteries [13], use in heavy industries for sensing strain [14], as coatings for steel specimens to incorporate self-healing behavior [15], and for the decomposition of organic matter for metal-free catalysis [16]. GFM is widely utilized in biomedical applications, ranging from being used as nucleotide sensors [17] to scaffolds for the growth of stem cells [18,19]. The extremely uniform atomic arrangement enables a defect-free structure and consequently renders graphene an extremely tough material in terms of tensile strength with a significantly high Young's modulus. The yield strength (σ) and elastic modulus (E) of the materials is defined with respect to the equation of density scaling, E ∝ Ebρ¯n as well as σ ∝ σbρ¯m, where ρ¯, Eb, and σb indicate the relative density, Young's modulus, and yield strength of the parent material, respectively [20,21].

Furthermore, graphene is highly conductive, thus it can serve as a suture or permanent implant for different roles in cancer theranostics as well as nerve tissue replacements in the body [22–24]. Graphene has also been used as an energy generator for miniature devices [25] from sunlight along with hydroelectric sources. Research regarding GFM has recently focused on their use for the fabrication of wearable sensors owing to their lightweight and highly repeatable signal detection [26]. (Fig. 2).

This review presents the significance of GFM, which has an excellent scope in the advancement of several niche avenues in science and technology. Furthermore, the literature regarding GFM and utilization of field-effect transistors (FETs), as well as their potential applications in sensors are summarized herein. This review is divided into eight sections. Section 1 introduces graphene and its derivatives, along with the scope and significance of this review. Section 2 describes the synthesis of GFM and surface functionalization strategies. Section 3 elaborates on surface-enhanced Raman scattering (SERS), which is adopted for the amplification of the Raman signal and identification of the analytes. Section 4 presents the basic details of various types of FETs and the fabrication of devices for real-time measurements. Section 5 emphasizes the significance of pH Sensors on GFM and defines their conductivity, surface properties, stability, and resistance, as well as their annual development from 2013 to date, (in graphene and its derivatives) in the design of specific target applications. Section 6 extends the potential application of GFM to the environment by describing various analysis techniques of sensing (CO_2, H_2O_2, heavy metals, volatile biomarker gases). Section 7 discusses the potential applications of GFM in healthcare (biological sensors, sensing of biomolecules). Finally, Section 8 presents the conclusions regarding the state of technology that will be impacted by GFM and highlights the promising future developments of GFM. This review highlights the use of graphene, graphene oxide (GO), and reduced graphene oxide (rGO) for applications in biomolecule sensing, pollutant detection, gas sensing, and biomedical applications, and aims to provide a comprehensive and in-depth overview of all technical aspects, in contrast to previous reviews that have concentrated on a specific subarea within this field, as shown in Fig. 3.

2. Synthesis methodologies and surface functionalization strategies

The variety of graphene and carbon-based nanomaterials is closely linked to the manufacturing process. Various processes, including the mechanical flaking of graphite or graphite oxide CVD, can be used to create graphene [27]. However, graphene composed by CVD or manually exfoliated graphene has numerous flaws that lead to degenerated outcomes/properties of the intended application. However, many graphene materials are typically fabricated using various techniques. For example, the thermal exfoliation of graphite oxide can result in a substance called thermally reduced graphene (TRGO), or sono-assisted exfoliation of graphite oxide, which results in GO undergoing additional chemical or electrical reduction. Compared with the flawless honeycomb lattice structure of pure graphene, TRGO has numerous defects. However, the uneven electron transfer owing to the electrochemistry with respect to the sp^2 carbons does not occur at the basal plane of graphene sheets but at the margins and defects. Owing to the architecture of the sp^2 carbon network, GO is not entirely flat and contains many oxygen-containing compounds that can facilitate functionalization via biomolecular action for bio-recognition events during biosensing. Chemical and electrochemical methods can also be used to reduce GO. These materials have a partially recovered sp^2 structure that includes certain oxygen-bearing groups. Electrochemically reduced graphene oxide (ERGO) or Chemically reduced graphene oxide (CRGO) are the common end products. The morphologies of GO, CRGO, TRGO, ERGO, and graphite oxide, indicate that these materials are chemically modified graphene. To select the appropriate variety of graphene for the application and transmission process, a large graphene "toolbox" may be required. The variations in the structural behavior are apparent; for example, sheets versus play a significant role in the design of nano-architectonic biosensors when compared to CNTs. Functionally, CNTs are formed from metallic fragments that may influence sensor reactions, whereas graphene is frequently manufactured using a variety of processes. The use of various graphene-based nanostructures in various sensor and analytical systems has been discussed in the

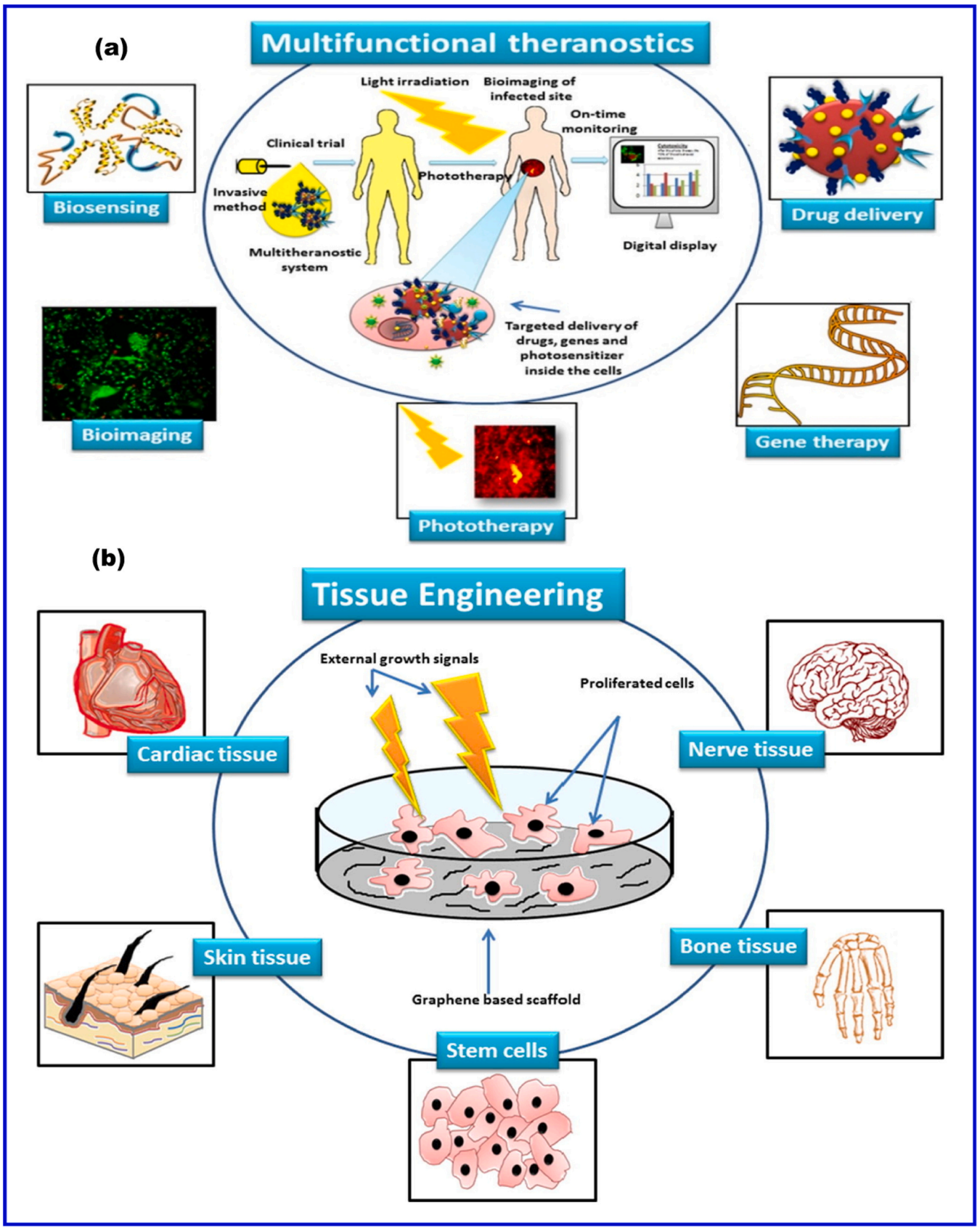


Fig. 2. Graphene in (a) different roles in cancer theranostics, and (b) stem cell engineering [22].

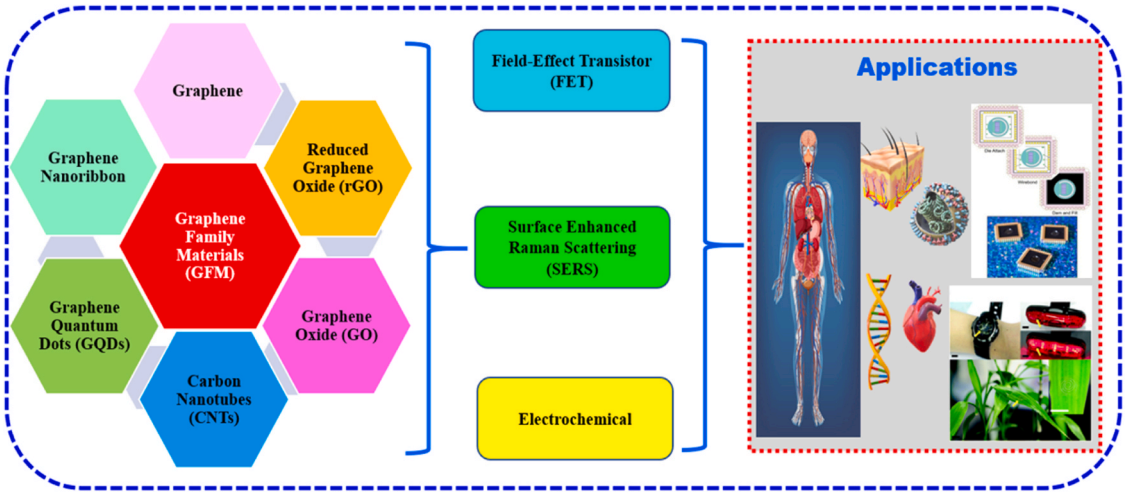


Fig. 3. Analytical evaluation of GFM for different sensor applications.

literature [28].

2.1. Methods to synthesize graphene

Broadly, both bottom-up and top-down approaches can be used to synthesize graphene, as shown in Fig. 4.

2.1.1. Top-down approach

The top-down approach utilizes exfoliation, electrochemical deposition, laser ablation, and chemical synthesis to either exfoliate or transform graphite-producing graphene.

2.1.1.1. Mechanical exfoliation. This technique utilizes a sticky tape to peel or remove graphite layers from a SiO_2 substrates. In 2004, Novoselov and Geim developed their first version of exfoliation, for which they were awarded the Nobel Prize [29]. Furthermore, Dasari et al. [30] demonstrated the exfoliation of graphene sheets using sticky scotch tape. As shown in Fig. 5(a-c), the graphite was peeled off using adhesive tape until a single sheet of graphene was formed. Although this process is simple and is often employed in laboratories, the resulting graphene has poor productivity and minor structural flaws. Fig. 5(d) presents the various methods used for large-scale production of graphene for optimal quality, size, and price for any application.

2.1.1.2. Electrochemical exfoliation. A graphite electrode is used for electrochemical exfoliation under the impact of several electrolytes in the electrochemical device to obtain pure graphene. Multiple films of the graphene sheets can be exfoliated to produce graphene from graphite. Composites can be incorporated during the platform design of the sensing device, considering its various benefits to the system. Factors such as enhanced sensitivity, permeability, and accessibility of the analyte to the sensor surface can be considered during the design.

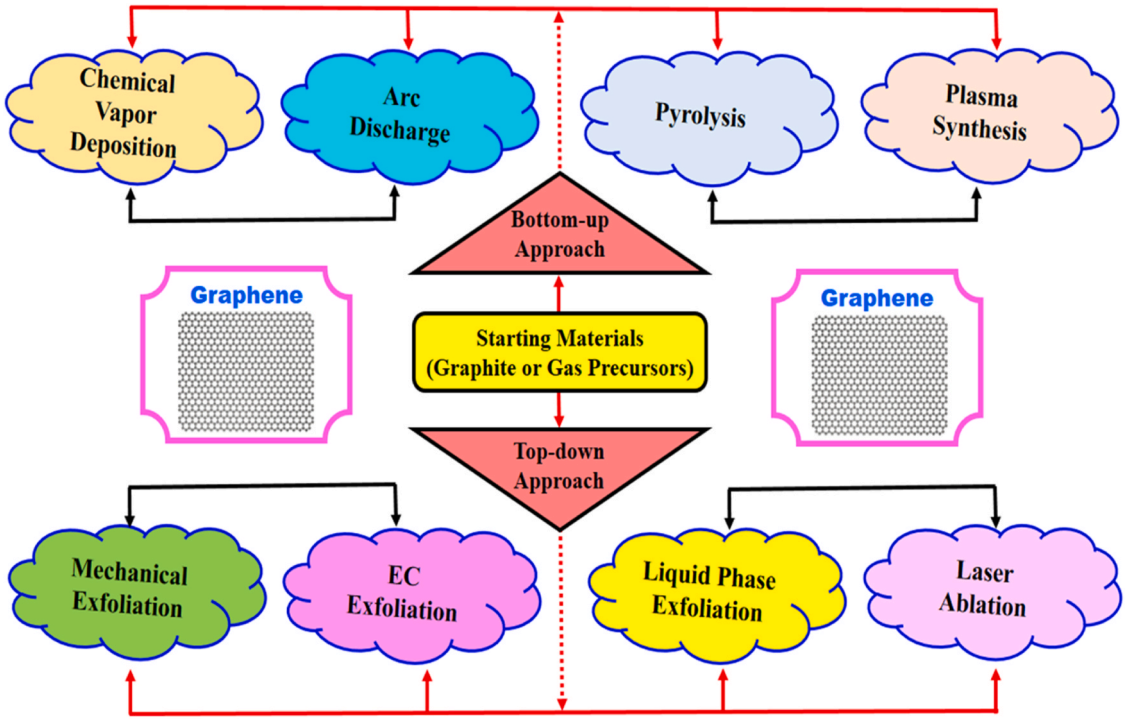


Fig. 4. Schematic of graphene synthesis.

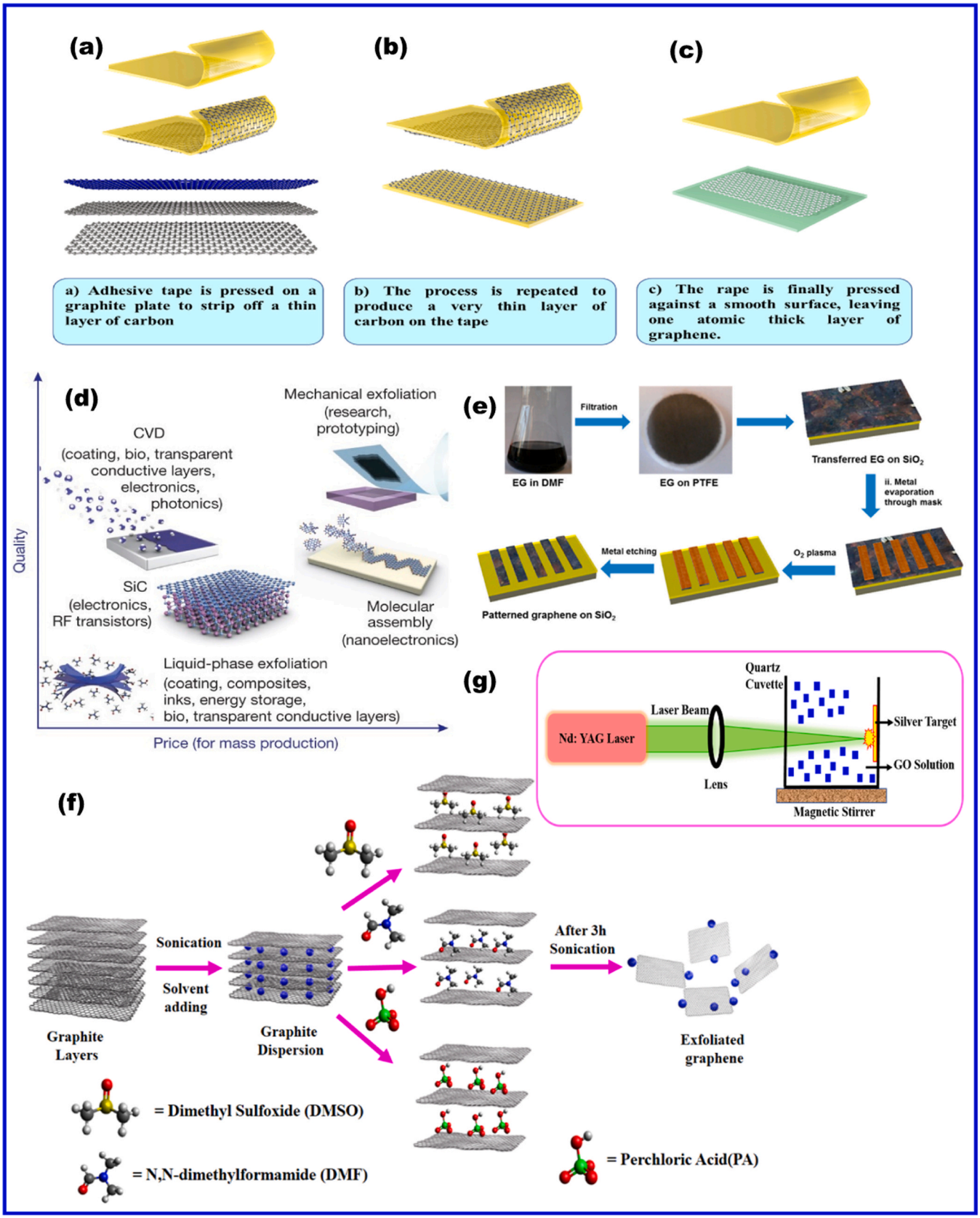


Fig. 5. Graphene synthesis via the top-down route. (a-c) Scotch tape procedure for the automatic exfoliation of graphene, (d) various methods used for the large-scale production of graphene [29], and (e) fabrication process of the patterned exfoliated graphene with source and drain electrodes [31], (f) schematic of the liquid-phase exfoliation process and (g) laser ablation technique for producing graphene.

Experiments have been performed with different electrolytes, with outputs varying in the graphene size, thickness, and chemical and electrical characteristics. Parvez et al. [31] used graphite as the anode, and platinum or another metal as the cathode, to create an electrolytic cell. After 10 min, the electrodes were submerged in a sulfuric acid electrolyte solution with a potential of +10 V. This technique produced more than 60% of its yield, and the graphene that was produced contained several layers. Similarly, Liu et al. [32] produced nonhomogeneous graphene with imperfections in the thickness and size distribution by using pencil graphite both together the electrodes and 1 M H_3PO_4 as the electrolyte. Consequently, the electrochemical exfoliation of graphite has gained attention as a rapid and environmentally friendly means of creating the most excellent graphene. Fig. 5(e) presents the fabrication process of the patterned exfoliated graphene with source and drain electrodes.

2.1.1.3. Liquid phase exfoliation. As shown in Fig. 5(f), an alternative top-down technique, liquid-phase exfoliation (LPE), employs sonication to exfoliate graphene sheets. Researchers have transformed graphite into graphene using LPE sonication by utilizing several solvents including hydrogen peroxide, sulfuric acid, and acetic acid. Typically, sonication was performed for 50–55 min at a source power of 280–500 W. Graphene nanoribbons with widths of less than 10 nm were created using the LPE approach. Green and Hersam used sodium cholate as a surfactant to exfoliate graphite [33]. LPE is a dependable and scalable process for producing better-quality graphene; however, its high-energy utilization and poor yield must be resolved.

2.1.1.4. Laser ablation technique. In this method, a high-power LASER beam ablates the surface of a carbon target to create singular carbon atoms that are arranged to form a graphene sheet. During the synthesis process, numerous factors such as the wavelength, pulse duration, and repetition rate of the LASER beam must be optimized. Furthermore, the substrate separation, processing temperature, and gas pressure must be optimized. Cappelli et al. [34] selected a silicon substrate. Fig. 5(g) presents the production of high-quality graphene using the NdYAG LASER at various temperatures. Additionally, Koh et al. [35] employed ultrashort-pulse laser technology to synthesize graphene on variety substrates, including nickel, copper, cobalt, and iron. The extracted graphene demonstrated an excellent quality, with a few imperfections that were significant in size.

Compared to the aforementioned top-down approaches, there are few other synthesis routes such as chemical methods, hydrothermal synthesis, and microwave-assisted techniques. In addition to the two primary processing approaches, exfoliation, and other CVD procedures, several alternative techniques have been to produce graphene, including chemical-based methods, a few of which were previously discussed as liquid-phase exfoliation in Section 2.1.1.3. Without requiring exfoliation, graphene films can be chemically extracted from graphite by other techniques. For example, Horiuchi et al. [36] synthesized carbon nanofilms (CNFs) from natural graphite and demonstrated the viability of this method for producing graphene. To remove the thinnest sheets from the dispersion, natural graphite was subjected to several oxidation and purification procedures, dilution in methanol, and centrifuged. One to six graphene layers were present in the product, and the dilution factor and thickness of the CNF were directly correlated. A distinct chemical process included intercalating sulfuric and nitric acids between the graphite layers, then rapidly heating the mixture to 1000 °C to cause the acid molecules to explosively evaporate and form thin graphitic sheets. Following sonication in a surfactant solution, oleum and tetrabutylammonium hydroxide (TBA) were used in the second stage of intercalation to create single- and few-layered graphene. In this study, the selection of intercalants guaranteed a small disruption of the sp^2 network in graphene, resulting in high-quality graphene. Choucair et al. [37] demonstrated the reaction of ethanol and sodium at a 1:1 molar ratio to create a graphene precursor, which was then quickly pyrolyzed. A high manufacturing yield of 0.1 g graphene per 1 mol of ethanol was obtained by identifying graphene in the suspended solid. The method demonstrated the capacity to produce graphene in large quantities. Graphene was prepared by chemical exfoliation, which is a completely different method. After quickly heating the graphite oxide to 1050 °C, it underwent a two-stage reduction process using hydrogen gas and N-methylpyrolidone. The research also asserted that the lateral dimensions and crystallinity of the input graphite determine the number of layers in the graphene. Thus, a potential method for regulating the number of graphene layers was presented, which may have a significant influence on electronic applications.

Furthermore, regarding the hydrothermal synthesis technique, a thermochemical transformation process called hydrothermal treatment effectively hydrolyzes, pyrolyzes, dehydrates, polymerizes, and aromatizes organic precursors, providing the end products with condensed aromatic molecules having numerous functional oxygenated groups. Huang reported a low-cost, low-impact, and effective technique for producing few-layered GOH via basic hydrothermal synthesis with HA as the base substance. This method is expected to be a viable substitute for Hummer's approach. Undissolved HA was partly dissolved in water and GOH solutions under hydrothermal conditions, although no tiny molecular component were simultaneously produced. The morphology, crystal structure, and chemical composition of the as-prepared GOH were thoroughly described. Krishnamoorthy et al. [38] reported the synthesis of graphene nanosheets using a one-step hydrothermal treatment, where the hydrothermal destruction of GO resulted in graphene nanosheets in a single step. To convert GO into monolayers, 0.05 g of the as-produced GO nanosheets was mixed with 50 mL of deionized water and exposed to ultrasonic irradiation for 30 min. KOH solution was added to the mixture to reduce the pH to 10. The solution was then moved into a Teflon tank and maintained at a constant temperature of 90 °C for 10 h while being covered with a stainless-steel reactor. Following the hydrothermal process, the resultant graphene nanosheets were thoroughly washed in distilled water before centrifugation for 10 min at 12000 rpm to remove any remaining material. This process was repeated until the synthesized product was devoid of any remaining contaminants. To eliminate the water content, the graphene nanosheets were further dried for 2 h at 150 °C in a hot air oven.

Regarding microwave-assisted techniques, Al-Hazmi et al. [39] developed a new method based on a microwave-aided solvothermal approach that uses methanol as a less expensive solvent to exfoliate and decrease graphite oxide in a single step under microwave irradiation. This process produces large quantities of high-quality graphene. Gurunlu et al. [40] suggested that the production of graphene in a regulated shape is possible by facilitating graphene exfoliation using microwave (MW) radiation treatment, which eliminates the need for high pressures and temperatures. The interplanar length and degree of disorder of graphite may be improved by using MW for the LPE of graphite. The van der Waals connections between the various graphite layers are weakened or broken by MW radiation. Consequently, the solvent molecules intercalated between the two graphite layers violently exfoliated and transformed into graphene. The spaces between the graphite layers can be penetrated by solvents with minimal surface tension. This causes a sudden expansion and creates a force that helps graphene exfoliate in a liquid. The intercalation of solvent molecules into the graphite layers is facilitated by the microwave treatment applied to graphite, which weakens the interlayer contacts for exfoliation. The solvents used for the experiment had surface tensions between 40 and 50 mJ m^{-2}, which is the ideal range for graphite exfoliation with MW assistance.

The liquid-phase exfoliation of graphite is a noteworthy approach for producing graphene on an extensive basis at an extremely affordable price. The development of a cost-effective process for the large-scale manufacturing of functionalized single- and few-layered graphene sheets is another major problem. This technique has several advantages and disadvantages. Considering the advantages, the technique is

potentially up-scalable, demonstrates excellent quality, is simple, and occasionally nonoxidative. Considering the disadvantages of this approach compared to other methods, although this technique is safe and environmental-friendly, it obtains a lower concentration of graphene (poor yield), demonstrates microscopic flakes (<5 μm), has a restricted dispersibility in graphene that is not functionalized, restricted processability, substantial fixed and with different expenses compared to other top-down methods [41,42].

2.1.2. Bottom-up approach

This approach typically employs four sub-techniques, namely temperature pyrolysis, arc discharge, CVD, and plasma-enhanced CVD to self-assemble or deposit nanoparticles. The context of these sub-techniques, pressure, environment, and flow rate are directly proportional to the quality of the graphene material that can be deposited. The subsequent product is of the highest quality, demonstrating no defects, and usually exhibits highly promising electrical features. However, the yield of the processed graphene is relatively low and only suitable for a limited number of rudimentary applications.

2.1.2.1. Chemical vapor deposition. As shown in Fig. 6(a), the basic CVD apparatus comprises substrates, a tube furnace, gas circulation, and tail gas treatment. The most popular catalysts are based on Group B elements, which provide a low-energy method for the production of graphene by creating intermediate molecules. Owing to their high availability and affordability, the first row of d-block metals, such as nickel, cobalt, copper, and iron, have gained significant attention [43]. Copper demonstrated the smallest carbon dissolution, whereas iron showed the greatest. This makes copper an ideal metal for creating monolayer graphene, compared to nickel and cobalt, which often result in several layers of graphene. By subjecting the precursors to intense heat, where a copper or nickel substrate is placed in a reactor at temperatures of 1000 °C [44], it is possible to create graphene with a large surface area. Additionally, several experts have indicated the large-scale production of graphene using Group B metals. In this manner, the synthesis of graphene is controlled by the substrate effectiveness, pressure, and temperature applied to the graphene surface. The optimization procedure for the performance of graphene using this method is highly challenging owing to the large number of interconnected factors.

2.1.2.2. Arc discharge. The arc discharge was originally used by Krastchmer and Hoffman. As illustrated in Fig. 6(b), in this approach, a direct-current arc voltage is applied between two graphite electrodes immersed in an inert gas in an electric arc oven that has two graphite electrodes and a steel chamber chilled by water. Wu et al. [45] suggested the use of an arc-discharge technique to create graphene in a gaseous atmosphere, where hydrogen and nitrogen gases were combined to produce high-quality graphene. The created graphene had fewer structural flaws compared to the chemical processes, and it was simple to disperse in organic solvents, which increased its potential uses. High-quality graphene can also be produced using other gas mixtures including helium and carbon dioxide. Kim et al. [46] demonstrated bi- and tri-layers of graphene with excellent quality by using the same procedure. Additionally, Cheng et al. [47] coupled vacuum arc discharge with the CVD process to synthesize graphene because arc discharge is cost-effective and environmentally friendly process that produces high-purity graphene.

2.1.2.3. Plasma-enhanced chemical vapor deposition synthesis (PECVD). For copper and nickel specimens, PECVD is often used to generate graphene using a combination of hydrogen and methane gas. This is a different approach for producing graphene that is on par with the thermal CVD procedure. Direct current (DC) arc discharge [49], radio frequency [50], and microwave (MW) [51] are a few examples of plasma drivers that may affect the process. Although other substrates have also been utilized, nickel and copper are often recognized as the main substrates for manufacturing PECVD graphene. The distinctive circumstances for the foundation of PECVD graphene on the substrate of a metal surface include the following: methane in hydrogen (5%-10%), substrate temperatures between 500 and 800 °C, and plasma power of 900 W. Compared to thermal CVD, the main advantage of this technique are the requirements of minimal time and low temperature. A schematic representation of the inductively coupled RF PECVD system for the deposition of a carbon nanosheet is shown in Fig. 6(c). The scanning electron microscopy (SEM) images of the carbon nanosheets grown on the Si substrate at CH_4 concentrations of 10%, 40%, and 100% are shown in Fig. 6(d–f).

2.1.2.4. Pyrolysis. The thermal decomposition of substances at elevated temperatures in an inert environment is termed as pyrolysis or devolatilization. The precursor is altered according to the expected output. Carbon atoms are deposited over metallic boats that act as thermal hotspots to create few-layered graphene. The thermal interruption of the silicon carbide (SiC) remains a reliable method for fabricating graphene [52]. Silicon withdraws at the maximum temperatures, releasing carbon at its site. The resulting graphene sheets can be up to 10 m thick. This method is both cost-effective and reproducible. Fig. 6(g) presents the technique used for the CO_2-laser induced epitaxial growth of graphene on the SiC wafer; the SEM image demonstrating the development of epitaxial graphene at Region 1 and the area under high magnification is shown in Fig. 6(h–i).

2.2. Surface functionalization strategies for GFMs

There are various types of surface functionalization approaches, such as covalent, noncovalent, surface modification with nanomaterials, and plasma hydrogenation methods, as discussed in Fig. 7(a).

2.2.1. Functionalization of covalent organic groups (polymer, DNA, proteins)

A stable graphene dispersion is required to fabricate composite materials with GFM [54]. The primary step requires enhancing the dispersibility and stability in solvents via the attachment or functionalization of specific organic groups to the GFMs. To enhance biocompatibility in bio- applications, GFM are modified or covalently functionalized with proteins, DNA, and polymers, leading to excessive things for a definite purpose in biological activities. For example, for the treatment or diagnosis of a disease, a specific target is directed towards particular organisms or cells in the body [55,56]. In most cases, the surfaces of GFM are attached to organic functional groups; the organic molecules that functionalize graphene through covalent bonding follow two main routes: a) between the organic functional group and oxygen groups of GO via the formation of a covalent bond, or b) between the free radicals or dienophiles and the C═C bonds of perfect graphene via the formation of a covalent bond [54]. By using reactive intermediates such as nitrenes, arynes, carbenes, and radicals, the GFM are normally functionalized; these types of reactive intermediates can also covalently transform GFM by a combination of free radicals via CH-insertion or cycloaddition reactions. Perfluorophenyl nitrenes are more efficient than alkyl nitrenes or phenyl compounds. Nitrenes are more commonly used than carbenes because nitrenes undergo CH-insertion and C═C cycloaddition interaction via GFM. Moreover, to simplify the Diel-Alder reaction with GFM, arynes act as dienophiles [57]. Compared with the graphene surface, GO has oxygen-holding groups that help simplify the formation of the covalent bond; furthermore, the presence of numerous epoxy, carboxyl, and hydroxyl groups at the top of GO facilitates certain common reactions such as isocyanation, carboxylic acylation, epoxy ring opening, and diazotization, among others [58]. For sensor and bio-applications, Jin et al. [59] developed a flexible and convenient approach for functionalization by producing 4-propargyloxyphenyl

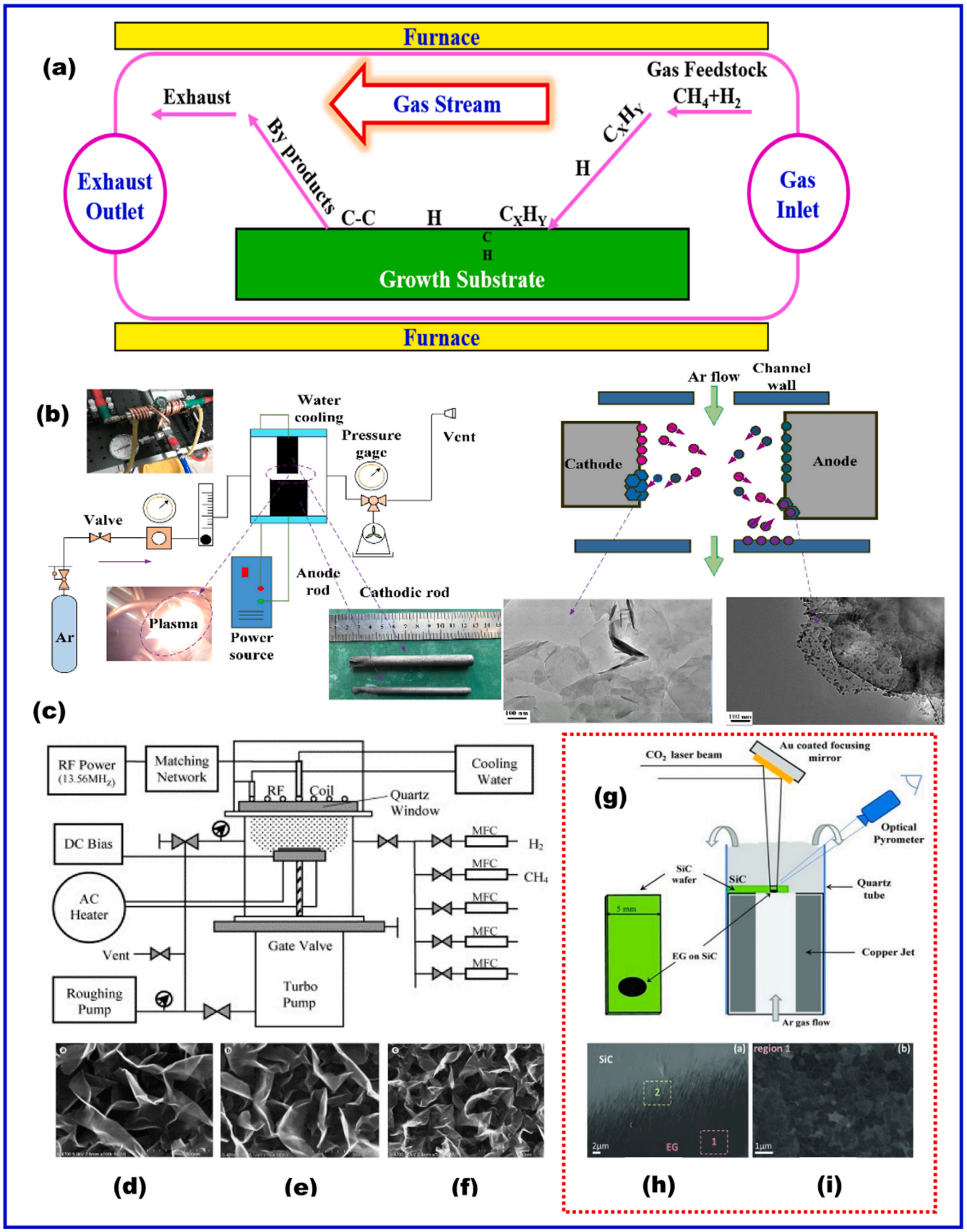


Fig. 6. Graphene synthesis via bottom-up route. (a) Schematic illustration of the CVD method, (b) arc discharge method [48], (c) schematic view of inductively coupled RF PECVD system for the deposition of carbon nanosheet, (d-f) SEM images of carbon nanosheets grown on the Si substrate at CH_4 concentrations of 10%, 40%, and 100% [50], (g) schematic representation of CO_2-laser-induced epitaxial growth of graphene on the SiC wafer, and (h-i) SEM image demonstrating the development of epitaxial graphene at Region 1 and its area under a high magnification [52].

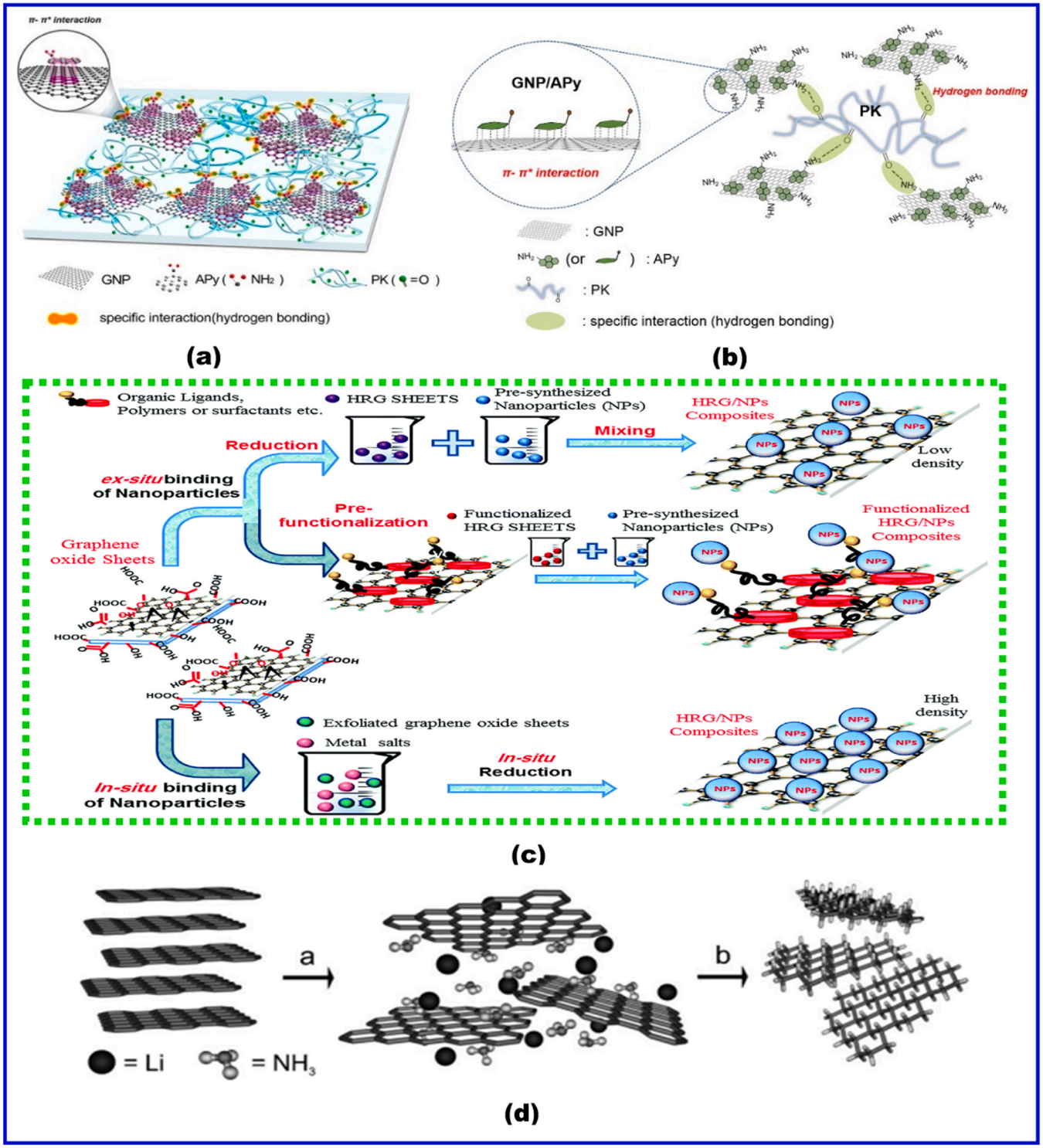


Fig. 7. (a) Types of functionalization possibilities and ssDNA functionalization of graphene, (b) Sufo-NHS esters on carboxylated graphene form an amide bond with amine-terminated ssDNA probes, resulting in (c) ssDNA functionalized graphene and (d) hybrid formation after incubation with cDNA. A:G:C:T [53] and (e) hydrofluorinated graphene synthesis. [69].

graphene (GC≡CH), which is further functionalized by azido polyethylene glycol carboxylic acid via an addition reaction. The other significant technique for covalently modifying graphene is via hydroxyl functionalization, where the existence of several OH^- groups at the top of GO enables hydroxyl-based functionalization by the reaction of esters or amidation produced by the GO, which are then further modified with other functional groups [60]. GO-containing edges with carboxyl groups are extremely reactive; therefore, they can be used for GO functionalization [61]. The deficiency of amino and hydroxyl groups on graphene facilities the production of ester or amide bonds by the effect of certain groups such as the carboxyl group, which is related to the activation of the reaction [62,63]. GO is widely used for sensing applications owing to its high surface area, aqueous stability, varied functional groups, and electrical and optical properties. The DNA probes covalently involved with the GFM are significantly resistant to nonspecific movement, thus increasing the constancy of biosensors [64]. In

EDC coupling chemistry, the GOs containing carboxyl groups are combined with DNA, which are amino-functionalized via the covalent attachment (Fig. 7(b-d)) [65]. A yield of approximately 50% is observed for this type of conjugation reaction after the necessary washing step for the eradication of the unwanted DNA from the surface of graphene, which typically provides an incorrect signal by the noncovalently attached and physisorbed probes. Bonnani et al. [66] developed a proficient method for covalently bonding single-stranded DNA (ssDNA) with graphene using the chemistry of carbodiimides and extended their usage in the geo-sensing. However, DNA functionalized by covalently bonding to graphene utilizing EDC has certain drawbacks, as well as the removal of physisorbed DNA from the surface of graphene materials, which not only indulge in reactions such as coupling. To solve this problem, Sharma et al. [67] demonstrated an ultrasensitive, label-free aptasensor for the detection of cardiac myoglobin using polyethylenimine (PEI)-functionalized rGO films via covalent modification. For advancing the miRNA sensing detection limit, Shin et al. [68] attached a dsDNA containing fluorescence-labeled probes on the surface of the GO using reactions such as covalent coupling for the detection of picomolar concentrations; the hydrofluorinated graphene synthesis is shown in Fig. 7(e) (Table 1).

2.2.2. *Functionalization of noncovalent approaches, with self-assembly*

The biocompatibility, high area of surface, and chemical stability are important features of GFM, making them useful for bioimaging, drug deliver, antibacterial, and gene delivery applications [83]. Graphene enables surface modification via π–π stacking interactions. These types of noncovalent interactions are generally observed in various materials, in which the force of repulsion and/or attraction occurs, and are found in many synthetic and natural entities. The surface of the GO sheet can be functionalized by hydrogen bonding and electrostatic interactions owing to the presence of oxygen-containing functional groups on the edge. As, Omidi et al. [83] revealed that the surface of rGO and graphene are loaded with a series of Schiff bases comprising azo pyridinium as well as chromene sections via noncovalent interactions. Various advantages of GFM involve their dispersion into the polymer matrix; however, owing to the existence of π-π collaborations in graphene, it is difficult to achieve a homogenous combination that leads to the restacking of the layers. To overcome this issue, an approach for achieving a similar dispersion in polymer matrix via a covalent- or noncovalent-based superficial alteration of graphene was proposed. A stable dispersion in organic solvents is accomplished via the covalent functionalization of graphene materials using aliphatic amines, aromatic compounds, and isocyanates molecules [84,85].

Alternatively, covalent functionalization degrades many of the beneficial characteristics of GFM, including their electrical, barrier, and mechanical properties. Layek et. al., [86] demonstrated that a polymeric matrix facilitates better interactions with the functional groups that exist on the basal-plane pyrene edge of graphene. The structure design and inherent characteristics of the self-assembled graphene facilitate its effective use in biosensors. For example, Luo et al. [87] demonstrated that self-ledged graphene with polyalinine composites can been used to construct supercapacitors and achieve a high electrochemical capacitance. Similarly, graphene self-assembled structures improved via glucose oxidase were utilized for the detection of glucose and achieved a sensitivity detection limit of up to ~20 μM [88]. Zhang et al. [89] reported that the self-assembled morphology of graphene can prove useful and stable 3D structures for sensor applications. Georgakilas et al. [90] demonstrated that noncovalent functionalization approaches have many significant advantages over covalent functionalization methods owing to a smaller amount of damage to the graphene structure along with respect to the intrinsic material properties. Several methods are used for achieving the noncovalent functionalization of GFM, such as π-π interactions and polymeric grafting by the small molecules containing surfactants or by aromatic rings [70,72,82]. Cho et al. [73] synthesized a noncovalent functionalized graphene using composites such as polyketones and pyrene derivates with improved barrier properties and graphene dispersion. A noncovalent functionalization approach is shown in Fig. 8(a–b), which improves the interfacial interactions and dispersibility of graphene in polymer matrices, thereby increasing the potential usage of GFMs in barrier film applications. Marcia et al. [91] synthesized noncovalent functionalized graphene using pyrene derivatives to overcome the cluster and enable superior compatibility between the polymer matrix and GFM. Jung et al. [92] utilized ss-DNA-modified graphene probes for the significantly precise examination of NH_3 and H_2S in blow-out breath tests despite the presence of excessive humidity.

Table 1
Functionalization strategies for graphene, GO and rGO.

Graphene Types	Type of Graphene Used	Functionalization Strategy Used	References
Graphene	Monolayer	Hydro fluorination	[69]
Graphene	Single layer	Non covalent	[70]
Graphene	Sheet	Covalent	[71]
Graphene	Sheets	Non covalent	[72]
Graphene	Sheets	Non covalent	[73]
Graphene	Sheets	Nanoparticles	[74]
Exfoliated Graphene	Monolayer	Covalent	[59]
Graphene Oxide	Single layer sheet	Covalent	[75]
Graphene Oxide	Sheet	Covalent	[64]
Graphene Oxide	Sheet	Covalent	[76]
Graphene Oxide	Sheet	Nanoparticles	[65]
Graphene Oxide	Sheets	Covalent	[77]
Graphene Oxide	Sheets	Covalent	[61]
Graphene Oxide	Sheets	Covalent	[78]
Graphene Oxide	Sheets	Nanoparticles	[79]
Graphene Oxide	Sheets	Nanoparticles	[80]
Graphene Oxide	NA	Covalent	[68]
Graphene Oxide	Multilayer stacked	Covalent	[66]
Reduced Graphene Oxide	Sheets	Covalent	[60]
Reduced Graphene Oxide	Sheets	Non covalent	[81]
Reduced Graphene Oxide	Multilayer	Covalent	[67]
CVD grown graphene	Monolayer	Plasma Hydrogenation	[82]

2.2.3. *Surface functionalized with nanoparticles*

For most heterogeneous catalysis, the binding of nanoparticles (NPs) to support surfaces with diverse properties is critical. A 2D carbon network with a flat basal plane creates graphene as the ultimate external support for the binding of metallic NPs and facilitates the study of interactions between the metallic supports. AuPd NP-based nanocomposites and polydopamine (PDA)-functionalized rGO nanosheets was synthesized using the chemical reduction method [79]. Xin et al. [74] studied the interfacial interactions between NPs and graphene using a 2D model. The p-phenyl SO_3H or p-phenyl NH_2 can be covalently attached to the graphene surface by promoting the uniform spreading of platinum NPs on the surface of graphene, as well as by reducing the size of NPs. The interface of the Pt NPs is significantly high with the functional groups, which helps reduce the migration and coalescence of the NPs. Therefore, the durability and activity of the Pt NPs were significantly improved by using this type of interface, as shown in Fig. 8(c).

For the NP-functionalization of graphene, the most frequently utilized method is metallic salt reduction by using ethylene glycol, sodium borohydride, and sodium citrate, among others [93,94]. The growth of NPs on the surface of the GO conspicuously occurs from the negatively charged functional groups on the surfaces of GO, thus enabling a nucleation interaction by attracting the positively charged metal salts.

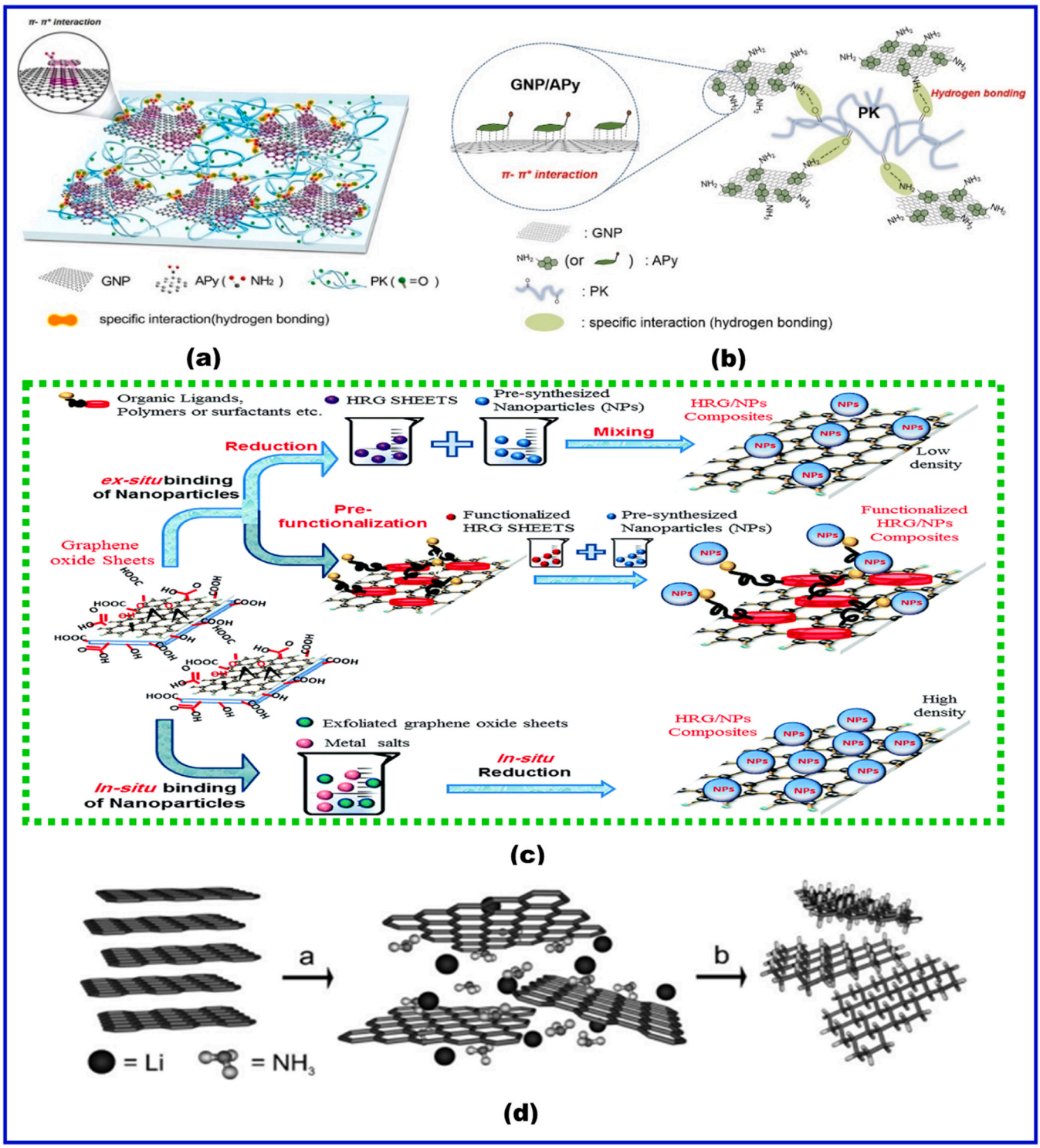


Fig. 8. (a) Hydrogen-based functionalization and the (b) interaction mechanism with the polyketone matrix [73], (c) nanoparticle functionalization with graphene via π–π stacking or C-C covalent coupling [103], and (d) Birch-type wet-chemical hydrogenation of graphene [108].

This type of reaction is similar to that of the conventional route of synthesizing metal oxide NPs, such as nucleation, growth, and reduction. The addition of a reducing agent reduces the cationic metal ions, resulting in the growth of NPs on the graphene surface [95]. Although this method appears simple for obtaining a good yield, controlling the size and morphology of the NPs is significantly challenging, and the chances of forming polydisperse NPs are high [96]. Xin et al. [74] used three different graphene supports to deposit Pt NPs. Gold NPs (AuNPs) were deposited on polydopamine-improvised graphene using a simple, green, and environmentally friendly method [97]. Chauhan et al. [80] has functionalized GO surfaces in the presence of folic acid and synthesized an AuNP GO composite for active tumor targeting.

The hydrothermal method is the main technique used by the scientists to avoid calcination or post-calcination after the synthesis of NPs and to succeed in achieving a small dispersion with a high crystallinity on graphene [98]. Metal oxide NPs such as SnO_2, TiO_2, and ZnO are commonly used for making graphene-metal oxide hybrid NPs via the hydrothermal method. Depending on the structure, size, and

crystallinity, there are various benefits in functionalizing metal oxide NPs onto graphene. This routine restacks the graph and reduces clumping [71]. Metal-oxide-functionalized graphene compounds are superior to individual graphene owing to the increased electron conductivity, condensed ion paths, and improved surface area [99]. Park et al. [57] described a one-pot synthesis via a hydrothermal process using hydrazine to completely synthesize rGO and SnO_2 nanocomposites. Zhang et al. [100] synthesized CdS NP-graphene nanocomposites with controlled density and size, leading to promising photoinduced photocatalysis and photoactivation. Rani et al. [101] demonstrated that the quantum confinement effect of the quantum dots (GQDs) less than 10 nm in size differed from that of graphene sheets. The band gaps of the hexagonal GQDs were studied by examining their HOMO and LUMO energies. With the help of electron-withdrawing substituents, optical properties such as emission and absorption spectra were obtained, and the resulting absorption spectra were redshifted. The size of the GQDs and type of atomic passivation (H or F) will result in absorption, which is useful information for optoelectronic devices and solar cells, respectively. Gebert et al. [102] synthesized ultrathin amorphous Ga_2O_3 on liquid Ga metal and demonstrated the formation of large passivation layers of graphene via a mechanical transfer. The author compared the temperature-dependent electrical measurements of bare graphene on SiO_2/Si; the millimeter-scale passivated graphene indicates its continued high field-effect mobility, which is desirable for applications. Electrical measurements and Raman spectroscopy showed that the passivation of Ga_2O_3 safeguards graphene from additional handling, such as the plasma-enhanced atomic layer deposition of Al_2O_3.

2.2.4. Plasma hydrogenation of graphene

Researchers widely use the hydrogenation of graphene as a new superficial functionalization method, and there are various ways for synthesizing hydrogenated graphene. Moreover, the activation of hydrogen (H activation) or the graphene lattice (C activation) is required for the reaction to proceed. The hydrogenation of graphene generally utilizes a synthetic route via plasma, in which the graphene is exposed to hydrogen plasma or argon gas [104]. Jones et al. [105] demonstrated that the hydrogenation of graphene in the presence of energetic electrons in plasma accelerates the breakup of water molecules assimilating on the surface of graphene. Wojtaszek et al. [106] determined that argon plasma did not increase the surface defect density of graphene, except when graphene was widely exposed to hydrogen/argon plasma, signifying that argon caused the fragmentation of water molecules. The role of physisorbed water with sufficient energy was further investigated. Felten et al. [107] suggested that the main species involved in hydrogenation include H^+, H^{2+}, H^{3+}, as well as their abundance and energy distribution, which differ at various locations in the plasma chamber, resulting in dissimilar reaction chemistries. A key advantage of plasma hydrogenation over other conventional methods is the ease of the chemical reactions; the interaction comprises hydrogen and carbon, which reduces the possibility of impurities including unwanted elements and molecules during the functionalization of graphene (Fig. 8(d)) [108]. Son et al. [69] indirectly exposed hydrogenated graphene to xenon difluoride to fabricate novel hydrofluorinated graphene. Moschetta et al. [83] described the monolayer graphene developed by CVD and treated with hydrogen plasma to obtain the hydrogenated graphene indicated by Betti et al. [109].

3. Surface enhanced Raman scattering (SERS) for GFM

High-performance and noninvasive analytical techniques, such as Raman spectroscopy, are employed for the precise fingerprinting of analyte molecules that are harmful to the environment, such as toxic pesticides [110]. However, certain factors such as an inferior signal conversion efficiency, significantly low signal scattering cross-section, and high fluorescence interference of the analyte, resulted in poor Raman signals with low intensity and sensitivity. Therefore, surface-enhanced Raman scattering (SERS) was adopted for the amplification of Raman signals and to identify the chemical footprints of the analytes [111]. The SERS process involves metal-based systems such as gold, silver, and platinum, which possess plasmonic properties [112]. The electromagnetic and chemical reactions occurring between the analyte molecules and metal surfaces are the major driving forces behind the SERS enhancement of the Raman signals. The direct photon-induced charge transfer from the analyte to the substrate is a chemical mechanism, whereas the photon-induced excitation of surface plasmons (hotspots) on the metal surface is an electromagnetic mechanism [113]. These two mechanisms typically participate simultaneously to significantly enhances SERS by up to 10^8 in some cases [114,115].

The evolution of SERS first occurred in the late 2000 s, with the utilization of graphene as a functional SERS substrate for analysis (Fig. 9 (a)). The graphene-induced enhancement of Raman signal platform is referred to as GERS, in which the graphene layer often acts as a substrate, or it is conjugated with metals to serve as a functional SERS substrate. Fig. 9(b-c) portrays the following: (b) surface passivation of metal substrate like Au and Ag in the absence of graphene, demonstrating dissimilar SERS features of R6G, which are highlighted by downward red arrows, and (c) presence of a graphene layer decorated with Au and Ag showing the exact Raman features of R6G [116]. The interlinked sp^2 architectural build-up of graphene or its different forms, such as GO, rGO, exhibit different adsorption sites for analyte molecules via electrostatic and p-p interactions [117]. These adsorption sites are vital for the chemical mechanism. The fluorescence-quenching ability of graphene-based composites as substrates is noteworthy, which enhances the signal-to-noise ratio of the obtained Raman spectrum and enables achieving a good limit of detection (LOD) [118]. The Fig. 9(d-e) shows the difference between the interaction of the normal SERS substrate (a) and GERS substrate (b) with the analyte molecules. The GERS-based plasmonic metal composite substrate provides an ideal arrangement for Raman signal enhancement owing to its superior chemical enhancement provided by the graphene, as well as the electromagnetic enhancement by the plasmonic metals. Fig. 9(f-h) displays the modules of a G-SERS tape, scalable production ($8 \times 8\ cm^2$ G-SERS substrate before the copper removal), AFM images showing the roughness of flat substrate in the range of + 2 nm, (i) analysis through a G-SERS(Au) tape, a real time and reversible G-SERS characterization of R6G directly in a 1×10^{-5} M aqueous solution (in which I, II, III are the raman spectra), self-assembled monolayer (SEM) of p-aminothiophenol on a flat gold surface measurement is shown in G-SERS (black line) and pristine (red line), cauliflower surface with adsorbed CuPc.

Jian et al. [119] recently decorated the surface of GO with Ag NPs, forming an efficient GERS functional substrate for environmental applications. The GERS (GO-Ag)-based sensing platform was tested using paraoxan, a toxic commercial pesticide. The SERS investigation revealed that the GO-Ag substrate exhibited an impressive enhancement factor (EF) of 10^6 and a LOD of up to 10^{-7} M for paraoxan detection. An efficient charge transfer process was achieved via the GO layer, and plasmonic Ag nanoparticle clusters on top of GO acted as hotspots, enabling an electromagnetic mechanism. These two processes were combined to provide a higher Raman signal enhancement for the paraoxan pesticide. Furthermore, to analyze the practicality of the GO-Ag GERS probe, it was tested in real water samples (mineral water), revealing significantly positive results with a LOD of 10^{-6} M. The GO-Ag GERS probe demonstrated superior stability until 240 days by reproducing the Raman signals of paraoxan. The fabrication and utilization of the GO-Ag-based SERS probe for paraoxan sensing are illustrated in Fig. 10(a). In another study, Li et al. [120] fabricated an economical, flexible, and rapid-sampling SERS swab substrate for on-site pesticide detection in fruits and vegetables. The flexible SERS swab substrates were prepared using cellulose paper, on which GO and Ag nanoparticles were printed using a screen-printing technique. One of the major advantages of the fabrication of SERS swabs by screen printing is that they

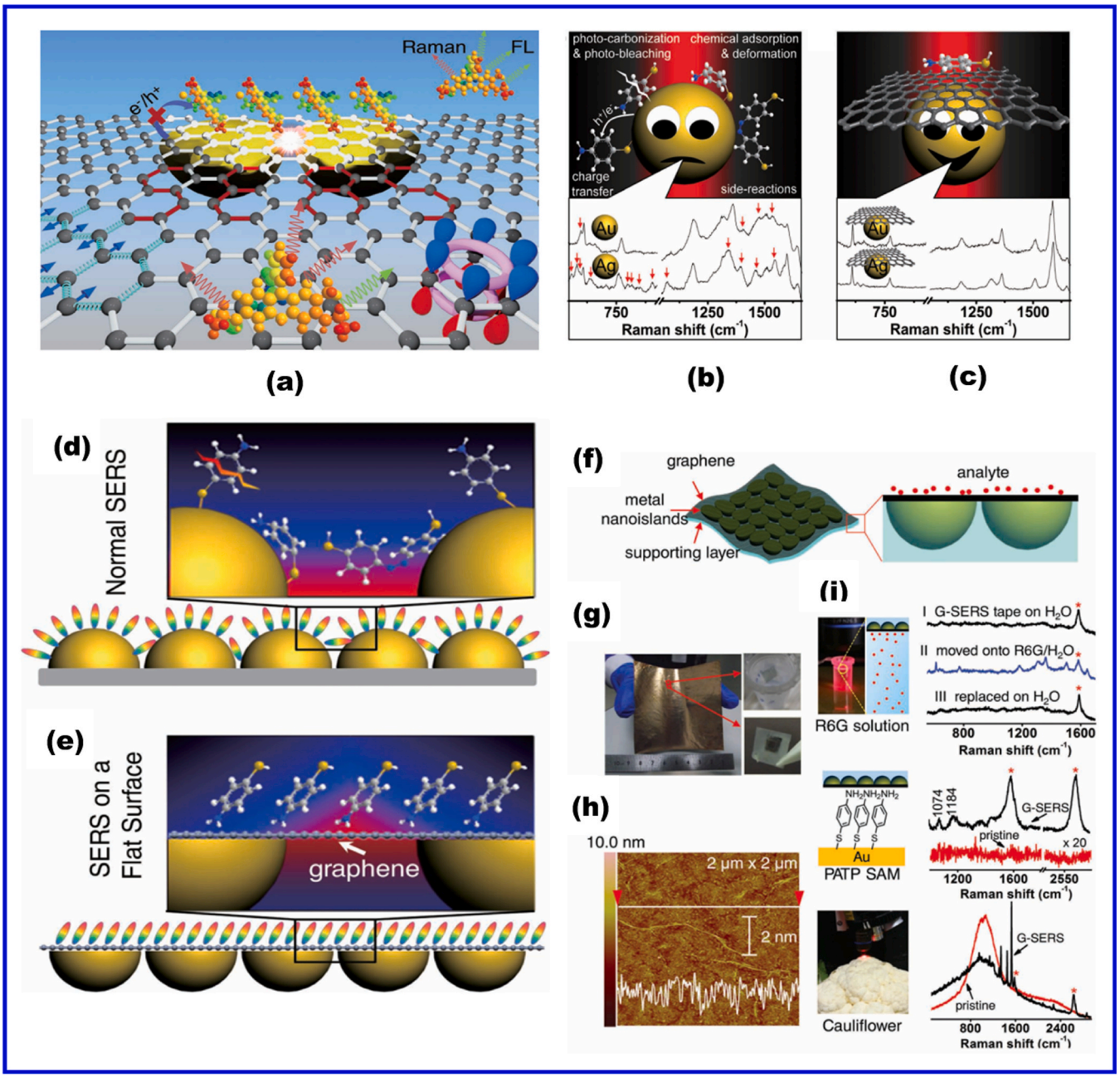


Fig. 9. (a) Graphene-based enhanced Raman scattering (GERS), (b) surface passivation of metal substrates such as Au and Ag in the absence of graphene present dissimilar SERS features of R6G, which are highlighted by downward red arrows, (c) Raman features of R6G are the same for the graphene layers decorated with Au and Ag, (d) Interaction of normal (metal) SERS substrate and analyte, (e) GERS substrate, (f) modules of a G-SERS tape, (g) scalable production (8 × 8 cm^2 G-SERS substrate before the copper removal), and (h) AFM images showing the roughness of the flat substrate in the range of + 2 nm: (i) analysis through a G-SERS(Au) tape, a real-time and reversible G-SERS characterization of R6G directly in a 1 × 10^{-5} M aqueous solution (in which I, II, III are the Raman spectra), self-assembled monolayer (SEM) of p-aminothiophenol on a flat gold surface measurement is shown in G-SERS (black line) and pristine (red line), cauliflower surface with the adsorbed CuPc (by soaking in a 1 × 10^{-5} M CuPc solution in ethanol for 10 min). "*" specifies the enhanced G-band and G'-band features of 1LG [116].

can be prepared in bulk batches for on-site pesticide analysis, which is economical compared to the conventional chemical fabrication of substrates. Screen-printed ink containing GO and Ag nanoparticles is periodically printed on the cellulose paper (Ag NP/GO SERS swabs), which helps achieve highly controlled and optimized SERS-active substrates for pesticide analysis. Three different pesticides including thiram, thiabendazole, and methyl parathion were investigated using Ag NP/GO SERS swabs, which revealed that the p-p-stacking electrostatic interaction arising from the GO and analyte molecules is a vital factor for the enhancement of the Raman signals of pesticides. The Ag NP/GO SERS swabs were further used to detect the pesticides in real samples such as apples, oranges, tomatoes, and cabbage. The multipesticide residues were spiked and analyzed using the Ag NP/GO SERS swabs, which demonstrated an excellent LOD for all the pesticide residues upon analysis: 28 ng cm^{-2} for thiabendazole, 7.4 ng cm^{-2} for methyl parathion, and 0.26 ng cm^{-2} for thiram. Fig. 10(b-c) shows the fabrication and application process of the Ag NP/GO SERS swabs. This study presents a compelling case for the utilization of graphene-based SERS substrates in environmental monitoring applications. A ternary heterojunction nanocomposite based on a g-C_3N_4/Ag/GO multifunctional composite membrane was employed by Zhao et al. [121] for SERS detection and the photocatalytic degradation of hazardous pesticides. A

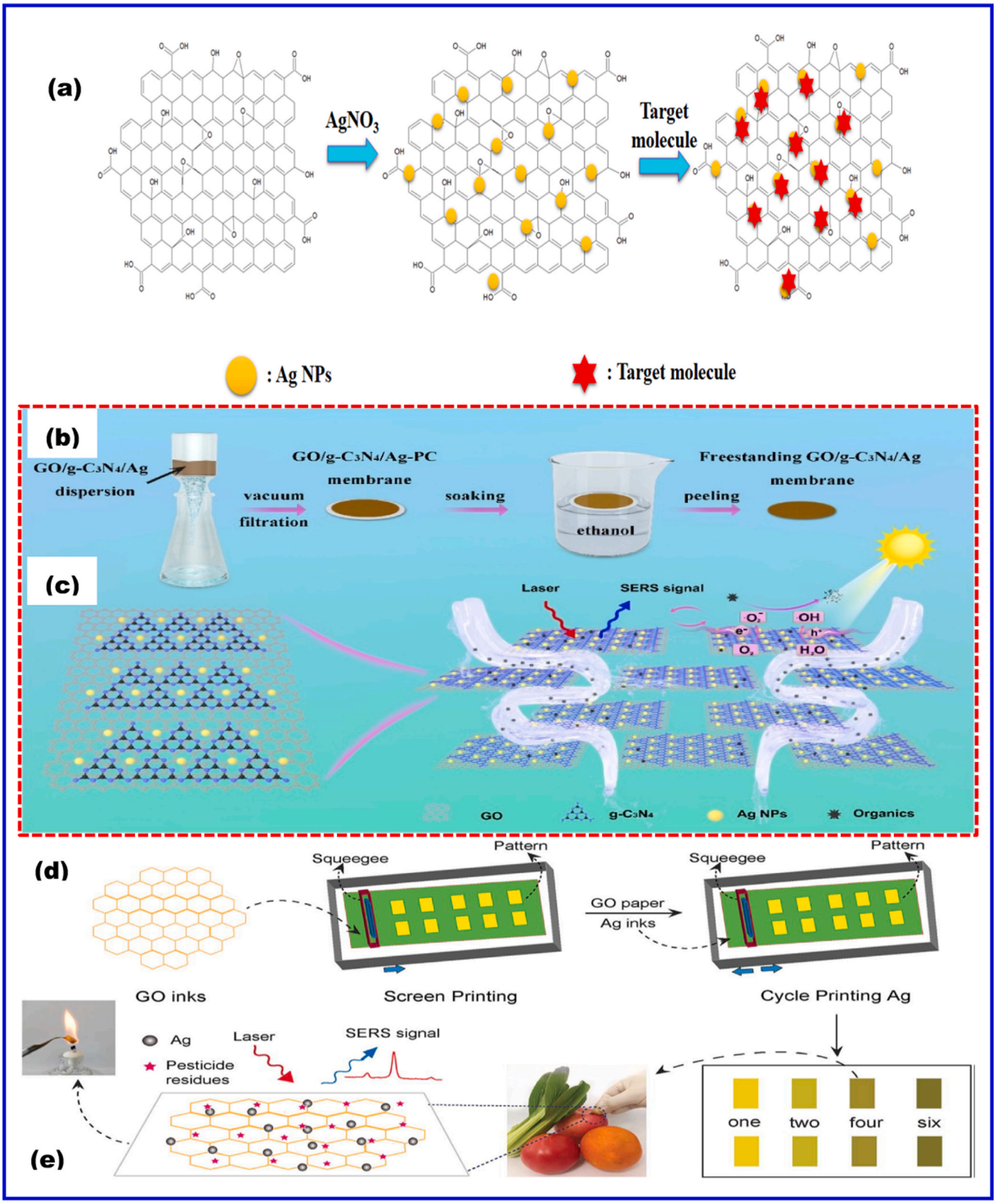


Fig. 10. (a) Construction of the GO-Ag GERS probe for paraoxan detection, (b-c) fabrication of Ag NP/GO SERS swabs for pesticide detection [121], (d) preparation of g-C_3N_4/Ag/GO multifunctional composite membrane, and (e) application process using g-C_3N_4/Ag/GO composite membrane [120].

multifunctional composite membrane was fabricated by the self-assembly of GO nanosheets with g-C_3N_4 and intercalated Ag nanoparticles. The fabrication strategy is shown in Fig. 10(d-e).

Fig. 11(a-g) shows the morphologies of the fabricated composite membranes. The SERS capability of the g-C_3N_4/Ag/GO multifunctional composite membrane was investigated using a hazardous pesticide (paraoxon-ethyl) at a concentration in the sub-nanomolar range. The detailed SERS analysis revealed a superior EF in the range of 10^7 for paraoxon-ethyl detection. Monodispersed silver nanoparticles on GO nanosheets apparently aid in the formation of localized surface plasmon resonances (LSPR), which is a significant factor in achieving a good EF, along with the enrichment ability of the GO nano sheets. Furthermore, the composite membrane displayed an exceptional LOD of 10^{-9} M for paraoxon-ethyl detection. Table 2 presents a comparison of the various pesticide detection methods using graphene-based SERS substrates.

4. Field effect transistor (FET)-based sensing

FET biosensors are composed of two essential elements; namely, a semiconductor based sensitive film for recognizing biomolecules and a conventional FET component for signal conduction, indicating its significance in a FET device [135–137]. The fabrication of a FET biosensor device mainly involves organizing the source (S) and drain (D), which is followed by placing the silica gel rubber in the middle after the engraving process, and finally organizing the gate (G) in the middle of S and D [138,139]. A sensitive film is prepared amongst the S and D of the FET, which is followed by attaching biological functional constituents to its surface; a measurement circuit is attached to the device to complete the FET biosensor [140,141]. Fig. 12 demonstrates that once a fixed biological functional substance encounters the material to be verified, a unique interaction occurs, prompting the movement of electrons in a delicate membrane, thereby revealing the quantity of the material to be verified. Generally, the techniques used to detect bias voltage in FET biosensors are classified as either back-, top-, or solution-gate.

4.1. Biosensor design via the back–gate technique

For a back-gate biosensor, the surface is occupied with an extreme

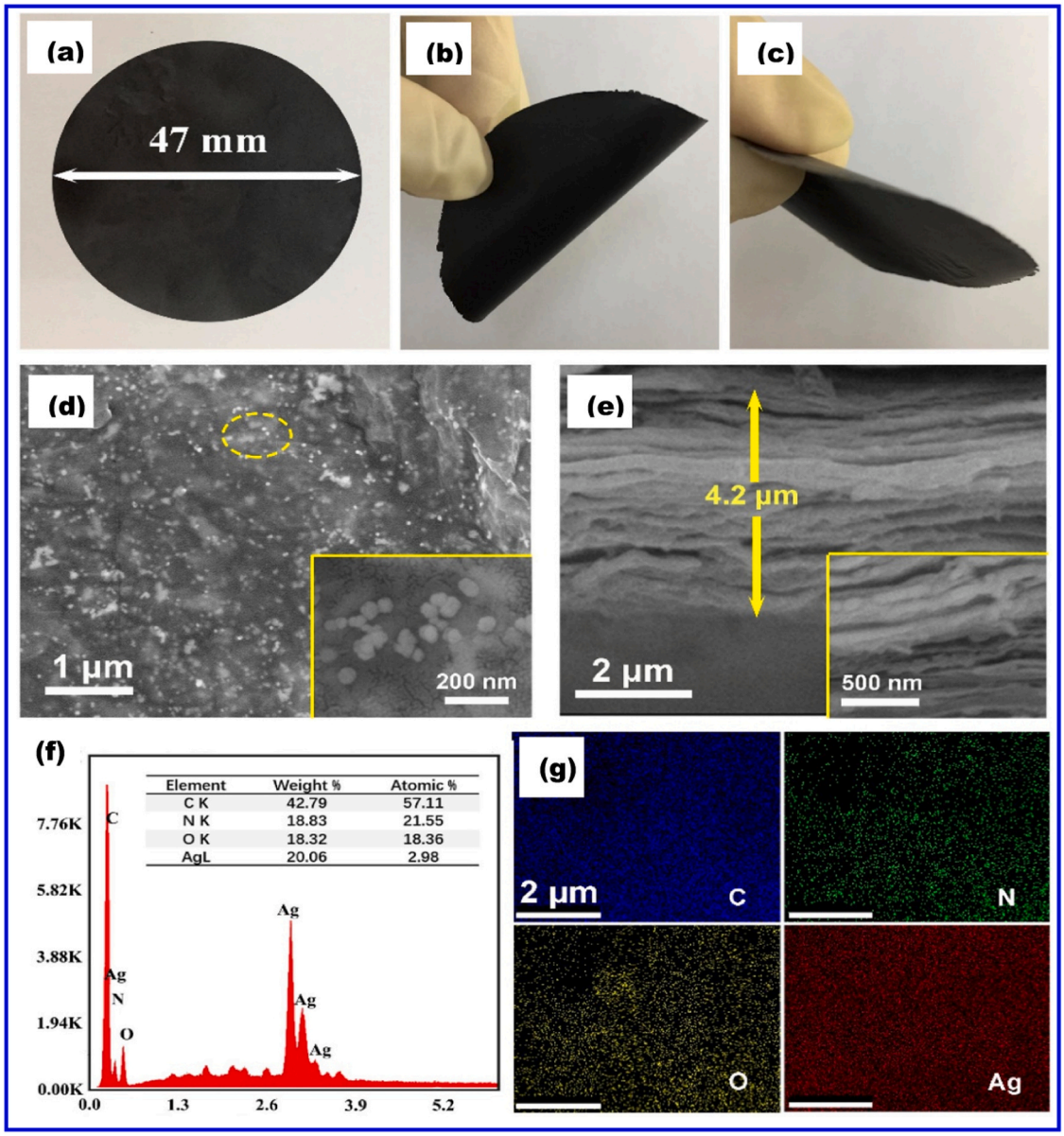


Fig. 11. g-C_3N_4/Ag/GO multifunctional composite membrane: (a–c) photograph, (d-e) SEM images, (f) EDAX spectra, and (g) elemental mapping investigation [121].

Table 2
GFM-based substrates for the detection of various analytes.

S. No.	SERS Substrate	Choice of Pesticide	Enhancement Factor (EF)	Limit of Detection (LOD)	References
1.	GO-Ag Nanoparticles	Paraoxon	10^6	10^{-7} M	[119]
2.	GO/g-C_3N_4/Ag Nanoparticles	Paraoxon – ethyl	10^7	10^{-9} M	[121]
3.	Ag nanoplate/graphene sheets	Thiram	-	10^{-9} M	[122]
4.	Ag nanoplate/graphene sheets	Methyl Parathion	10^8	10^{-9} M	[123]
5.	Graphene-Au film-Au nanorods	Azinphos – methyl	-	10^{-6} M	[124]
6.	Au@Ag nanoparticles/GO/Au@Ag nanoparticles sandwich	Dithio - carbamate	10^7	10^{-6} M	[125]
7.	Graphene wrapped Ag array	Malachite Green	10^8	10^{-11} M	[126]
8.	PMMA/Ag/Graphene	Thiram	-	10^{-8} M	[127]
9.	Ag nanocubes/GO	4-chlorobiphenyl	10^8	10^{-12} M	[128]
10.	Au-Ag-porous GaN/Graphene monolayer	Lead	3.85×10^8	10^{-11} M	[129]
11.	Au-Graphene-Cu	Glucose	39–74%	2 mM – 33.82 mM	[130]
12.	GO/Au	Aβ protein 1–42	-	0.45 mM	[131]
13.	GO-Au	Crystal Violet & Rhodamine 6 g	$2.73\times10^5 - 1.04\times10^6$	5×10^{-11} M	[132]
14.	Au-Graphene monolayer	Rhodamine 6 g	2.12×10^7	10^{-12} M	[133]
15.	Au-Ag-Graphene	Cyanide and Pyocyanine	-	50×10^{-9} M	[134]

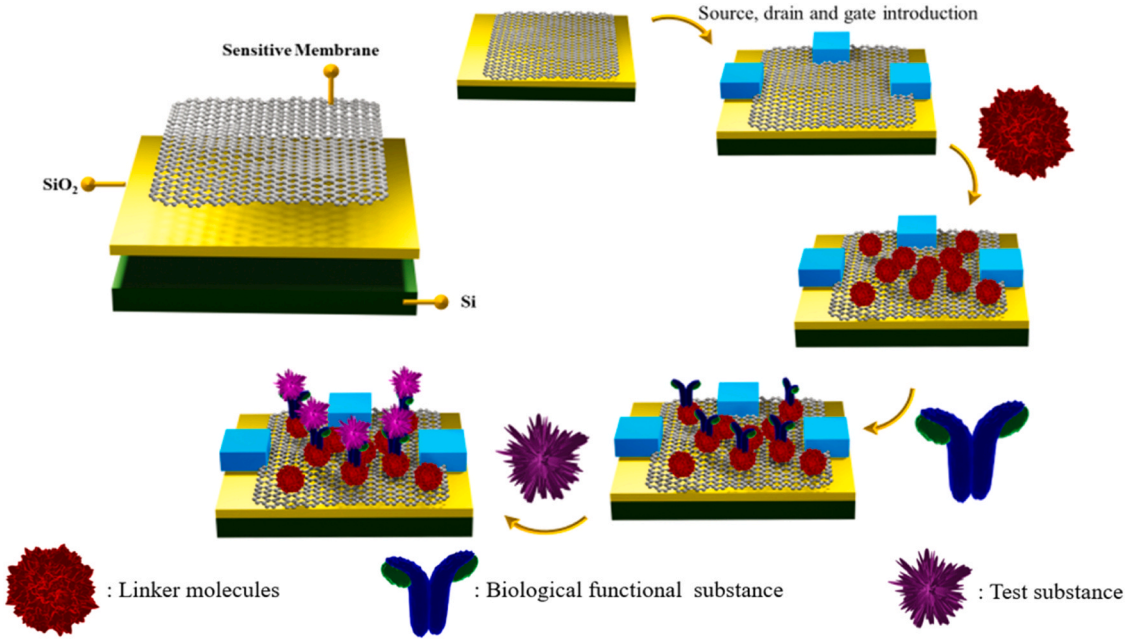


Fig. 12. Schematic representation of a FET biosensor.

recognition area on which a silicon substrate is commonly considered as the back gate, and silicon dioxide is used as the gate dielectric layer for this type of FET biosensors [142]. Through sputtering deposition, patterned metal layers such as titanium are designed as a source and drain on the substrate. Subsequently, CNTs must be cultivated in an environment in which oxygen plasma triumphs; the growth of electrode sections via vapor deposition requires photoresist coating and patterning. At that juncture, the organic solvents are used for the elimination of the photoresist. The device was annealed in vacuum, as shown in Fig. 13(a) [143], and the Debye shielding consequence in the back-gate graphene FET is shown in Fig. 13(b) [144], where the channel of the FET attracts the positive ions that are present in the solution using back-gate FET channel for the detection of antibodies. If the analyte is larger than the Debye length of the biosensor, it attracts the receptor, and the recognition reaction is reduced if the antibodies are large. Compared to other testing details, the maximum detection area is relatively simple using the back-gate biosensor method.

4.2. Biosensor design via the top-gate technique

The top-gate (T-G) biosensor is generally used for remarkably effective detection, and the groundwork process for the fabrication of biosensors is relatively simple compared to other fabrication methods. The signal emitted by the FET can be improved by using a piezoresistive effect, and the top gate can be employed as the sensing component. Accordingly, the cantilever strain minimizes the movement of the base electrons by reducing the current leakage. As shown in Fig. 13(c), Chalklen and Wang et al. [145] used a T-G biosensor to study the adsorption of the analytes and to detect the deflection of the cantilever. Bungon et al. [146] used a T-G biosensor to investigate the adsorption of the analyte, detect the deflection of the cantilever, sputter gold on a p^{++} SiO_2/Si substrate, and illustrate the use of evaporated chromium. The T-G FET biosensor was designed by using metal lift-off and contact lithography patterning for the detection of the clusterin protein biomarker of Alzheimer's disease, as shown in Fig. 13(d-e). Jeseung et al. [147] used a CNT film to develop a metal-semiconductor FET biosensor. The probing antibody is stationary to the gold top-gate by an *Escherichia coli* outer membrane with the Z domain of protein A, or an antibody that is a binding protein G and the gold top-gate is engaged at the center of the CNT channel. The sensitivity of this biosensor is relatively high, as shown in Fig. 13(f); different designs such as MESFET-G, MESFET-Z, FET-C are shown in Fig. 13(g-i).

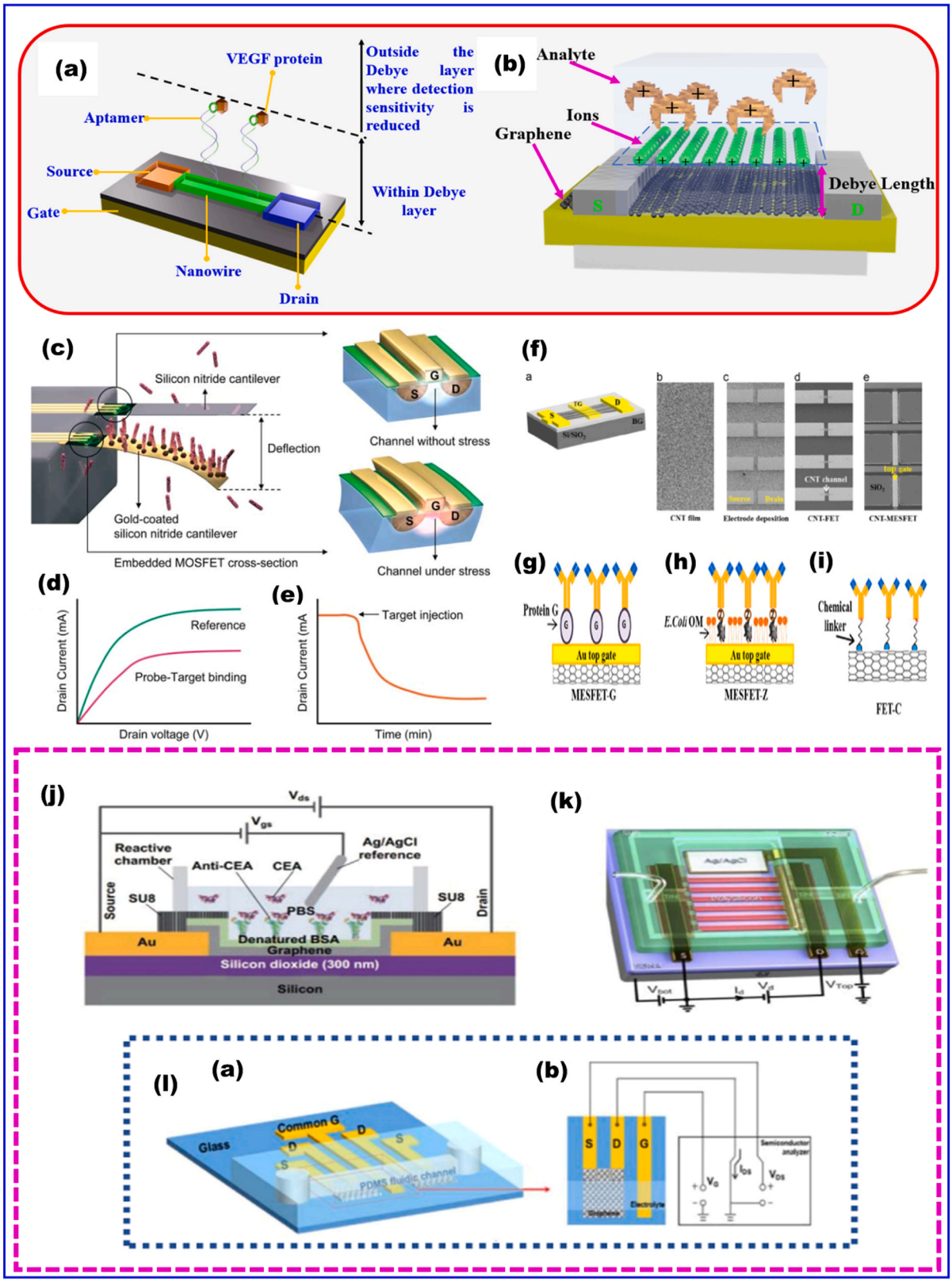


Fig. 13. (a) Back-gate NW-FET sensor, (b) sensing schematic, (c) schematic of the top-gate FET biosensor, (d) schematic showing the change in the MOSFET drain current upon probe-target binding, (e) variation in the drain current with respect to time owing to the deflection of a microcantilever [148], (f) (a) schematic of top-gate FET device, (b-e) FET device fabrication, (g) representation of MESFET-G, (h) MESFET-Z, and (i) FET-C [149], (j) Schematic of the solution-gate FET biosensor [152], (k) schematic of the Ag/AgCl electrode measurement configuration [154], (l) schematic of the (a) side and (b) top views of a solution-gate FET biosensor without an Ag/AgCl electrode [155].

4.3. Biosensor design via the solution-gate technique

The most prominent procedure results in a solution-gate FET biosensor that further eliminates the physiological background of human beings. Silicone was utilized as a substrate, on which a reaction chamber fabricated with polydimethylsiloxane (PDMS) was attached. For sample functionalization in the reaction chamber, a miniaturized Ag/AgCl electrochemical reference electrode acting as a gate electrode was submerged, as shown in Fig. 13(j). Solution-gated FETs employing graphene or rGO as active materials are better than that employ different active materials [150]. Aiming to fabricate device biosensors that employ graphene or reduction, gate-source voltage (V_{gs}) and drain-source voltage (V_{ds}) were applied to the device [151,152]. In addition, this device demonstrated a maximum sensitivity for numerous analytes as well as functions at minimum potentials owing to the nano-electric double layer (EDL) at the edge of the graphene solution and the Ag/AgCl liquid gate electrode most commonly used in the process [153]. As shown in Fig. 13(k), Zeimpekis et al. [154] used Ag/AgCl as the gate electrode and provided a detailed assessment of the pH and protein sensing. Under water-based conditions, FETs are mostly unstable owing to their low sensitivity, and traditional Ag/AgCl electrodes must be used for gating. Han et al. [155] obtained real-time observations of a micro-scale loop-mediated isothermal DNA amplification by projecting a solution-gated graphene FET and using gold electrodes as the source, drain, and gate of the sensor, as shown in Fig. 13(l).

5. Significance of pH sensors on GFM

5.1. pH sensors based on graphene

The aforementioned application of graphene has several advantages as a pH-sensitive material in pH-ISFETs when compared to glass electrodes owing to its configuration; pH-ISFET is smaller in size and has a longer durability compared to a glass electrode, which has a weaker package compared to that of pH-ISFET. Moreover, the pH-ISFET does not consist of any bulb-like part that must be stored wet with a sufficient amount of electrolyte solution, thus it can be stored in a dry condition and there is no extra electrolyte solution needed for storage compared to that of the glass electrode. Furthermore, in exclusively biological measurements, such as the pH of cells, owing to their noncontact (optical) measurement and small size, GQDs have become a viable option.

5.1.1. Solution-gated ISFETs

5.1.1.1. Effect of different electrolyte solutions. The mechanisms related to the response of graphene to the pH of the different electrolyte solutions were further investigated for a better understanding. Heller et al. [156] used a constant pH (i.e., pH = 7) and different concentrations of KCl solution, which were normalized to 1 M KCl within a range [1 mM – 1 M], demonstrating a linear dependence between log(KCl) concentration and V_{Dirac} shift. At pH = 3, similar results were achieved via LiCl; the surface potential decreased, and the double-layer capacitance on the surface, as well as the buffer of the graphene, increased at a high ionic strength. Considering the concentration of the buffer solution with respect to pH = 7, the shift of V_{Dirac} altered near −42.7 mV/decade. However, at pH = 3 the V_{Dirac} shift inversed with respect to the concentration by +18.9 mV/decade, which was most likely owing to the supporting SiO_2 layer. In reality, groups such as silylamine and silanol are ionized by SiO_2; for example, $SiNH_3^+$, $SiOH_2^+$, and SiO^- can positively or negatively charge the surface. For the pH measurement, the effect of different ions was confirmed such as tetraethylammonium (TEA^+), Li^+, K^+. However, the authors did not explain this effect. Conversely, Heller et al. assumed that the specific adsorption or ionic radius of graphene may play a major role. Fu et al. [157] related the pH to a range of graphene sensitivity and indicated that it was significantly large (i.e., 12–99 mV/pH). Consequently, the author set up a three-electrode experiment, as shown in Fig. 15(a). Using the CVD method, graphene was exfoliated or developed on a copper foil and then relocated to the top of a SiO_2/Si substrate. For $V_G \in [0.1, 0.8]$ V and $V_{DS} \in [10,50]$ mV, the leakage current was 1 nA, which is negligible when compared with the measured I_{DS}. From pH values ranging from 5 to 10, the observed sensitivity was nearly 6 + 1 mV/pH, with respect to a previous study, where V_{Dirac} positively shifted as the pH increased. Subsequently, by adding fluorobenzene for 35 s, the graphene surface became more hydrophobic and dried the FET. However, for pH values ranging from 4 to 10, the sensitivity of graphene was nearly zero. Conversely, for pH values ranging from 3 to 8, the sensitivity of the graphene increased to 17 mV/pH by depositing a significantly slim Al_2O_3 layer (below 2 nm), as confirmed by atomic layer deposition at 100 °C. The author indicates that by depositing Al_2O_3, the OH functional groups transformed graphene into a moderately hydrophilic material. Fu et al. indicated that flawless graphene is inefficient for pH sensing and that the presence of defects such as carbonyl and hydroxyl groups will upsurge the graphene response towards the pH. The reported values sensitivity values such as 20 and 99 mV/pH [158,159] correspondingly have a maximum leakage gate current.

Lin et al. [160] demonstrated the growth of graphene on nickel and copper foils. The author used the CVD technique, and before transferring it onto a SiO_2/Si substrate, it was suspended on an arrangement of Pb/Cr drains and sources; the width of the channel was approximately 20 μm. The author correlated both the nickel and copper growths of graphene and indicated that the graphene spread on copper foil (GrCu) consisted of a single crystal monolayer and was quasi-continuous, whereas the graphene developed on the nickel (GrNi) consisted of a significantly small amount of defects, and was a continuous film entailing less than 10 years. The response measured owing to the exponential decay with respect to the time of I_{DS} is expressed as $(I_{DS}\text{-}I_{DSin})/I_{DSin}$, where I_{DSin} is the initial value. A linearly increasing response was observed when GrNi was tested at different pH values including 7, 10, 11, and 13; considering an increase in the pH, the reaction values at a pH of 7 and 13 were 4.75% and 45.1%, respectively, and the resolution was approximately a pH of 0.1. At different pH values, the I_{DSin} was not constant and fluctuated; for example, at pH values of 7 and 13, the I_{DSin} values were approximately 250 μA and 1.5 mA, respectively, at V_{DS} = 0.1 V and V_G = 0 V. This indicates irreversible ion adsorption on graphene. Experiments with another type of graphene such as GrCu was tested, for which the sensitivities were found to be 34.5% at a pH 7.35, 47.6% at a pH 7.59, 57.4% at a pH 7.86; the pH resolution was 0.01. The author did not report error bars on the plots or the number of measurements obtained. Lee et al. [161] investigated the V_{Dirac} shift when an SGFET interacted with hydrochloric acid (HCl), potassium hydroxide (KOH), and sodium hydroxide (NaOH). A graphene film was grown on a copper film in the presence of a H_2 and CH_4 gas mixture at 1000 °C. Before transferring the graphene onto the SiO_2/Si wafer after complete etching of the copper, the graphene was coated with PMMA, which was dispersed in chlorobenzene. The wafer already comprises of drain, Au/Cr electrodes, and a source; the coated PMMA was completely separated by soaking the fabricated chip in an acetone solvent followed by deionized water. The graphene was patterned using standard photolithographic techniques. The range of pH values was altered (pH = 6, 7, and 8), and different concentrations of K^+, Na^+, Cl^- solutions were obtained in a 0.05 M solution of phosphate (Tables 3 and 4). Depending on the ionic strength and composition of the buffer solutions, the author demonstrated a negative shift in V_{Dirac}, whereas other studies regarding SGETs have reported a positive shift in V_{Dirac} as the pH increases. The pH sensitivities were −78.5, −38.5, and −7.5 mV/pH in the buffer solutions containing diverse concentrations of K^+, Cl^-, Na^+ ions, respectively, for buffer solutions with pH values of 6, 7, and 8 at $V_G \in [0,1]$ V as well as at V_{DS} = 50 mV. However, in the reference buffer (0.05 M), the reported sensitivity was approximately +69 mV/pH. Consequently, the observed shift for the commercially available reference buffers was towards the

Table 3
Implications of different electrolytes by using various solutions.

Electrolyte	pH	Concentration (M)	Ionic Strength (M)
K^+	6	0.0556	0.1225
	7	0.0779	0.2116
	8	0.0963	0.2852
Na^+	6	0.0056	0.1224
	7	0.0279	0.2116
	8	0.0463	0.2852
Cl^-	6	0.0444	0.2112
	7	0.0221	0.2558
	8	0.0037	0.2926

positive side, whereas for the buffers with the electrolytes, upon increasing the pH, the shift was towards the negative side. Although the ionic strengths of the potassium and sodium buffers were identical, the results described herein cannot be explained by the strength of the ions. Here, the V_{Dirac} sensitivity shifted towards the Na^+ ionic concentration because it played a more significant role than the concentrations of K^+ or Cl^-. The author assumed that the V_{Dirac} shift was owing to the significance of ionic charge screening, as it depended on the proportion of hydration, ion size, and attraction approaching the surface of graphene. Because the ionic charge shield is more important at higher concentrations, the authors suggested that pH measurements should only be performed in diluted solutions. In this experiment, the sensor sensitivity observed was greater than before (from −7 to −27 mV/pH) with respect to the 0.1 M potassium solution owing to the dilution of the sodium solution by 5–10 times, the V_{Dirac} shift observed was toward the positive direction for as the pH increased.

Kwon et al. [162] prudently examined graphene-mesh FETs (GM-FETs) and the role of defects in sensitivity. To reduce the contamination and disorder of the carbon atoms, silica spheres were used to synthesize the graphene mesh structure and to avoid photolithographic patterning. The copper foil was protected by a hexagonal close-packed monolayer of silica spheres; the separation of the carbon atoms was stimulated as a graphene mesh at the copper–silica interface (Fig. 14a). A single layer of graphene was grown on the top of the copper for an FET comparison (Fig. 14b). The resultant mesh had an average interspacing and diameter of 600 and 300 nm, respectively, with circular holes arranged hexagonally. The sensitivity of the monolayer graphene FETs and GM-FETs were 16 and 90 mV/pH, respectively. considering the different pH values ranging from 6.50 to 8.25, and V_{DS} = 50 mV (Fig. 14(c-f)). Kwon et al. proposed that owing to the numerous unsaturated carbon atoms due to the edge flaws, they might bind or adsorb the H^+ ion, on which the GM-FETs super-Nernstian sensitivity may depend. Although the sensitivity increases owing to the development of the bonds, the use of GM-FETs is limited owing to the irreversibility of this reaction. After five 3-min testing cycles for pH values including 8.25, 7.85, 7.40, 6.95, and 6.55 with respect to the GM-FETs, the sensitivity of the mixtures decreased approximately 7 mV/pH. Graphene defects should be minimized for reliable and reproducible results.

Parizi et al. [164] demonstrated a significant improvement in an ion-sensitive field-effect transistor (ISFET) sensor under the circumstances of pH sensitivity. Based on the investigation of the authors regarding the theory and simulations, the sensor exhibited a remarkably enhanced sensitivity, which can exceed the Nernst limit when utilizing pH buffer solutions that contain counter-ions larger than a certain size. Using an extended-gate ISFET pH sensor, the author confirmed the theory by studying the response of the pH. With stable operations and no hysteresis, the results of the measurement were consistent and reproducible. To confirm the validity and accuracy of the investigation results, the author tested various conditions, such as using dissimilar oxide dielectrics as a layer for sensing, numerous solutions, and IC versus off-the-shelf transistors as the foundation of the ISFET sensor. Yawson et al. [165] investigated the retreat of the active layer and systematically studied the improvements in the movement of electrolyte-gated organic field-effect transistors (OFETs) by utilizing polymer solid-state electrolyte gate insulators (SEGIs). Here, the SEGI consisted of a P(VDF-HFP) [poly(vinylidene fluoride-co-hexafluoropropylene] polymer solution-ion gel at 1 Hz composite and large areal capacitance of >10 μF cm^{-2}. Ultraviolet photoelectron spectroscopy studies have revealed that the downward vacuum-level shift causes a substantial hole injection barrier that originates from the formation of numerous interfacial dipole layers while scaling up the P3HT [poly(3-hexylthipehen)] semiconducting layer by an order of magnitude ranging from to 5–50 nm. The ultrathin size of 5.1 nm is better than most of the devices by

Table 4
Various sensors composed of GFM and their respective applications, analytes, and concentrations.

S. No.	GFM used	Sensing modality	Analyte	Concentration	References
1.	ZnS:Cu,Cl phosphor layer and drop-coating of graphene	Resistance based gas sensor	Co_2	100–1000 ppm	[202]
2.	Graphene Chitosan composite	Electrochemical	Hemoglobin	6.5 and 230 μM	[204]
3.	CMP/poly(lactic acid) (PLA) - Graphene sandwich	Electrochemical	Nitroaromatic, benzoquinone vapors and oxidizing of metal ions	Mm Hg DNBa- 4.55×10^{-5} TNBb- 6.44×10^{-6} BQc- 0.1	[205]
4.	Graphene	FET	Hg^{2+}	10 pM	[206]
5.	AgNW–graphene hybrid electrodes	FET	Dimethylmethyl phosphonate	5–25 ppm	[207]
6.	Au/SnO_2/RGO	Electrocatalysis	Ethanol, toluene, ammonia, formaldehyde, methanol, butanol, Npropanol and acetone	1–1000 ppm	[208]
7.	Graphene	Fluorescence spectroscopy	HIV DNA	50 nM	[216]
8.	Graphene	FET	DNA	0.01–500 nM	[217]
9.	Graphene-Chitosan	Electrochemical	Glucose	3–10 mM	[218]
10.	Graphene Quantum Dots	Photoluminescence	Protein Kinase	0.01 – 0.34 μM	[219]
11.	Graphene	FET	Insulin	1.3 nM	[220]
12.	Graphene nanoribbon	Electrochemical	HIV gene	100 aM	[212]
13.	Graphene nanoribbon	FET	Interlukin 6	0.2 nM – 2.083 μM	[213]
14.	Graphene quantum dots	Electrochemical	Glucose	10 nM – 1.9 μM	[214]
15.	Graphene quantum dots	Photoluminescence Spectroscopy	Metal Ions and dye	90–800 μM	[215]
16.	Graphene-Gold hybrid	SERS	Bilirubin protein	0.436 μM	[221]

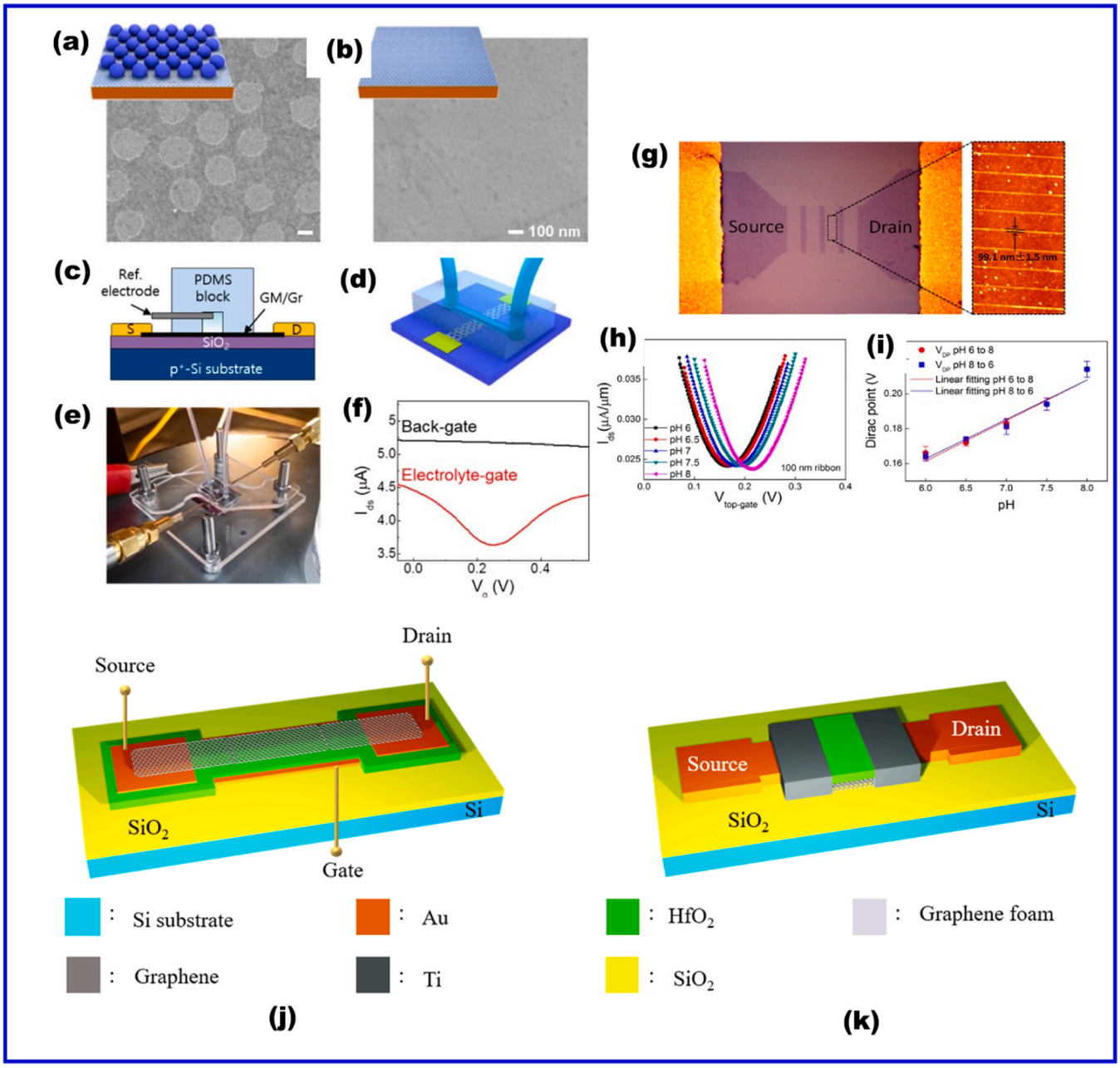


Fig. 14. SEM (top) image of the (a) graphene mesh and (b) monolayer graphene; (c) cross-sectional and (d) 3D view of electrolyte-gated Gr-FET, (e) measurement setup, (f) typical *I-V*$_g$ curves of GM-FET versus the electrolyte gate and back-gate voltage [162], (g) graphene FET after EBL edge-patterning (left), graphene nanoribbons, (h) source-drain current density I_{ds} of various pH buffer solutions, (i) dirac point shift at various pH values and the standard deviation of the pH response [163], (j) FET with a fixed gate under the HfO_2, (k) Graphene-foam 3D-FET layered with a 20 nm HfO_2 layer.

expressing its excellent stability, demonstrating a maximum field-effect suppleness of >2 cm^2 V^{-1} s^{-1}; namely, a device generating active suppleness of 0.83 + 0.05 cm^2 V^{-1} s^{-1}, small threshold voltage of less than −0.6 V, on/off ratio of ~10^6, and a low gate-leakage of current levels (~10^5) below the on-current levels in a 10-μm channel length device. The author reduced the semiconductor thickness and observed a positive shift in the threshold voltage for the P3HT/SEGI FETs, which was 10 times higher than that of the neat P(VDF-HFP) devices, revealing an outstanding approach for the reliability assessment and carrier mobility enhancement in low-voltage-functioned electrolyte-gated OFETs. Awais et al. [166] explored the transport properties of silicon carbide nanowire field-effect transistor (SiCNW-FET) with respect to the pH effect by considering key factors such as the resistivity, transconductance, repeatability, and stability of the fabricated device for sensing applications in harsh environments. The author used various pH solutions ranging from 5 to 9 for the study of transport properties; a pH 5 and a 2 V bias voltage demonstrated a minuscule resistivity of 0.065 mΩ cm and a high trans conductance of 4.5 mS. Awais et al. reported that the conductivity improved from 2.66 to 4.5 mS at a pH of 5 but significantly declined from 4.5 to 0.15 mS at a pH of 9; this device achieved repeatability and good stability after being rinsing with DI water demonstrate a full recovery. Consequently, fields such as biomedicine, biosensing, and environmental sensing can effectively contribute to the development of cost-effective and low-power 3 C-SiCNW-based FETs. Ranjan et al. [167] examined the nonideal behavior around the isoelectric point for the first-time using MATLAB and commercial Silvaco tools for the analytical model of the β-MIS-$(AlGa)_2O_3$ /Ga_2O_3 ion-sensitive FET, and studied the electrical double layer with the

electrolyte using the Gouy-Chapman-Stern theory. In this study, the dielectric in between electrolyte and $(AlGa)_2O_3$ was Al_2O_3; to examine the sensitive parameters such as the charge density, surface potential, β_{int}, C_{DL}, Alpha and C_{diff} for various pH values, they used various concentrations of electrolyte solutions such as 1 mM, 0.01 M, and 0.1 M in aqueous solution. The intensity of 2DEG at the interface of Ga_2O_3 and $(AlGa)_2O_3$ in β-MIS-$(AlGa)_2O_3$ /Ga_2O_3 HEMT undergoes changes owing to the sensitive parameters and surface potential; in the aforementioned study, they observed that higher electrolyte concentration demonstrated a low sensitivity and vice versa. The I_{ON} /I_{OFF} ratio of β-MIS-$(AlGa)_2O_3$ /Ga_2O_3 HEMT, threshold voltage, and transfer characteristics were further examined with dissimilar pH values; when the pH increased from being acidic to basic medium, the threshold voltage has also respectively increased.

5.1.1.2. Chemical reactivity of graphene edges. Based on the aforementioned experiments, graphene boundaries are chemically reactive. Zhang et al. [168] fabricated suspended GNR-ISFET for assessing cancer markers and the pH of a solution; aiming to improve the sensitivity of the graphene towards the pH, the author has further investigated the ideas of Cheng et al. [169]. In this experiment, the GNR-ISFET was driven with $V_G \in$ [-1.8, 1.8] V and $V_{DS} = 1$ V, and the thickness of the GNRs was approximately 50 nm. Zhang et al. presented the equation $(I_{DS} - I_0)/I_0$ at a pH of 9, where I_{DS} is stabilized by the current I_0. Compared with the normal SGFET, unsuspended GNR FET, and suspended GNR FET, the sensitivity increased, which was nearly 1.5 times more sensitive and approximately 25 mV/pH at pH values ranging from 5 to 9.

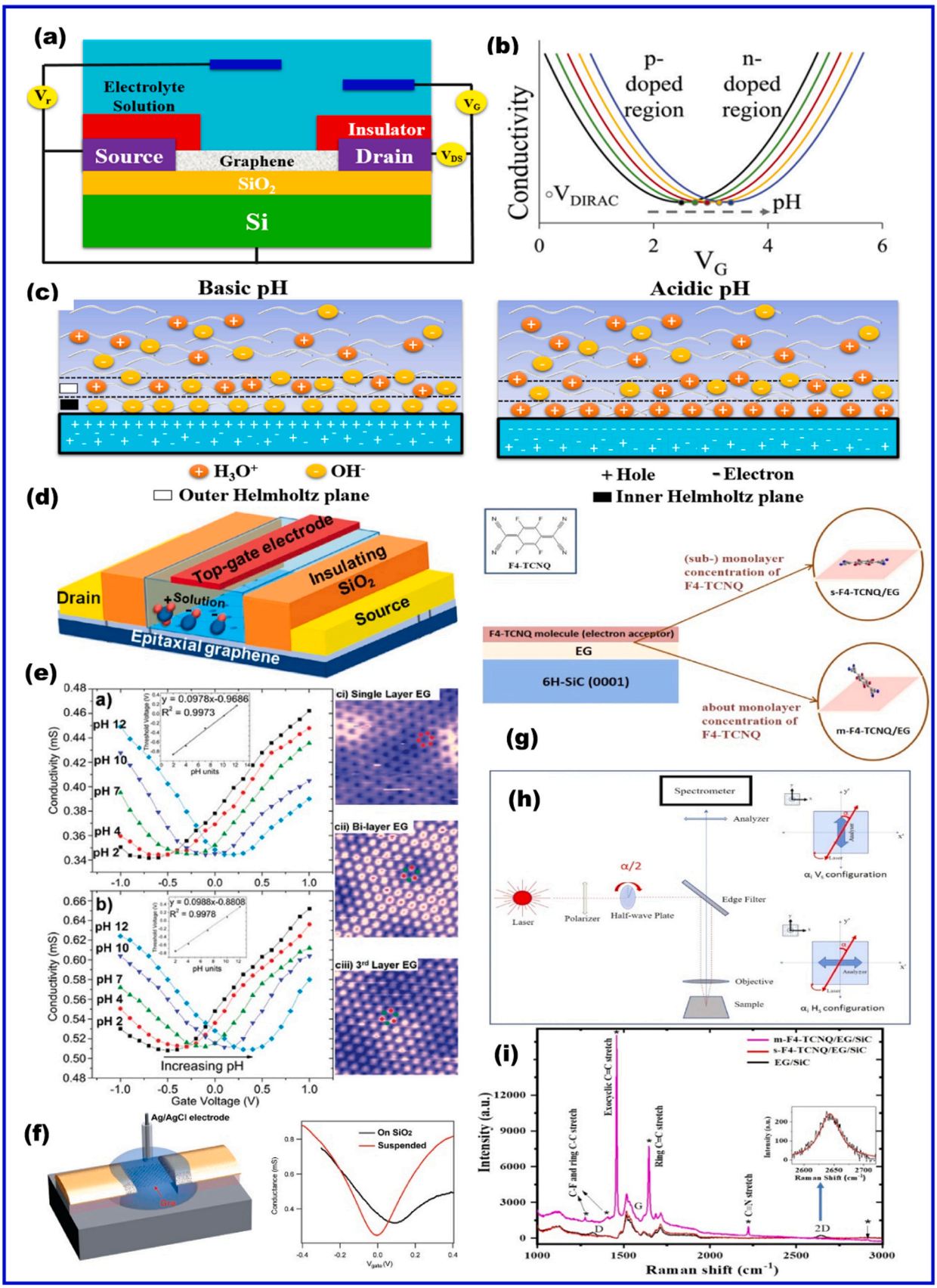
Conversely, Ristein et al. [159] reported that the voltage values in the foundation of defects, which are proficient in varying the measurement during the experiment. To improve the number of hydroxyl groups on the graphene layer, Tan et al. [166] decorated its surface using electron beam lithography (EBL), followed by exposing it to oxygen plasma to obtain 4 columns of 5.5-μm long and 99.1+1.5-nm wide graphene nanoribbons (GNRs). This decoration is illustrated in Fig. 14 (g). At pH values ranging from 6 to 8, owing to the decoration on the layer, its sensitivity improved from approximately 6.5 to 23.6 mV/pH at a constant $V_{DS} = 10$ mV. Unlike the basal plane defects, an advantage of edge defects is that they cannot affect the current flow with respect to the graphene channel. The author reported that this improvement of sensitivity does not depend on the impurities such as hydrogen silsesquioxane (HSQ), which was used in the photoresist and residual PMMA used in the photolithographic process (Fig. 14h). The SGFETs were characterized, any variation in the solution can affect the response of the sensor, as shown in Fig. 14(i). The dielectric layer sandwiched between the graphene channel and gate is an additional FET configuration that deals with the fabrication of the solid gate above the graphene, which is attached above the SiO_2 substrate (Fig. 14j). This improves the microfabrication and integration, and a bulky gate electrode is not required, compared to the transistor dimensions. The arrangement of the 3D graphene FET is shown in Fig. 14(k).

5.1.1.3. Epitaxial graphene over 6H-SiC. A solution-gated FET (SGFET) is a well-known ISFET, in which graphene is used as a conduction pathway. The SGFET consists of a 3-electrode cell, in which the electrolyte is in direct contact with a Pt counter electrode, a reference electrode (Ag/AgCl, Pt, or calomel) to pass the gate voltage V_G, and a graphene (working) electrode that concludes the device. Although the counter electrode is frequently absent, the source and drain of the TG-FET with Cr/Au or Ti/Au are common for pH measurements (Fig. 15a). CVD synthesis and exfoliation of graphite are the most common procedure for the fabrication of graphene [170–174].

In the CVD process, graphene is deposited over a copper foil, which acts as a supporting material; however, during fabrication process, the film is protected with poly(methyl methacrylate) or poly(dimethylsiloxane), and copper is selectively etched in a solution containing sodium persulfate and then deposited over ISFET substrates composed of 6 H-SiC or SiO_2/Si. Ang et al. [176] deposited a graphene layer over 6 H-SiC for pH sensing. The author assumed that the conductivity (σ) of the graphene will be modulated by the adsorption of the hyroxonium (H_3O^+) and hydroxyl (OH^-) ions. In a p-type doping, they observed that the hydroxyl moiety linked with the inner Helmholtz plane of the solution/graphene in the negative V_G interface attracted their counter ions in graphene by using a $V_G \in$ [-1, 1] V, in addition to a stable drain-source voltage (V_{DS}) value such as −1 V. Conversely, the adsorption of the H_3O^+ ions induced a positive V_G or acidic pH in n-type doping. For example, considering an increase in the pH from 2 to 13, V_{Dirac} (Dirac voltage) is a voltage where the channel conductance is minimized by balancing the electrons and holes, which demonstrates a positive shift (Fig. 15b and c), hence allowing the investigation of the pH. However, with respect to a negative V_G, graphene with three out of four layers with a sensitivity of approximately 99 mV/pH was reported, which is higher than the Nernst limit of 59.16 mV/pH. The solution-gated field effect transistor (SGFET) was fabricated on few-layered graphene (FLG); the gate potential versus conductivity of the SGFET fabricated on (a) 1–2 and (b) 3–4 EG layers is shown in Fig. 15(d). The measurement was obtained in 10 mM KCl/10 mM PBS using a pH 2 and 12 at a constant source-drain voltage of −1 V, with 3 ×3 nm^2 STM images of the (i) monolayer, (ii) bilayer, and (iii) trilayer graphene epitaxially grown on 6 H-SiC(0001) with $V_{tip} = 0.1$ V (Fig. 15e(a-c)). By considering a structure similar to that shown in Fig. 15(a), Ohno et al. [177] addressed the leakage of current that was lower than 10 nA in a graphene monolayer. At this juncture, the conductance of two FET configurations was measured: back-gate and top-gate, for which the T-G demonstrated three times the capacitance of the back-gate with an n-doped silicon wafer as a result of endorsing the preference of T-G for sensing applications. When the pH increased from 4 to 8.3, the V_{Dirac} shifted positively and linearly. Here, a sensitivity of 30 mV/pH was observed at $V_G \in$ [-50, 50] mV. Notably, the author reported that owing to the scattering of charged impurities at different pH values, V_{Dirac} may shift in the opposite direction, which may be owing to the graphene defects or residues from the fabrication step.

A ~1-μm shorter graphene layer was suspended between the Au/Cr contacts of the source and drain on the SiO_2 etched substrate by Cheng et al. (Fig. 15f) [178]. The author observed a high conductivity at V_{G-}, that is, the majority of holes when compared with the V_{G+}, and majority of electrons from the FET were directed to a V_{Dirac} of 0.1+ 0.2 V. The suspended graphene led to a significant positive inference in the FET features compared with the standard configuration. The sensitivity increased by 2 and 1.5 times for the electrons and holes, and the SNR was elevated by 14 dB at frequencies less than 1 kHz for a prominent symmetric σ-V_G curve. The complete details of this experiment are lacking owing to reduced scattering; furthermore, when tested with various buffers between pH values ranging from 6 to 9 and $V_G \in$ [-50, 50] mV, the FET sensitivity was near 17 mV/pH. Ristein et al. used a monolayer graphene on a 6 H-SiC single crystal [159]. At pH values ranging from 3 to 12, V_G versus the source drain current (I_{DS}) was investigated at $V_{DS} = -50$ mV. Here, the outflow current was lower than 1 nA in a solution-gated FET (SGFET) and the linear I-V features up to $|V_{DS}| = 0.1$ V. Therefore, the sensitivity obtained in this study was as 19 + 1 mV/pH for the V_{Dirac} shift per unit pH. As the transistors were similar with respect to Ang et al. [176], the potential for the obtained value of the graphene channel, such as 3.5×10^{-5} S, was compared to that of the reported value (3.5×10^{-4} S). The difference of one order of magnitude in the conductivity was possibly owing to the defects triggered by the creation of holes that led to a significant Nernstian sensitivity, as Ang et al. confirmed an SGFET at $V_G > 0.3$ V.

Lei et al. deposited a graphene sheet onto a SiO_2/Si substrate that was exfoliated from graphite and designed a chemiresistor, which was a gate-free FET [179]. The sensitivity of the device was measured for pH values ranging between 4 and 10 with an initial resistance of 86 kΩ and a constant current flow of 10 μA was approximately 2.13 kΩ/pH. The



(caption on next page)

Fig. 15. (a) Three electrode FET configuration for a pH analysis, (b) V_{Dirac} shift during pH change presents excess electrons towards the right and excess holes towards the left channel [175], (c) distribution of donors or ions (electrons or holes) in the electrolyte solution at various pH values, (d) solution-gated field effect transistor (SGFET) fabricated on few-layer graphene (FLG), (e) gate potential versus the conductivity of the SGFET fabricated on (a) 1–2 and (b) 3–4 EG layers; the measurement is obtained in 10 mM KCl/10 mM PBS with pH values of 2 and 12 at a constant source-drain voltage of −1 V; (c) 3 ×3 nm^2 STM images of the (i) monolayer, (ii) bilayer, and (iii) trilayer graphene epitaxially grown on 6 H-SiC(0001) with $V_{tip} = 0.1$ V [176], (f) enhanced concert of suspended graphene field effect transistors (Gr-FETs) as sensors in aqueous solutions [178], (g) concentration-dependent change of the molecular orientation of F4-TCNQ on BLG, (h) Raman spectroscopy setup, (i) Raman spectra (unpolarized) of the pristine BLG on SiC(0001) (black line), after the deposition of 0.3 mL F4-TCNQ (red line), G, 2D, and D peaks of the graphene [184].

ratio between the sensitivity of the device and the maximum standard deviation of the resistance values for repeated trials was considered in the resolution calculation. Here, the author reported the resolution for acid acidic pH as well as basic pH as 0.97 and 0.33, correspondingly. This is mainly due to the assumption that OH^- ions are well-organized in the internal Helmholtz plane to that of H_3O^+ ions. This sensor was reusable regardless of the hysteresis of approximately 2 kΩ. Despite the lack or reporting any further explanation or specific value regarding the reusability, the author suggested that considering the extremely small thickness, this will undoubtedly useful for the facile removal of electrolytes form the top of graphene. Lee et al. [169] proposed another model of a gate-free FET based on a paper substrate. In sodium dodecyl sulfate (SDS) solution, graphene was first dispersed and sonicated, and subsequently transferred on top of the paper substrate under a vacuum using a metal mask. A total of 6 U-shaped graphene sensors were designed after rinsing with deionized water and letting it dry for 20 min at 80 °C. A paraffin pen was used to define the area for the closed measurements around each sensor. The deposition of 0.5 mg of graphene between the vacuum filtration resulted in the greatest fabrication repeatability and electrical stability at a sensing layer thickness of approximately 100 μm. Approximately 10-μL drops of various solutions with pH values ranging from 1 to 10 were used to measure the responses in each of the six measurement areas. The association with respect to the pH and resistance resulted in a recession line with a coefficient of determination $R^2 = 0.93$ at $V_{DS} \in$ [-1, 1] V, with a sensitivity of approximately 30.8 Ω/pH.

Yang et al. [180] reported the growth of graphene on the Si face of 6 H-SiC using an inner and external carbon synergy (IECS) technique, which combines traditional epitaxial growth (EG) on the silicon carbide and CVD for a realistic approach of the graphene grown on the SiC substrate; the process required only 3 min, which is significantly faster than the traditional EG technique at a temperature approximately 200 °C lower than that used for the traditional technique. The author reported that the directly-grown graphene is compatible with the semiconductor method and is significantly useful in the approach for graphene-centered microelectronic devices. Kotousova et al. [181] examined the epitaxial graphene structure achieved by the thermal desorption of a silicon carbide layer in an Ar medium and under a vacuum synthesis by reflection electron diffraction. Consequently, the author achieved a uniform buffer-layer coating of the SiC layer by the epitaxial graphene while developing a passive intermediate on the surface of the 4 H- and 6 H-SiC(0001) polytypes, in comparison to the graphene grown under a high vacuum. Thus, the degree of perfection of the original single crystal influenced the performance of the coating.

Yang et al. [182] investigated the epitaxial growth of graphene on SiC and the thermal transport at a 6 H-SiC/graphene buffer layer/GaN heterogeneous interface, from which the graphene buffer layer (GBL) was epitaxially grown using the annealing method, illustrating that the Tersoff-Erhart-Albe potential (TEA) is higher than that of the environment-dependent interatomic (EDI) potential based on the assessment of the average atomic binding energy, nucleation temperature, bond length, atomic structure, and radial distribution function. The author also stated that the interface thermal resistance (ITR) can be minimized by defect engineering by using the thermal relaxation method at the 6 H-SiC/GBL/GaN heterogeneous interface with an extreme reduction of 9.6%. Moreover, the ITR exhibited a maximum decline of 17.9% by increasing the nucleation areas, which further clarifies that the energy is tranquil for passing through the interface, demonstrating the reliability of graphene for an interfacial heat transfer. Therefore, Yang et al. concluded that the ITR is sensitive to temperature (300 K to 1100 K), with a large decrease of 19.6% as the temperature increased. The thermal design of graphene-based semiconductor devices was determined based on the selection of the potential and analysis of the heat transfer of the three-materials heterogeneous interface. Lebedev et al. [183] grew the graphene films on semi-insulator 6 H-SiC substrates at approximately 1700 °C via the thermal decomposition of SiC. The presence of single-layer graphene on the surface of the SiC was confirmed via Auger and Raman spectroscopy. The author presented a theory of adsorption on epitaxial graphene using the Green's function method to obtain analytical results with simple substrate models for the transfer of charge between the substrate and adsorbed molecules. The sensor structure was molded onto the graphene film by using a laser; the developed sensor was sensitive towards NO_2 gas concentration levels ranging from 1 to 0.01 ppb. This method was also tested for the detection of protein using an immunochemical system consisting of monoclonal antibodies (mAbs) and fluorescein, which bind to the dye.

Chattopadhyay et al. [184] used the thermal deposition of the molecular electron acceptor tetrafluoro-tetracyanoquinodimethane (F4-TCNQ) to grow bilayer epitaxial graphene (BLG) on 6 H-SiC(0001) (EG/SiC), which was modified as shown in Fig. 15(g). The surface-modified system was investigated by angle-resolved polarized Raman spectroscopy (ARPRS) and X-ray photoelectron spectroscopy (XPS). The XPS analysis revealed that the concentration bonding of the deposited F4-TCNQ molecules agreed with the Raman spectroscopy, as shown in Fig. 15(h-i). Consequently, the variation in the sum of the layers with respect to the graphene as well as the concentration of the acceptor further control the doping and charge, which is suitable for the applications in the device. Ichou et al. [185] used an ultrahigh vacuum environment (UHV) for combining Kelvin probe microscopy (KPFM) and noncontact atomic force microscopy (nc-AFM) to directly measure the work function and height of monolayer graphene on the Si-face of 6 H-SiC(0001), enabling the distinguishment of the following three types of graphene structures with a good precision: Quasi free-standing monolayer graphene (QFMLG), bilayer graphene (BLG) and zero layer graphene (ZLG). The work function and height of QFMLG are 4.63 ± 0.05 eV and 4.09 ± 0.11 Å, the work function of BLG is 4.83 ± 0.05 eV, and the work function and height for ZLG were 4.42 ± 0.05 eV and 2.62 ± 0.22 Å, respectively. Compared to the various techniques, the nature of nanometer-sized graphene islands, which have an early nuclei of monolayer graphene grown on 6 H-SiC(0001), can be identified by CVD using a local nc-AFM/KPFM dual probe.

Solution-gated graphene transistors (SGGTs) were recently developed and improved for a variety of biosensing applications, including the detection of bacteria and biomolecules and the monitoring of cell activity. Compared to other sensing approaches, SGGTs may attain an equivalent or greater sensitivity to bacteria, DNA, proteins, and other substances after undergoing certain modifications. SGGTs have demonstrated to be significantly promising as high-throughput, ultrasensitive, and highly selective biosensors for various applications because they are readily miniaturized and incorporated into microfluidic systems.

5.2. Electrochemical pH sensors based on graphene oxide

Although there are several means for restoring electrical conductivity, GO is one of the most prominent methods for generating electrical insulators owing to its disordered sp^2 bonding network, unlike graphene [186]. However, its detailed chemical structure is currently under investigation [150]. The most extensive conventional model was developed by Klinowski and Lerf in 1998 [187,188], in which the authors described GO as graphitic platelets categorized by carbonyl groups on the edges, and hydroxyl and epoxy groups on the basal plane. Therefore, GO is highly hydrophilic owing to its numerous polar groups, making it an excellent material for measuring the pH of solutions. Investigations regarding the pH-dependency of GO in a liquid solution indicate that the protonation and deprotonation of carboxyl groups is responsible for the change in the hydrophilicity of GO [189–191]. The hydrophilicity is highly improved at higher pH values, at which point the GO behaves as a surfactant but softens in an aqueous solution as a regular salt owing to its lower surface tension. Conversely, the degree of protonation is weak at low pH values, and GO forms floating clusters such as GO-water-GO sandwich structures, which are bounded by water molecules.

Sun et al. [192] investigated hydrogels containing GO and poly (N-isopropylacrylamide) for the ionization process of carboxyl groups, which occurs mainly as the pH increases, and simultaneously reduces the number of hydrogen bonds. Qin et al. [193] synthesized and disseminated approximately 25–55 mg of GO in 1 mL of filtered water without preprocessing to obtain a self-assembled GO hydrogel, similar to another revised description of the Hummers method [194]. The GO nanosheets were approximately 0.607- and 0.911-nm thick, with an average size of approximately 500 nm. At the lowest GO concentration of 30 mg/mL, a hydrogel was achieved during the synthesis process. The gel formed only at an acidic pH and was pH-dependent, which may be owing to the fact that the hydrophobic interactions and the π-π stacking inhibited the pH-response, and the formed GO hydrogel was stable when the concentration exceeded 5 wt%.

Wang et al. [195] modified the existing Hummer's method to synthesize GO colloids for the formation of a hydrogel and investigated the role of pH by adjusting it with aqueous ammonia for basic solutions and HCl for acidic solution. At pH values of < 5 or > 10, the GO colloid is accumulated into a cylindrical hydrogel; it was converted into a black dispersion. The obtained results depend on the following three factors: i) concentration of GO, ii) use of ammonia and HCl to reduce the GO sheets thickness of the electrical double layer, and iii) the degree of dissociation of the carboxyl groups of the GO sheets for controlling the attraction-repulsion by the charge state. Hosseinzadeh et al. [196] extended the work of Sun et al. by mixing hydrogels consisting of GO and starch-based superabsorbent nanocomposites with Fe_3O_4 nanoparticles and starch-*g*-poly(acrylic acid-*o*-acrylamide) to investigate the ionization of the carboxyl groups as the pH increased by reducing the number of hydrogen bonds.

Melai et al. [197] demonstrated a gold 3-electrode screen printing set-up as an electrochemical GO pH sensor, which included the following 3 electrodes: 1) Ag/AgCl was used as the reference electrode (RE), the 2) working electrode (WE) was coated by a 400-nm layer of GO, and the 3) counter electrode (CE) was short-circuited with the RE. The author suggested that the sensitivity of the WE and RE was approximately 32 mV/pH, and the potential of the open circuit between the two electrodes of the WE and RE was directly proportional to the pH values ranging from 4 to 10 in buffer solutions. During the course of a four-day testing period of human exudate, the fluid was generally obtained from the swelling area as well as from multiplication segments of the wound; this sensor was designed for monitoring the pH of the wound, and the deviation of the pH unit recorded values were limited to <0.1 compared to a typical pH meter available in the market [198]. Liu et al. [199] designed a GO/cysteic acid combined film following the same methodology of Melai et al. by using a three-electrode configuration. The addition of sulfonated and carboxylate pH-sensitive groups to the structure of GO was the main advantage of using cysteic acid. The oxidation of *L*-Cysteine (CySH) measured by cyclic voltammetry in a 0.04 M HCl solution with 2.5×10^{-3} M CySH at a scan rate of 200 mV s^{-1} over the range of [-0.8 m to +2.2] V produced cysteic acid, and 0.15 mg mL^{-1} was the optimum GO concentration. For pH value ranging from 2 to 12, a sensitivity of approximately 50 mV/pH was obtained, and a linear response ($R^2 = 0.997$) was observed for the GO/cysteic acid electrochemical sensor, indicating that the response of a sensor is <1. The relative standard deviation obtained from the stability test at a pH of 5 at 25 °C for 11 h was approximately 0.8%, which can be stored for one month. Liu et al. measured the pH value of tap water as well as Coca Cola by using GO/cysteic acid sensor for a comparison with that of a commercially available pH meter, the results of which demonstrated a relative deviation of 0.7% and 1.6%, respectively. Reagent-less pH electrodes that are sensitive to changes in their surroundings and have longer durability are required, such as for usage in sewage, industrial effluents, and the food industry. Carbon-based materials have been extensively studied for electrochemical applications owing to their low cost, easy of availability, and adaptability. The GO-based electrochemical sensor utilizes a simple technique to monitor the pH and is fabricated using GO-modified carbon electrodes. In an earlier study, Salvo et al. [200,201] developed a pH-responsive film within the desired range using GO dispersion (4 mg/mL). When tested in human plasma over a month, the performance of the resultant sensor was comparable to that of a commercial pH meter (error = 0.14 ± 0.09 pH units) with a sensitivity of approximately 40 mV/pH, consistency of ± 4 mV, and strong linearity (R2 = 0.99). The proposed pH sensor was evaluated in human blood over a week, and the mean difference between it and a commercial pH meter (glass electrode) was approximately 0.1 ± 0.1 pH units. The standard deviations of the GO sensor and pH meter were 0.1 and 0.05 pH units, respectively. This GO pH sensor demonstrated a hysteresis of 0.15 pH units and a temperature dependency of approximately 0.01 pH/°C at temperatures ranging between 25 and 45 °C. Under a broth medium containing human fibroblast cells (MRC-5 (p33)) and 10% fetal bovine serum (FBS), the biocompatibility of the GO film was satisfactory.

6. GFM for environmental usage (analysis of toxic gas using GO)

6.1. Gas sensing

Seekaew et al. [202] indicated that graphene can be used as a sensor material, particularly for detecting carbon dioxide (CO_2) at room temperature. CVD was used to create the graphene substance, which demonstrated high repeatability, precision, and consistency. Additionally, the sensor performance of the graphene for CO_2 concentrations ranging between 100 and 1000 ppm was 25.12%. Regardless, the composition of the sensing materials, and operational temperature impact the effectiveness of gas sensors. The most frequently investigated metal oxides include ZnO, Cu_2O, SnO_2, NiO, WO_3, and TiO_2. The integration of modified graphene and various metal oxide materials has demonstrated enhanced sensor responsiveness. However, n-type semiconductors constitute the majority of experimental metal oxide compounds. Zhang et al. [203] indicated that the substitution of graphene with TiO_2 may enhance the performance of sensors for the measurement of acetone, including sensitivity, effectiveness, and response duration/recovery time. The adhesion and diffusion of gas molecules may be enhanced by combining graphene and metal oxide. Temperature has a significant impact on the performance of gas sensors composed of metal oxide composites because it results in ionized oxygen species, such O_2^-, O, and O_2, developing on the surface of nano-oxide materials.

Owing to the processes that occur on the electrodes, the production of this species has a significant impact on the effectiveness of the sensors. Fig. 16(a) demonstrates the fabrication of TiO_2/Fe_3O_4/GN-SO_3H nanocomposites dispersed in water; Fig. 16(b) presents the TEM image of the

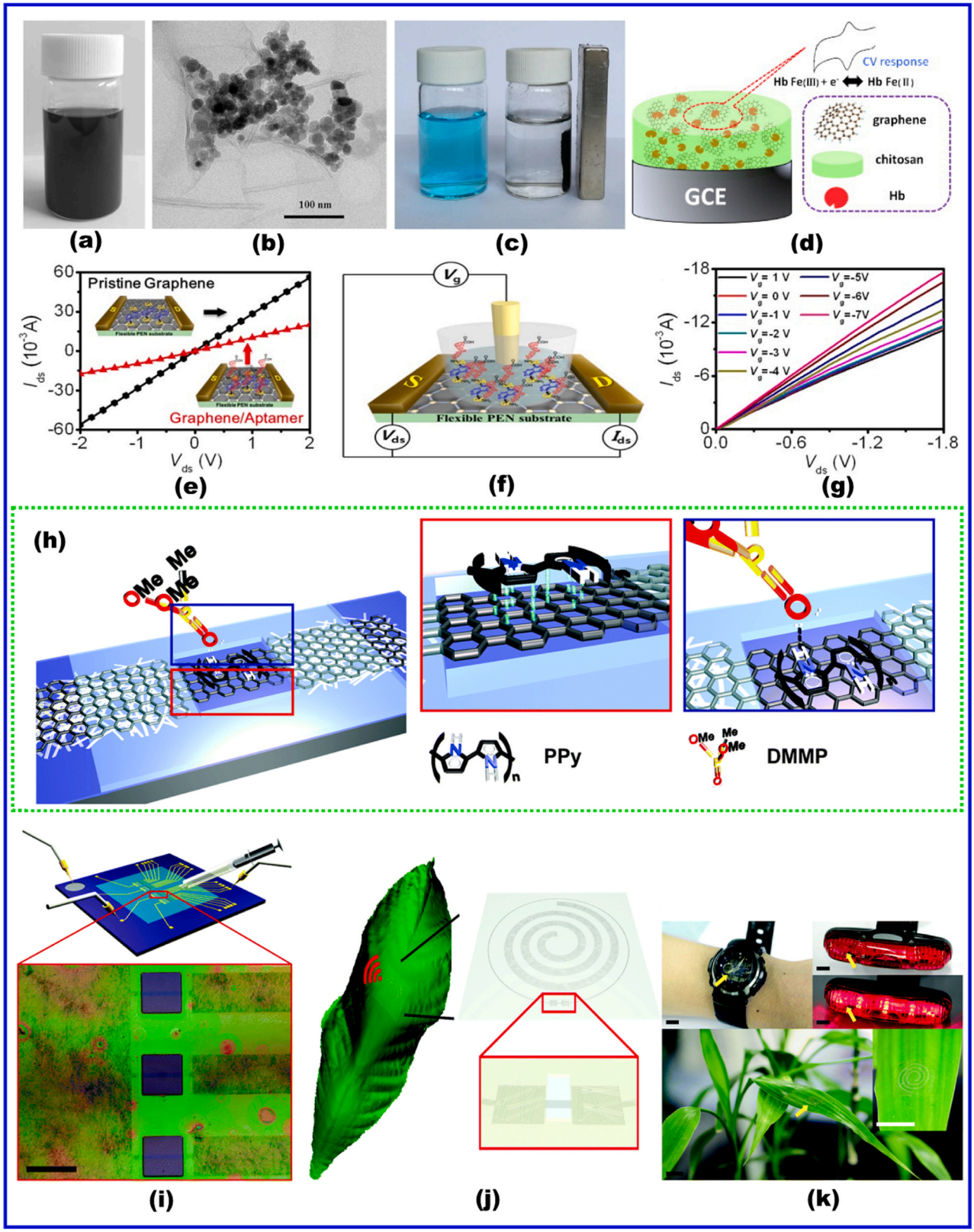


Fig. 16. (a) Digital photographs of the TiO_2/Fe_3O_4/GN-SO_3H composites, (b) TEM images, (c) (i) methylene blue solutions; (ii) Photocatalytic degradation and XPS spectra of the nanocomposites [203], (d) schematic illustration of Hb-graphene-chitosan/GCE [204], (e) *I-V* curves of the graphene aptasensor before and after introducing the aptamer, (f) schematic illustration of a liquid-ion gated FET for the aptamer on the top of the graphene, (g) I_{ds}-V_{ds} output of the graphene aptasensor at various V_g from 1 to −7 V in a step of −1 V [206], (h) FET-based sensor for detecting DMMP via π–π stacking interactions amongst graphene and PPy, (i) schematic and microscopic image of the sensor; scale bar = 50 μm, (j) wireless and real-time sensing of a graphene-based sensor integrated with an antenna on a leaf, (k) images of graphene gas sensors connected with an antenna on a wristwatch, leaf, bicycle light [207].

$TiO_2/Fe_3O_4/GN\text{-}SO_3H$ nanocomposites, demonstrating the typical microstructure along with wrinkled and ultrahin sulfonated graphene nanosheets with sizes ranging from 15 to 25 nm. The author selected methylene blue (MB) as a model dye owing of its wide industrial usage; here, TiO_2/graphene strongly interacted with the delocalized π-bond of the aromatic functionalized graphene basal plane via π-π interactions and successfully removed MB (6 mg/L) from aqueous media, demonstrating a removal rate of 99.99% as shown in Fig. 16(c). The immediate electron transfer reaction of GOD at the enhanced electrode and its electrochemical behavior at the graphene-chitosan enhanced electrode are presented. These findings suggest that graphene supports direct electron transport at the electrode surface and offers an enzyme-friendly atmosphere. Chitosan is crucial for creating a suspended state of well-dispersed graphene and for immobilizing enzyme particles. This graphene-based enzyme sensor exhibited outstanding sensitivity and long-term stability for glucose detection. The development of a unique, extremely sensitive, and stable electrochemical sensor may provide a new method for this purpose.

H_2O_2 is a metabolic byproduct of several biological processes; therefore, H_2O_2 detection is crucial. Bunch et al. [6] created an H_2O_2 sensor (Fig. 16d) by employing an rGO-chitosan composite film with hemoglobin (Hb) molecules trapped inside. Compared to the traditional H_2O_2 detecting techniques, this sensor has a significantly low limit of detection (LOD; 0.51 mM) and a larger linear range (6.5–230 mM). This enables the preservation of the enzyme in its natural form, and the rGO-chitosan matrix densely supplied with hemoglobin particles presents a friendly environment. Additionally, rGO allows the transport of electrons from the matrix to the electroactive center of hemoglobin, and the percolating 3D network of rGOs offers multiplexing pathways for the rapid conductivity of charges. Horseradish peroxidase (HRP) was employed in another H_2O_2 detector to hydrolyze H_2O_2, and the electrodes were upgraded with highly ordered mesoporous carbon (1.61 mM), CNT/silica/Au/Pt hybrid nanomaterial (0.5 mM), and tiny graphene sheets that were noncovalently exfoliated by the electrode (10.3 mM). Additionally, an extensive spectrum of linear responses (1–500 mM) was attained. Platinum nanoparticles may be evenly coated on rGO nanosheets, demonstrating significant solidity; furthermore, a rapid charge transfer is guaranteed via the close connections between the metal nanoparticles and rGO, which are extremely electrical in nature. All these factors contributed to the outstanding performance of this sensor. The same team also fabricated a sensor with an identical layout based on a hybrid gold nanoparticle/rGO. Here, rGO was combined with AuNPs and an enzyme (microperoxidase-11); the AuNPs not only act as catalysts in this arrangement but also cooperate with the rGO layer to facilitate charge transfer. The rGO thin film was decorated with in situ-generated Prussian blue, which is a better electrocatalyst (artificial peroxidase) for H_2O_2 elimination, to achieve the maximum sensitivity (45 nM) in all H_2O_2 sensors [204].

6.2. Heavy metals sensing

Furthermore, the inhibitory effects of graphene for the detection of harmful heavy metal ions including Cd^{2+}, Hg^{2+}, and Pb^{2+} are outlined. Conjugated microporous polymers (CMPs) and polylactic acid (PLA) were included in the light-emitting nanofibrous films via electrospinning, as suggested by Yuan et al. [205]. The cutting-edge chemical sensor demonstrated excellent porosity, outstanding adaptability, and a high surface-to-volume ratio, which improved its capacity for identifying nitro aromatic and oxidizing heavy metal ions. A liquid-gate FET-type and transparent graphene-based hazardous Hg^{2+} sensor was proposed by An et al. [206], which demonstrated significant adaptability and specificity for Hg^{2+} despite the presence of various chemical contaminants. The *I-V* curves of the graphene aptasensor demonstrate the before and after overview of the aptamer; a schematic illustration of a liquid-ion gated FET for the aptamer on top of the graphene with its measurement is shown in Fig. 16(e-g) [206].

6.3. Industrial volatile organic chemical-sensing

Although the identification of electrolytes and metabolites is significant, volatile biomarker gases constitute important data. For example, measuring exhaled NO may indicate asthma, whereas detecting ammonia from gases in the human breath can identify stomach diseases caused by *Helicobacter pylori*. More than 2600 volatile organic compounds (VOCs) from the blood, urine, skin, and breath are reportedly essential auxiliary diagnostic indicators. Therefore, a new method of clinical diagnosis that utilizes the accurate examination of VOCs produced by the human metabolism is being developed. Target gases have a significantly high selectivity and sensitivity; they mix with thousands of other gases, and only a few particles per billion gas particles can be identified, which is the main barrier to the accurate detection of VOCs. Volatile biomarker petrol sensors must also have a high degree of stability, repeatability, and rapid recovery time. Based on the aforementioned specifications, graphene and its derivative are demonstrated to be promising as VOC sensors owing to their high strength-to-weight ratios. Owing to these properties, graphene is highly sensitive to gas particle detection. A novel DMMP gas sensor with outstanding adaptability and visibility is shown in Fig. 16(h-k) [207,208], which was created by drop-coating polypyrrole onto graphene. Large graphene-based biological sensors distinguishing dimethyl methyl phosphonate (DMMP), ethanol, NO_2, SO_2, and tumour indicators are currently available. This gas sensor demonstrated high selectivity and exceptional straining ability (up to 20%) in the presence of acetone, methanol, water, and tetradecane.

7. GFM in biomedical and healthcare fields

7.1. Biocompatibility of graphene

For the advanced integration of graphene with human tissue, especially when inserted into the human body, it is critical to consider the consequences of graphene and its byproducts on the well-being of humans, including their biocompatibility, toxic effects, and potential environmental risks. Graphene-based sensors have gained significant attention for use in health surveillance and bio-applications. Several studies regarding graphene-based nanomaterials (GBNs) have been conducted. However, a comprehensive investigation regarding the consequences on human health and the environment is currently lacking. In-depth safety studies are a crucial component of innovative materials. Notably, “grapheme” refers to a group of GBNs encompassing GO and rGO in experimental articles. Owing to the absence of standardized definitions of GBNs, the number of layers, median lateral size, and carbon-to-oxygen (C/O) ratio are important factors used for categorizing graphene in various production processes. A biosensor is an analytical tool used for detecting biological analytes that combines useful substances or biological components with a biophysical detector. This system can transform biological data into another signal that is easier to quantify. In biological systems, graphene exhibits outstanding biological compatibility, environmental sensitivity, and equilibrium, all of which are crucial for point-of-care and real-time sensing applications (Fig. 17). Chemical sensing is a rapidly expanding discipline that is increasingly reliant on innovative materials. As previously indicated, the intriguing features of graphene enable it to meet the necessary conditions for the development of highly active sensors. Implementing innovative sensory systems that utilize the unique properties of graphene is a key challenge. A single biochemical molecule or biomolecule on or near the surface of graphene may change its electrical and optical characteristics by transferring a charge or energy owing to a local deformation. A potential signal can be easily converted into an event that can be monitored electrically or optically using field-effect transistors (FETs), nanoscale electrodes, or other essential transducers based on graphene. Considering their diversity, more than half of these sensors do not actually use perfect single-layer graphene but utilize the various techniques

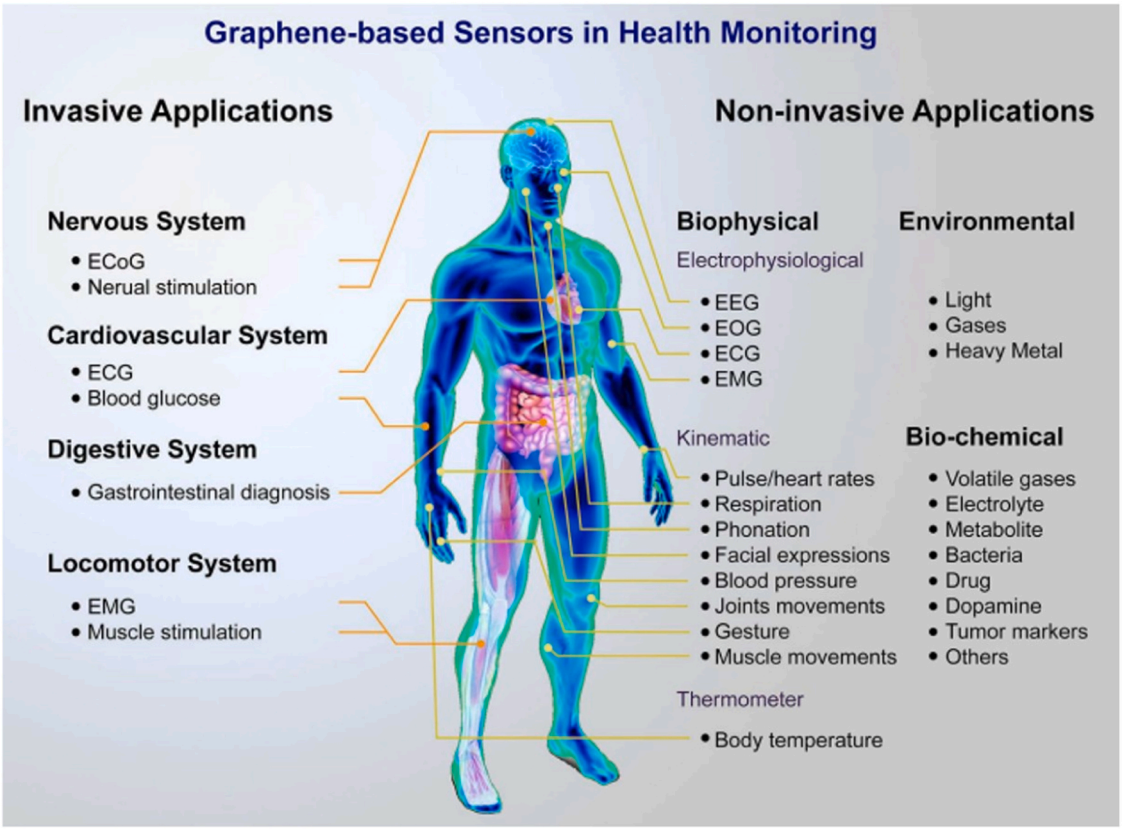


Fig. 17. Schematic of graphene-based sensors [211].

available for creating graphene and their different levels of success. However, the number of residual chemical groups, ripples, shapes, sizes, and layers at the outermost boundaries of graphene significantly affect the sensory functionality of these sensors. The sensitivity limitations of these devices considering the recent intriguing discoveries are concerning; however, the lack of selectivity is apparently a bigger issue. The most current nanomaterial-based sensor applications are briefly outlined in this section [209,210].

7.2. Biological sensing

As the field of biological sensing is rapidly expanding, researchers such as Swamy et al. [212] have proposed the possibility of using graphene nanoribbons derived from multiwalled carbon nanotubes (MWCNTs) to detect the HIV-1 gene using electrocatalytic interactions. Oxidative unzipping was used to unravel the MWCNTs into atomic-layered nanoribbons, which were then deposited over a glassy carbon electrode to fabricate the chip, over which the probe DNA of the HIV gene was immobilized and evaluated for targeted DNA detection using cyclic voltammetry. The setup was able to detect approximately 100 aM of DNA by using this novel chip. Hasler et al. [213] fabricated clickable graphene nanoribbons for electrochemical sensor fabrication to detect Interleukin 6, while also using nanoribbons as an interface linker for rGO-based FET sensors. This resulted in the simultaneous assessment of optical and electronic detection modalities. The concentration of the analyte was in the nanomolar range.

Gholamalizadeh et al. [214] devised a flexible electronic platform for glucose detection using N-doped graphene quantum dots via a screen-printing technique. The sensitivity and LOD were 40.76 mA. $mM^{-1}.cm^{-2}$ and 0.098 mM, respectively. Li et al., [215] hydrothermally synthesized graphene quantum dots for detection of reactive red −2 dye, as well as an array of ions including the following: Al^{3+}, Ni^{2+}, Fe^{2+}, Co^{2+}, Cr^{3+}, $PdCl_4^{2+}$, Au^{3+}, Rh^{3+}, Fe^{3+}, Ca^{2+}, Zr^{4+}, Ru^{3+}, Pt^{4+}, Na^{+}, Cu^{2+}, K^{+} and Zn^{2+}. Photoluminescence spectroscopy was used to detect the aforementioned analytes in the 90–800 μM range.

7.3. Graphene for sensing biomolecules

7.3.1. DNA sensing

Fig. 18(a) presents the use of water-soluble GO as an infrastructure for the accurate and focused identification of DNA, demonstrating a simplified representation of this novel detection equipment. We predicted that GO may bind dye-labeled ssDNA and completely quench the fluorescence of the dye because the significant noncovalent binding of GO with nucleobases and aromatic compounds has been documented (step (a) in Fig. 18a). The connection between the dye-labeled DNA and GO is disrupted when a target is present because the attachment of the dye-labeled DNA to the target molecule changes its conformation. Such exchanges of these interactions enable the release of the dye-labeled DNA from the GO, which returns the dye fluorescence (step (b) in Fig. 18a). Fluorescence-improved sensing, which is sensitive and focuses on the targeted molecule, may be achieved by this approach. This study demonstrated that similar to CNTs, GO can be used as a platform for quick, sensitive, and targeted biomolecule detection; regardless, GO is a more advantageous material than CNTs for creating biosensors than carbon nanotubes owing to its low cost and wide manufacturing scale. Between 1 nm and 1 mm, the fluorescence of this mixture was observed after approximately 30 min, allowing it to hybridize at room temperature. The aptamer GO dyed with fluorescein reacts fluorescently with thrombin. A fluorescein-based dye-labeled aptamer (50 nm) was produced in Tris-HCl buffer (20 mM, pH 7.4, containing 100 mM NaCl, 5 mM KCl, and 5 mM $MgCl_2$) and mixed with GO for 5 min before thrombin was added. The final thrombin concentrations of the samples varied between 5 and 100 nm. This type of combined fluorescence was observed after approximately 30 min of bonding at an ambient temperature.

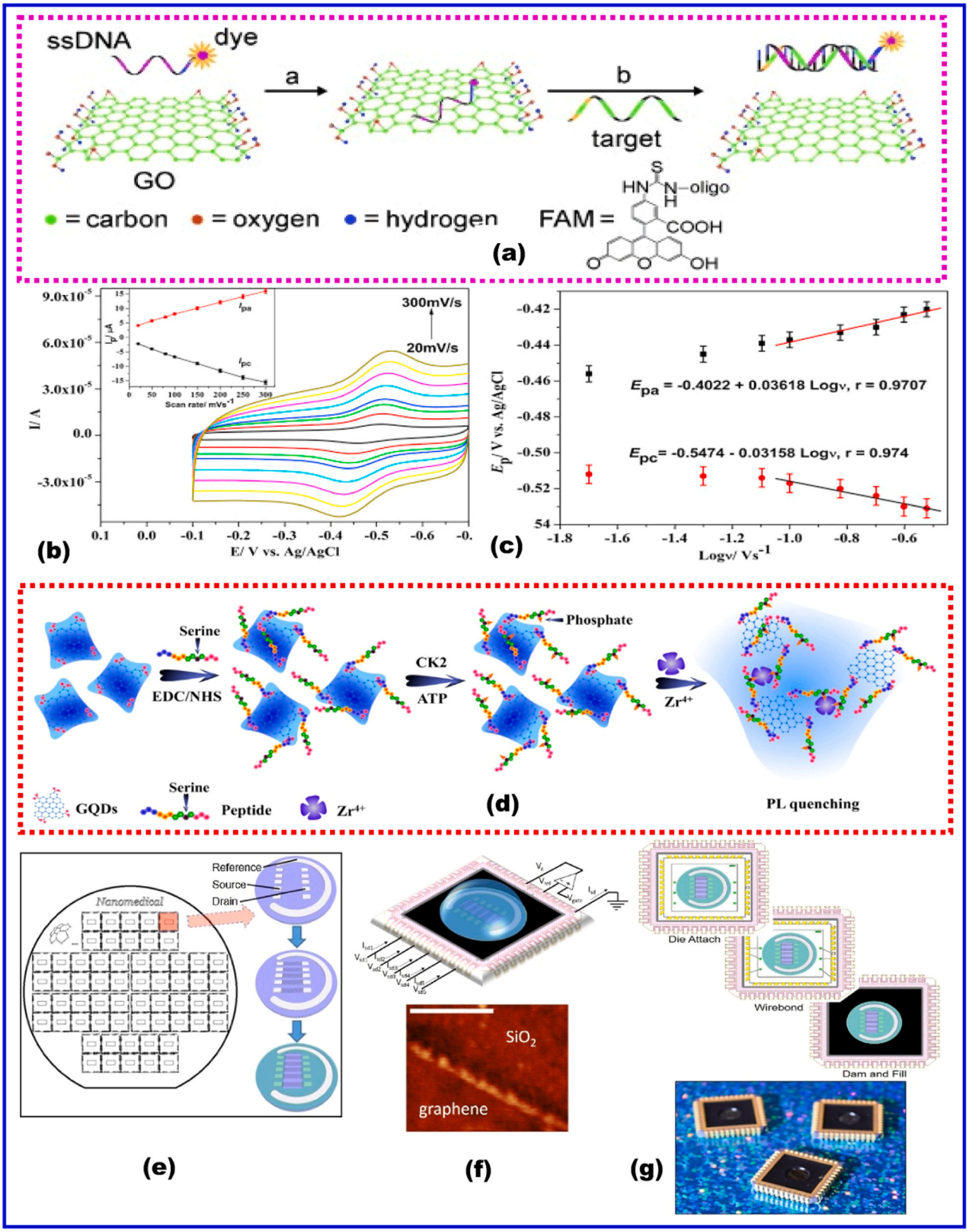


Fig. 18. (a) Schematic of the target-induced fluorescence variation by the ssDNA-FAM-GO complex [216], (b) CV of the GOD-graphene-chitosan electrode at various scan rates: peak current versus scan rates, (c) peak potential (E_p) versus the logarithm of the scan rate (log ν) [218], (d) schematic illustration of phosphorylation peptide-GQDs that are aggregated and quenched by PL via the Zr^{4+} ion connection providing the basis for the CK_2 kinase test [219], (e) wafer-level graphene--transistor fabrication process, Pt/Ti drain, source, and patterned reference electrodes, followed by etching and graphene deposition, (f) graphene liquid gate of the graphene/SiO_2 interface, (g) chip packaging consisting of a dye attached to a 44-pin CQFJ package, followed by Au-ball wire bonding [220].

7.3.2. Glucose sensing

Chemically functionalized graphene can be easily combined with polymers in a solution to produce a unique variety of electrically conducting nanocomposites. The glassy carbon electrode (GCE) surface was used to construct and modify the combined graphene-chitosan nanocomposite before GOD was absorbed onto the nanocomposite film. Electrochemical and scanning electron microscopy techniques were used to characterize the films. The nanocomposite film was able to establish favorable surroundings for GoD to achieve DET. Compared to well-studied carbon nanotubes-based glucose sensors, the GoD-Graphene-Chitosan (GoD-GC) nanocomposite exhibited excellent sensitivity. This provides new opportunities for the development of outstanding electrochemical biosensors [217].

The Cyclic Voltammetry analysis of GoD-G-C on the electrode in the solution with various levels of glucose and oxygen saturation is shown in Fig. 18(b), which demonstrates that the initial level of reduction decreased as the glucose level increased, suggesting an increase in oxygen usage. According to research, the oxygen intake exponentially increases as the level of glucose increases from 0.08 to 12 mM, with an R-value of 0.9993, and a maximum sensitivity of approximately 37.93 A mM^{-1} cm^2 (Fig. 18c). Consequently, this tiny combination of GOD, graphene, and chitosan can be used as a glucose sensor. The fact that glucose concentrations in diabetics are higher than 7.0 mM suggests that this biosensor is practically appropriate for determining the concentration of human blood sugar. This linear range is substantially larger than that of 0.08–0.28 mM for the immobilization of GQD on a granular gold-enhanced carbon paste electrode and that of 0–7.8 mM for GOD on the MWCNT-chitosan framework [6].

7.3.3. Protein sensing

Regarding the selective aggregation of phosphopeptide-graphene quantum dot (GQD) complexes induced by the collaboration of Zr^{4+} ions, a straightforward and accurate emission spectroscopy (photoluminescence) test for the expression of protein kinases was developed, as shown in Fig. 18(d). Additional enzymes can be potentially detected with a more intricate construction of the peptide substrate sequences. Using a detection limit of 0.03 U mL^{-1}, it is possible to develop a linear connection between the reduced PL intensity of peptide GQDs and the concentration of casein kinase II (CK_2) under ideal circumstances. The estimated value for CK2s EC50 (the enzyme concentration at which 50% of the substrate was transformed) was 0.34 U mL^{-1}. The proposed technique was demonstrated to be promising for the study of kinase inhibitors. The reduction of CK_2 phosphorylation activity by four distinct inhibitors including quercetin, emodin, dichlorobenzimidazole-l-d-ribofuranoside (DRB), and ellagic acid was examined in human serum by comparing samples incubated with inhibitors and those without. The following experiments were performed to demonstrate the potential of these GQD-based platforms for the examination of kinase inhibitors in biological environments. As anticipated, the severity of PL improved in the presence of the inhibitors as their effectiveness increased. The IC50 value of Ellagic acid (inhibitor concentration causing 50% inhibition) was calculated to be 0.041 M. This developed procedure provided researchers with a novel and highly effective instrument for studying both enzymes and their opponents [219]. Lerner et al. [220] fabricated high-quality graphene transistors for large-scale production using ceramic chip carriers (Fig. 18e). They fabricated a liquid-gated FET that was able to detect insulin using reproducible biomolecular interaction kinetics. The chip is shown in Fig. 18 (f)–(g).

Researchers have developed a quick and accurate PL test using GQDs to measure the protein kinase activity. Kinase-catalyzed peptide phosphorylation was monitored using an innovative approach based on the particular accumulation of phosphorylated peptide-GQDs triggered by the Zr^{4+} ion coordination. This approach offers a fresh and alluring replacement for the frequently employed FRET quenching mechanisms in fluorescence-based enzyme experiments. This technique, which employs peptide-conjugated GQDs, has several significant benefits compared to other fluorescent kinase techniques, including rapid detection (<5 min) and a simple investigational procedure that avoids complex protein recognition procedures (Fig. 18d). The suggested approach demonstrates the potential for use in the production of kinase-related drugs and kinase inhibitor screening. GO was used to fabricate hybrid paper-based sensors [221]. This study presents using a GO-gold nanoparticle hybrid sensor for the label-free detection of serum bilirubin. SERS sensing was performed by detecting bilirubin signatures controlled by using the GO hybrid nanostructures. An SPR-based graphene-gold biosensor was fabricated [222]. The grating was designed to be single-, double-, and triple-step for an increased sensitivity to detect water, glucose, and blood, which have different refractive indices. Furthermore, a MoS_2-graphene hybrid was designed [223]; thus, a highly sensitive platform is required for single-molecule detection. The platform was designed with pores of different diameters and was assessed to slow the translocation of a single BSA protein molecule via the pores. λ-DNA was also tested without significant variations.

7.3.4. Bio-electrochemical sensors

Owing of the massive pores, analyte transit increases, aiding in the identification of binding partners. Direct detection methods using graphene can detect relevant biological components at lower levels. Owing to its distinct electrochemical and morphological characteristics, graphene was developed as a material of interest for novel electrochemical sensors. The ability to detect compounds with maximum oxidation or reduction prospective, such as nucleic acids, is enabled owing to the broad electrochemical prospective range of graphene (approximately 2.5 V in a 0.1 mM phosphate buffer saline solution). Moreover, the corners and flaws of graphene have a high electron transport rate [208], suggesting that the rGO layers or tiny fragments of pure graphene remain suitable for observation during electrochemical experiments. Owing to the distinctive electronic structure of rGO, particularly the significant solidity of the electronic states across a broad energy range, the electron transfer rate from $Fe^{3+}/^{2+}$ to rGO was approximately one order of magnitude greater than that on a glassy carbon electrode (GCE). In addition, directly connecting an electrode to the active centers of tiny graphene flakes of the redox enzymatic agent may improve electron transport.

rGO is intriguing because it displays inherent catalytic activity with several minor enzymatic products such as H_2O_2 and NADH, which makes it desirable for sensor-based enzymes. Electrodes grounded with graphene offer a sizable operational reaction area and a high capacity for enzymatic packing owing to their extraordinarily high surface-area-to-volume ratio (theoretically 2600 m^2 g^1). Its high strength-to-weight ratio renders it suitable for functional composites, in which a small amount of graphene may provide percolating charge conduction routes. The majority of sensors based on graphene have used rGO for the following reasons: (1) the numerous faults and chemical groups enable the transfer of charge, ensuring good electrochemical action; (2) chemical molecules above the rGO exterior offer suitability and suppleness for numerous functions that improve the performance of the sensor; (3) the electrical and chemical characteristics of rGO remain extremely tunable; and (4) unlike nonconductive GO, rGO effectively conducts electricity.

8. Conclusions

GFM have gained significant interest in modern scientific society owing to the sheer value of their new applications and the improvement of existing technologies such as sensors, coatings, and composite fillers. Their high strength-to-weight ratios, increased surface areas, and unique catalytic behaviors have revolutionized the fields in which they are incorporated. The synthesis of GFM is relatively easy using CVD, exfoliation, and LASER ablation. Although yield properties are difficult to obtain in the same spectrum, the synthesis conditions can be easily optimized. Modification of the GFM surface is also simple using

appropriate chemicals to treat the surface of the GFM to suit the intended applications. The GFM tends to be temperamental when introduced into analytical techniques, with repeatability being a challenging issue for multiple iterations of the same sample. Surface characterization techniques such as SEM, TEM, LASER profilometry, and AFM are traditionally used. This review focuses on the potential applications of GFM in pH sensing, highlighting an important tool in healthcare and environmental applications, where a shift in the pH is crucial for controlling an industrial or bio-process.

The superficial adsorption of macromolecules to GFM via π–π interactions has been sufficiently reported by researchers, demonstrating their important role in ligand binding and targeting by GFM-based sensors. Back-gate, top-gate, and solution-gated sensors based on GFM have provided new perspectives for sensing molecules of interest with higher transconductance and lower power requirements. Gas sensing has always been a priority for heavy industrial activities by corporations that deal with numerous toxic gases that are harmful to the environment; thus, a highly sensitive cascade is needed to assess the leakage of spreading gases as early as possible. GFM-based gas sensors, which have a high sensitivity, must be sufficient to prevent toxic gases or effluents from reaching the environment outside industrial activity or effluent treatment plants. In addition to sensing toxic gases and chemicals, GFM can also be used to treat aqueous and gaseous effluents owing to their excellent filtration properties. Catalysis is another area that this review presents, providing insights into the augmentation of existing catalytic processes as well as processes unique to the GFM. Considering the emerging manipulative strategies such as the monoaxial and biaxial crumpling of GFM, the sensitivity of biosensors is increasing and will only improve over time.

With modern science, an increasing number of characterization techniques will be used to evaluate GFM in different technological fields. The defect-free, atomic-layered architecture of GFM-based sensors indicates that the sensitivity achieved will be at an unforeseen level, reaching zeptomolar (~zM) concentrations with the possibility of having arrays of sensors integrated into a small setup. GFM-based sensors have also enabled achieving multimodal sensing in a single platform owing to their unique optical, electrical, and electrochemical properties. This implies that a fabricated chip can be assessed using multiple instruments that can be operated using the layman approach. Although a GFM can be highly advantageous in terms of sensing and multimodality, the fragile nature of graphene renders it a highly sensitive component in the sensor platform, which can be easily damaged if mishandled in storage or during an erroneous production step. However, as demonstrated by large-scale manufacturing, these difficulties will always be optimized with sufficient input from researchers, making GFM-based sensors a potent asset in the field of precision sensing.

CRediT authorship contribution statement

Ramaswamy Sandeep Perala: Writing – review & editing, Writing – original draft, Investigation, Conceptualization. **Narendhar Chandrasekar**: Writing – review & editing, Writing – original draft, Methodology, Data curation. **Ramachandran Balaji**: Writing – original draft, Validation. **Pinky Steffi Alexander:** Writing – original draft, Data curation. **Nik Zulkarnine Nik Humaidi**: Software. **Michael Taeyoung Hwang**: Supervision, Resources, Project administration.

Declaration of Competing Interest

The authors declare that they have no known competing financial interests or personal relationships that could have appeared to influence the work reported in this paper.

Data availability

Data will be made available on request.

Acknowledgements

No Acknowledgements.

References

[1] M.T. Hwang, M. Heiranian, Y. Kim, S. You, J. Leem, A. Taqieddin, V. Faramarzi, Y. Jing, I. Park, A.M.V. Zande, S. Nam, N.R. Aluru, R. Bashir, Ultrasensitive detection of nucleic acids using deformed graphene channel field effect biosensors, Nat. Commun. 11 (2020) 1543.
[2] A. Ganguli, V. Faramarzi, A. Mostafa, M.T. Hwang, S. You, R. Bashir, High sensitivity graphene field effect transistor-based detection of DNA amplification, Adv. Funct. Mater. 30 (2020) 2001031.
[3] P. Snapp, M. Heiranian, M.T. Hwang, R. Bashir, N.R. Aluru, S. Nam, Current understanding and emerging applications of 3D crumpling mediated 2D material-liquid interactions, Curr. Opin. Solid State Mater. Sci. 24 (3) (2020) 100836.
[4] J. Luo, H.D. Jang, T. Sun, L. Xiao, Z. He, A.P. Katsoulidis, M.G. Kanatzidis, J. M. Gibson, J. Huang, Compression and aggregation-resistant particles of crumpled soft sheets, ACS Nano 5 (11) (2011) 8943–8949.
[5] S. Deng, V. Berry, Wrinkled, rippled and crumpled graphene: an overview of formation mechanism, electronic properties, and applications, Mater. Today 19 (4) (2016) 197–212.
[6] J.S. Bunch, A.M.V. Zande, S.S. Verbridge, I.W. Frank, D.M. Tanenbaum, J. M. Parpia, H.G. Craighead, P.L. Mceuen, Electromechanical Resonators from Graphene Sheets, Science 315 (5811) (2007) 490–493.
[7] X. Dong, Y. Shi, W. Huang, P. Chen, L.J. Li, Electrical detection of DNA hybridization with single-Base specificity using transistors based on CVD-Grown Graphene sheets, Adv. Mater. 22 (14) (2010) 1649–1653.
[8] F.P.D. Disouza, R. Sundaresan, S.M. Chen, B. Ramachandran, N. Chandrasekar, Electrochemical monitoring of sulfadiazine via La@CeO incorporated with reduced graphene oxide, Analytica 4 (3) (2023) 300.
[9] N. Chandrasekar, R. Balaji, R.S. Perala, N.Z.N. Humaidi, K. Shanmugam, Y. C. Liao, M.T. Hwang, S. Govindaraju, A brief review of graphene-based biosensors developed for rapid detection of COVID-19 biomarkers, Biosensors 13 (3) (2023) 307.
[10] S. Maheshwaran, R. Balaji, S.M. Chen, E. Tamilalagan, N. Chandrasekar, S. Ethiraj, M.S. Samuel, Construction of graphene oxide wrapped gadolinium vanadate nanocomposites as an efficient electrocatalyst for the amperometric sensing of sulfadiazine, Process Saf. Environ. Prot. 168 (2022) 77–87.
[11] A.P. Steffi, R. Balaji, N. Chandrasekar, N. Prakash, T.P. Rajesh, S. Ethiraj, M. S. Samuel, S. Vuppala, High-performance anti-corrosive coatings based on rGO-SiO2-TiO2 ternary heterojunction nanocomposites for superior protection for mild steel specimens, Diam. Relat. Mater. 125 (2022) 108968.
[12] A.P. Steffi, R. Balaji, N. Prakash, T.P. Rajesh, S. Ethiraj, M.S. Samuel, A.K. Nadda, N. Chandrasekar, Incorporation of SiO_2 functionalized gC_3N_4 sheets with TiO_2 nanoparticles to enhance the anticorrosion performance of metal specimens in aggressive Cl^- environment, Chemosphere 290 (2022) 133332.
[13] G. Kucinskis, G. Bajars, J. Kleperis, Graphene in lithium ion battery cathode materials: A review, J. Power Sources 240 (2013) 66–79.
[14] S.H. Bae, Y. Lee, B.K. Sharma, H.J. Lee, J.H. Kim, J.H. Ahn, Graphene-based transparent strain sensor, Carbon 51 (2013) 236–242.
[15] Y. Ye, H. Chen, Y. Zou, Y. Ye, H. Zhao, Corrosion protective mechanism of smart graphene-based self-healing coating on carbon steel, Corros. Sci. 174 (2020) 108825.
[16] X. Duan, S. Indrawirawan, H. Sun, S. Wang, Effects of nitrogen-, boron-, and phosphorus-doping or codoping on metal-free graphene catalysis, Catal. Today 249 (2015) 184.
[17] M. Nihar, V. Berry, Graphene-based single-bacterium resolution biodevice and DNA transistor: interfacing graphene derivatives with nanoscale and microscale biocomponents, Nano Lett. 8 (12) (2008) 4469–4476.
[18] S.H. Ku, C.B. Park, Myoblast differentiation on graphene oxide, Biomaterials 34 (8) (2013) 2017–2023.
[19] W.C. Lee, C.H. Lim, H. Shi, L.A. Tang, Y. Wang, C.T. Lim, K.P. Loh, Origin of enhanced stem cell growth and differentiation on graphene and graphene oxide, ACS Nano 5 (9) (2011) 7334–7341.
[20] X. Zheng, H. Lee, T.H. Weisgraber, M. Shusteff, J. Deotte, E.B. Duoss, J.D. Kuntz, M.M. Biener, Q. Ge, J.A. Jackson, S.O. Kucheyev, N.X. Fang, C.M. Spadaccini, Ultralight, ultrastiff mechanical metamaterials, Science 344 (6190) (2014) 1373–1377.
[21] L.J. Gibson, M.F. Ashby. Cellular Solids: Structure and Properties, second ed., Cambridge Univ. Press, 1999.
[22] R.G. Bai, N. Ninan, K. Muthoosamy, S. Manickam, Graphene: a versatile platform for nanotheranostics and tissue engineering, Prog. Mater. Sci. 91 (2018) 24–69.
[23] K. Zhang, H. Zheng, S. Liang, C. Gao, Aligned PLLA nanofibrous scaffolds coated with graphene oxide for promoting neural cell growth, Acta Biomater. 37 (2016) 131–142.
[24] D. Depan, T. Pesacreta, R. Misra, The synergistic effect of a hybrid graphene oxide–chitosan system and biomimetic mineralization on osteoblast functions, Biomater. Sci. 2 (2014) 264–274.
[25] H. Zhong, Z. Wu, X. Li, W. Xu, S. Xu, S. Zhang, Z. Xu, H. Chen, S. Lin, Graphene based two-dimensional hybrid nanogenerator for concurrently harvesting energy from sunlight and water flow, Carbon 105 (2016) 199–204.
[26] S. Xia, M. Wang, G. Gao, Preparation and application of graphene-based wearable sensors, Nano Res. 15 (2022) 9850–9865.

[27] R. Goyat, Y. Saharan, J. Singh, A. Umar, S. Akbar, 2022, , Molecules 276433.
[28] S. Viswanathan, T.N. Narayanan, K. Aran, K.D. Fink, J. Paredes, P.M. Ajayan, S. Filipek, P. Miszta, H.C. Tekin, F. Inci, U. Demirci, P. Li, K.I. Bolotin, D. Liepmann, V. Rneugopalakrishanan, Mater. Today 18 (9) (2015) 513–522.
[29] K.S. Novoselov, V.I. Falko, L. Colombo, P.R. Gellert, M.G. Schwab, K. Kim, A roadmap for graphene, Nature 490 (2012) 192–200.
[30] B.L. Dasari, J.M. Nouri, D. Brabazon, S. Naher, Graphene and derivatives-synthesis techniques, properties and their energy applications, Energy 140 (2017) 766–778.
[31] K. Parvez, R. Li, S.R. Puniredd, Y. Hernandez, F. Hinkel, S. Wang, X. Feng, K. Mullen, Electrochemically exfoliated graphene as solution-processable, highly conductive electrodes for organic electronics, ACS Nano 7 (2013) 3598–3606.
[32] J. Liu, H. Yang, S.G. Zhen, C.K. Poh, A. Chaurasia, J. Luo, X. Wu, E.K.L. Yeow, N. G. Sahoo, J. Lin, Z. Shen, A green approach to the synthesis of high-quality graphene oxide flakes via electrochemical exfoliation of pencil core, RSC Adv. 3 (2013) 11745–11750.
[33] A.A. Green, M.C. Hersam, Solution phase production of graphene with controlled thickness via density differentiation, Nano Lett. 9 (2009) 4031–4036.
[34] E. Cappelli, S. Orlando, M. Servidori, C. Scilletta, Nano-graphene structures deposited by N-IR pulsed laser ablation of graphite on Si, Appl. Surf. Sci. 254 (2007) 1273–1278.
[35] A.T.T. Koh, Y.M. Foong, D.H.C. Chua, Comparison of the mechanism of low defect few-layer graphene fabricated on different metals by pulsed laser deposition, Diam. Relat. Mater. 25 (2012) 98–102.
[36] S. Horiuchi, T. Gotou, M. Fujiwara, T. Asaka, T. Yokosawa, Y. Matsui, Single graphene sheet detected in a carbon nanofilm, Appl. Phys. Lett. 84 (2004) 2403–2405.
[37] M. Choucair, P. Thordarson, J.A. Stride, Gram-scale production of graphene based on solvothermal synthesis and sonication, Nat. Nanotechnol. 4 (2009) 30–33.
[38] K. Krishnamoorthy, M. Veerapandian, G.S. Kim, S.J. Kim, A one step hydrothermal approach for the improved synthesis of graphene nanosheets, Curr. Nanosci. 8 (2012) 934–938.
[39] F.S. Al-Hazmi, G.H. Al-Harbi, G.W. Beall, A.A. Al-Ghamdi, A.Y. Obaid, W. E. Mahmoud, One pot synthesis of graphene based on microwave assisted solvothermal technique, Synth. Met. 200 (2015) 54–57.
[40] B. Gurunlu, C.T. Yucedag, M. Bayramoglu, One pot synthesis of graphene through microwave assisted liquid exfoliation of graphite in different solvents, Molecules 27 (2022) 5027.
[41] A. Amiri, M. Naraghi, G. Ahmadi, M. Soleymaiha, M. Shanbedi, A review on liquid-phase exfoliation for scalable production of pure graphene, wrinkled, crumpled and functionalized graphene and challenges, FlatChem 8 (2018) 40–71.
[42] M. Lopes, A. Candini, M. Urdampilleta, A.R. Plantey, V. Bellini, S. Klyatskaya, L. Marty, M. Ruben, M. Affronte, W. Wernsdorfer, N. Bendiab, Surface enhanced raman signal for terbium single molecule magnets grafted on graphene, ACS Nano 4 (2010) 7531–7537.
[43] M.P. Lavin-Lopez, J.L. Valverde, S.O. Lozoya, A.P. Carrero, A. Romero, Role of inert gas in the Cvd-graphene synthesis over polycrystalline nickel foils, Mater. Chem. Phys. 222 (2019) 173–180.
[44] W. Liu, H. Li, C. Xu, Y. Khatami, K. Banerjee, Synthesis of high-quality monolayer and bilayer graphene on copper using chemical vapor deposition, Carbon 49 (13) (2011) 4122–4130.
[45] X. Wu, Y. Liu, H. Yang, Z. Shi, Large-scale synthesis of high-quality graphene sheets by an improved alternating current arc-discharge method, RSC Adv. 6 (2016) 93119–93124.
[46] S. Kim, Y. Song, J. Wright, M.J. Heller, Graphene bi- and trilayers produced by a novel aqueous arc discharge process, Carbon 102 (2016) 339–345.
[47] G.W. Cheng, K. Chu, J.S. Chen, J.T.H. Tsai, Fabrication of graphene from graphite by a thermal assisted vacuum arc discharge system, Superlattices Micro 104 (2017) 258–265.
[48] H. Tan, D. Wang, Y. Guo, A strategy of synthesize multilayer graphene in arc-discharge plasma in a semi-opened environment, Materials 12 (14) (2019) 2279.
[49] A. Malesevic, R. Vitchev, K. Schouteden, A. Volodin, L. Zhang, G.V. Tendeloo, A. Vanhulsel, C.V. Haesendonck, Sythesis of few-layer graphene via microwave plasma-enhanced chemical vapor deposition, Nanotechnology 19 (2008) 305604.
[50] J. Wang, M. Zhu, R.A. Outlaw, X. Zhao, D.M. Manos, B.C. Holloway, Synthesis of carbon nanosheets by inductively coupled radio-fruequency plasma enhanced chemical vapor deposition, Carbon 42 (2004) 2867–2872.
[51] V.A. Krivchenko, V.V. Dvorkin, N.N. Dzbanovsky, M.A. Timofeyev, A.S. Stepanov, A.T. Rakhimov, N.V. Suetin, O.Y. Vilkov, L.V. Yashina, Evolution of carbon film structure during its catalyst-free growth in the plasma of direct current glow discharge, Carbon 50 (2012) 1477–1487.
[52] S.N. Yannopoulos, A. Siokou, N.K. Nasikas, V. Dracopoulos, F. Ravani, G. N. Papatheodorou, CO_2-Laser-Induced growth of epitaxial graphene on 6H-SiC (0001), Adv. Funct. Mater. 22 (2012) 113–120.
[53] Z. Guo, S. Chakraborty, F.A. Monikh, D.D. Varsou, A.J. Chetwynd, A. Afantitis, I. Lynch, Peng, Zhang, Surface functionalization of graphene-based materials: Biological behavior, toxicology, and safe-by-design aspects, Adv. Bio. 5 (9) (2021) 2100637.
[54] V. Georgakilas, M. Otyepka, A.B. Bourlinos, V. Chandra, N. Kim, K.C. Kemp, P. Hobza, R. Zboril, K.S. Kim, Functionalization of graphene: covalent and non-covalent approaches, derivatives and applications, Chem. Rev. 112 (2012) 6156–6214.
[55] S. Pattnaik, K. Swain, Z. Lin, Graphene and graphene-based nanocomposites: biomedical applications and biosafety, J. Mater. Chem. B 4 (2016) 7813–7831.
[56] G. Reina, J.M.G. Dominguez, A. Criado, E. Vazquez, A. Bianco, M. Prato, Promises, facts and challenges for graphene in biomedical applications, Chem. Soc. Rev. 46 (2017) 4400–4416.
[57] J. Park, M. Yan, Covalent functionalization of graphene with reactive intermediates, Acc. Chem. Res. 46 (2013) 181–189.
[58] J. Park, X. Yang, D. Wickramasinghe, M. Sundhoro, N. Orbey, K.F. Chow, M. Yan, Functionalization of pristine graphene for the synthesis of covalent graphene-polyaniline nanocomposite, RSC Adv. 10 (2020) 26486–26493.
[59] Z. Jin, T.P. McNicholas, C.J. Shih, Q.H. Wang, G.L.C. Paulus, A.J. Hilmer, S. Shimizu, M.S. Strano, Click chemistry on solution-dispersed graphene and monolayer CVD graphen, Chem. Mater. 23 (2011) 3362–3370.
[60] Y. Xiong, Y. Xie, F. Zhang, E. Ou, Z. Jiang, L. Ke, D. Hu, W. Xu, Reduced graphene oxide/hydroxylated styrene-butadiene-styrene tri-block copolymer electroconductive nanocomposites: preparation and properties, Mater. Sci. Eng., B 177 (2012) 1163–1169.
[61] H.K. Choi, Y. Oh, H. Jung, H. Hong, B.C. Ku, Nam H. You, Y.K. Kim, E.S. Shin, J. Yu, Influences of carboxyl functionalization of intercalators on exfoliation of graphite oxide: a molecular dynamics simulation, Phys. Chem. Chem. Phys. 20 (2018) 28616–28622.
[62] W. Yu, L. Sisi, Y. Haiyan, L. Jie, Progress in the functional modification of graphene/graphene oxide: a review, RSC Adv. 10 (2020) 15328–15345.
[63] A. Bonanni, C.K. Chua, M. Pumera, Rational design of carboxyl groups perpendicularly attachted to a graphene sheet: a platform for enhanced biosensing applications, Chem. Eur. J. 20 (2014) 217–222.
[64] A. Lopez, J. Liu, Covalent and Noncovalent functionalization of graphene oxide with DNA for smart sensing, Adv. Intell. Sys. 2 (2020) 2000123.
[65] J. Huang, C. Zong, H. Shen, M. Liu, B. Chen, B. Ren, Z. Zhang, Mechanism of cellular uptake of graphene oxide studied by surface-enhanced raman spectroscopy, Small 8 (2012) 2577–2584.
[66] A. Bonanni, A. Ambrosi, M. Pumera, Nucleic acid functionalized graphene for biosensing, Chem. Eur. J. 18 (2011) 1668–1673.
[67] A. Sharma, J. Bhardwaj, J. Jang, Label-free, highly sensitive electrochemical aptasensors using polymer-modified reduced graphene oxide for cardiac biomarker detection, ACS Omega 5 (2020) 3924–3931.
[68] B. Shin, W.K. Kim, S. Yoon, J. Lee, Duplex DNA-functionalized graphene oxide: a versatile platform for miRNA sensing, Sens. Actuators B: Chem. 305 (2020) 127471.
[69] J. Son, N. Buzov, S. Chen, D. Sung, H. Ryu, J. Kwon, S. Kim, S. Namiki, J. Xu, S. Hong, K. Watanabe, T. Taniguchi, W.P. King, G.H. Lee, A.M.V. Zande, Tailoring surface properties via functionalized hydrofluorinated graphene compounds, Adv. Mat. 31 (39) (2019) 1903424.
[70] J.A. Mann, W.R. Dichtel, Noncovalent functionalization of graphene by molecular and polymeric adsorbants, J. Phys. Chem. Lett. 4 (2013) 2649–2657.
[71] S. Sun, Y. Cao, J. Feng, P. Wu, Click chemistry as a route for the immobilization of well-defined polystyrene onto graphene sheets, J. Mater. Chem. 20 (2010) 5605–5607.
[72] D. Parviz, S. Das, H.S.T. Ahmed, F. Irin, S. Bhattacharia, M.J. Green, Dispersion of Non-covalently functionalized graphene with minimal stabilizer, ACS Nano 6 (2012) 8857–8867.
[73] J. Cho, I. Jeon, S.Y. Kim, S. Lim, J.Y. Jho, Improving dispersion and barrier properties of polyketone/graphene nanoplatelet composites via noncovalent functionalization using aminopyrene, ACS Appl. Mater. Interfaces 9 (2017) 27984–27994.
[74] L. Xin, F. Yang, S. Rasouli, Y. Qiu, Z.F. Li, A. Uzunoglu, C.J. Sun, Y. Liu, P. Ferreira, W. Li, Y. Ren, L.A. Stanciu, J. Xie, Understanding Pt nanoparticle anchoring on graphene supports through surface functionalization, ACS Catal. 6 (2016) 2642–2653.
[75] Z. Liu, S. Chen, B. Liu, J. Wu, Y. Zhou, L. He, J. Ding, J. Liu, Intracellular detection of ATP using an aptamer beacon covalently linked to graphene oxide resisting nonspecific probe displacement, Anal. Chem. 86 (2014) 12229.
[76] Z. Xu, S. Wang, Y. Li, M. Wang, P. Shi, X. Huang, Covalent functionalization of graphene oxide with biocompatible poly(ethylene glycol) for delivery of paclitaxel, ACS Appl. Mater. Interfaces 6 (2014) 17268–17276.
[77] X. Yang, L. Ma, S. Wang, Y. Li, Y. Tu, X. Zhu, Clicking graphite oxide sheets with well-defined polystyrenes: a new strategy to control the layer thickness, Polymer 52 (2011) 3046–3052.
[78] A. Bonanni, C.K. Chua, M. Pumera, Rational design of carboxyl groups perpendicularly attached to a graphene sheet: a platform for enhanced biosensing applications, Chem. Eur. J. 20 (20) (2013) 217–222.
[79] P. Das, S.V. Mudigunda, G. Darabdhara, P.K. Boruah, S. Ghar, A.K. Rengan, M. R. Das, Biocompatible functionalized AuPd bimetallic nanoparticles decorated on reduced graphene oxide sheets for photothermal therapy of targeted cancer cells, J. Photochem. Photobiol. B 212 (2020) 112028.
[80] G. Chauhan, V. Chopra, A. Tyagi, G. Rath, R.K. Sharma, A.K. Goyal, Gold nanoparticles composite-folic acid conjugated graphene oxide nanohybrids for targeted chemotherapy cancer ablation: in vitro screening and in vivo studies, Eur. J. Pharm. Sci. 96 (2017) 351–361.
[81] S. Qu, M. Li, L. Xie, X. Huang, J. Yang, N. Wang, S. Yang, Noncovalent functionalization of graphene attaching [6,6]-Phenyl-C61-butyric acid methyl ester (PCBM) and application as electron extraction layer of polymer solar cells, ACS Nano 7 (2013) 4070–4081.
[82] M. Moschetta, J.Y. Lee, J. Rodrigues, A. Podesta, O. Varvicchio, J. Son, Y. Lee, K. Kim, G.H. Lee, F. Benfenati, M. Bramini, A. Capasso, Hydrogenated graphene improves neuronal network maturation and excitatory transmission, Adv. Biol. 5 (2021) 2000177.

[83] S. Omidi, A. Kakanejadifard, F. Azarbani, Noncovalent functionalization of graphene oxide and reduced graphene oxide with Schiff bases as antibacterial agents, J. Mol. Liq. 242 (2017) 812–821.
[84] Q. Su, S. Pang, V. Alijani, C. Li, X. Feng, K. Müllen, Composites of graphene with large aromatic molecules, Adv. Mater. 21 (2009) 3191–3195.
[85] P.G. Ren, H. Wang, H.D. Huang, D.X. Yan, Z.M. Li, Characterization and performance of dodecyl amine functionalization graphene oxide and dodecyl amine functionalized graphene/high-density polyethylene nanocomposites: a comparative study, J. Appl. Polym. Sci. 131 (2014) 39803.
[86] R.K. Layek, S. Samanta, A.K. Nandi, The physical properties of sulfonated graphene/poly(vinyl alcohol) composites, Carbon 50 (2012) 815–827.
[87] Y. Luo, D. Kong, Y. Jia, J. Luo, Y. Lu, D. Zhang, K. Qiu, C.M. Li, T. Yu, Self-Assembled graphene@PANI nanoworm composites with enhanced supercapacitor performance, RSC Adv. 3 (2013) 5851–5859.
[88] S. Liu, J. Tian, L. Wang, Y. Luo, W. Lu, X. Sun, Self-assembled graphene platelet-glucose oxidase nanostructures for glucose, Biosens. Bioelectron. 26 (2011) 4491–4496.
[89] D. Zhang, K. Wang, J. Tong, B. Xia, Characterization of layer-by-layer nano self-assembled carbon nanotube/polymer film sensor for ethanol gas sensing properties, et al. Microsyst. Technol. 20 (2014) 379–385.
[90] V. Georgakilas, J.N. Tiwari, K.C. Kemp, J.A. Perman, A.B. Bourlinos, K.S. Kim, R. Zboril, Noncovalent functionalization of graphene and graphene oxide for energy materials, biosensing, catalytic, and biomedical applications, Chem. Rev. 116 (2016) 5464–5519.
[91] M. Marcia, A. Hirsch, F. Hauke, Perylene-based non-covalent functionalization of 2D materials, Flatchem 1 (2017) 89–103.
[92] Y. Jung, H.G. Moon, C. Lim, K. Choi, H.S. Song, S. Bae, S.M. Kim, M. Seo, T. Lee, S. Lee, H.H. Park, S.C. Jun, C.Y. Kang, C. Kim, Humidity-tolerant single-stranded DNA-Functionalized graphene probe for medical applications of exhaled breath analysis, Adv. Funct. Mater. 27 (2017) 1700068.
[93] H.W. Tien, Y.L. Huang, S.Y. Yang, J.Y. Wang, C.C.M. Ma, The production of graphene nanosheets decorated with silver nanoparticles for use in transparent conductive films, Carbon 49 (2011) 1550–1560.
[94] J. Lin, Z. Peng, C. Xiang, G. Ruan, Z. Yan, D. Natelson, J.M. Tour, Graphene nanoribbon and nanostructured SnO_2 composite anodes for lithium ion batteries, ACS Nano 7 (2013) 6001–6006.
[95] W. Gao, L.B. Alemany, L. Ci, P.M. Ajayan, New insights into the structure and reduction of graphite oxide, Nat. Chem. 1 (2009) 403–408.
[96] P.T. Yin, S. Shah, M. Chhowalla, K.B. Lee, Design, synthesis and characterization of graphene nanoparticle hybrid materials for bioapplications, Chem. Rev. 115 (2015) 2483–2531.
[97] J. Luo, N. Zhang, R. Liu, X. Liu, *In Situ* green synthesis of Au nanoparticles onto polydopamine-functionalized graphene for catalytic reduction of nitrophenol, RSC Adv. 4 (2014) 64816–64824.
[98] S. Bai, X. Shen, Graphene-inorganic nanocomposites, RSC Adv. 2 (2012) 64–98.
[99] Z.Q. Wang, N.J. Zhou, J. Guo, X.Y. Wang, Fluid selection and parametric optimization of organic Rankine cycle using low temperature waste heat, Energy 40 (2012) 107–115.
[100] B. Wang, D. Yang, J.Z. Zhang, C. Xi, J. Hu, Stimuli-response polymer covalent functionalization of graphene oxide by Ce(IV)-induced redox polymerization, J. Phys. Chem. C. 115 (2011) 24636–24641.
[101] P. Rani, R. Dalal, S. Srivastave, K. Tankeshwar, Tuning the properties of graphene quantum dots by passivation, Phys. Chem. Chem. Phys. 24 (2022) 26232–26240.
[102] M. Gebert, S. Bhattacharyya, C.C. Bounds, N. Syed, T. Daeneke, M.S. Fuhrer, Passivating graphene and suppressing interfacial phonon scattering with mechanically transferred large-area Ga_2O_3, Nano Lett. 23 (2023) 363.
[103] M. Khan, M.N. Tahir, S.F. Adil, H.U. Khan, M.R.H. Siddiqui, A.A. Al-warthan, W. Tremel, Graphene based metal and metal oxide nanocomposites: synthesis, properties and their applications, J. Mater. Chem. A 3 (2015) 18753–18808.
[104] D.C. Elias, R.R. Nair, T.M.G. Mohiuddin, S.V. Morozov, P. Blake, M.P. Halsall, A. C. Ferrari, D.W. Boukhvalov, M.I. Katsnelson, A.K. Geim, K.S. Novoselov, Control of graphene's properties by reversible hydrogenation: evidence for graphene, Science 323 (2009) 610–613.
[105] J.D. Jones, W.D. Hoffmann, A.V. Jesseph, C.J. Morris, G.F. Verbeck, J.M. Perez, On the mechanism for plasma hydrogenation of graphene, Appl. Phys. Lett. 97 (2010) 233104.
[106] M. Wojtaszek, N. Tombros, A. Caretta, P.H.M. van Loosdrecht, B.J. van Wees, A road to hydrogenating graphene by a reactive ion etching plasma, J. Appl. Phys. 110 (2011) 063715.
[107] A. Felten, D. McManus, C. Rice, L. Nittler, J.J. Pireaux, C. Casiraghi, Insight into hydrogenation of graphene: effect of hydrogen plasma chemistry, Appl. Phys. Lett. 105 (2014) 183104.
[108] R.A. Schafer, J.M. Englert, P. Wehrfritz, W. Bauer, F. Hauke, T. Seyller, A. Hirsch, On the way to graphene-pronounced fluorescence of polyhydrogenated graphene, Angew. Chem., Int. Ed. 52 (2013) 754–757.
[109] M.G. Betti, E. Placidi, C. Izzo, E. Blundo, A. Polimeni, M. Sbroscia, J. Avila, P. Dudin, K. Hu, Y. Ito, D. Prezzi, M. Bonacci, E. Molinari, C. Mariani, Gap Opening in double-sided highly hydrogenated free-standing graphene, Nano Lett. 22 (2022) 2971–2977.
[110] L.M. Malard, M.A. Pimenta, G. Dresselhaus, M.S. Dresselhaus, Raman spectroscopy in graphene, Phys. Rep. 473 (2009) 51–87.
[111] R. Balaji, R. Vengudusamy, S.M. Chen, T.W. Chen, X. Liu, M.R. Khan, Z. A. Alothman, M.A. Ali, S.M. Wabaidur, High-performance SERS detection of pesticides using BiOCl-BiOBr@Pt/Au hybrid nanostructures on styrofoams as 3D functional substrate, Microchim. Acta 187 (2020) 1–11.
[112] E.S. Kumar, T. Makaryan, A. Melikyan, H. Minassian, Y. Gogotsi, M. Yoshimura, One-step solution processing of Ag, Au and Pd@MXene hybrids for SERS, Sci. Rep. 6 (2016) 32049.
[113] N. Valley, N. Greeneltch, R.P.V. Duyne, G.C. Schatz, A look at the origin and magnitude of the chemical contribution to the enhancement mechanism of surface-enhanced raman spectroscopy (SERS): theory and experiment, J. Phys. Chem. 4 (2013) 2599–2604.
[114] R. Balaji, V. Renganathan, S.M. Chen, V. Singh, Ingenious design and development of recyclable 2D BiOCl nanotiles attached tri-functional robust strips for high performance selective electrochemical sensing, SERS and heterogenous dip catalysis, Chem. Eng. J. 385 (2020) 123974.
[115] R. Balaji, S. Maheshwaran, S.M. Chen, N. Chandrasekar, S. Ethiraj, M.S. Samuel, V. Renganathan, High-performance catalytic strips assembled with BiOBr nano-rose architectures for electrochemical and SERS detection of theophylline, Chem. Eng. J. 425 (2021) 130616.
[116] W. Xu, N. Mao, J. Zhang, Graphene: a platform for surface-enhanced raman spectroscopy, Small 9 (2013) 1206–1224.
[117] S. Sun, Z. Zhang, P. Wu, Exploring graphene nanocolloids as potential substrates for the enhancement of raman scattering, ACS Appl. Mater. Interfaces 5 (2013) 5085–5090.
[118] P.V. Shanta, Q. Cheng, Graphene oxide nanoprisms for sensitive detection of environmentally important aromatic compounds with SERS, ACS Sens 2 (2017) 817–827.
[119] Y. Jiang, J. Wang, L. Malfatti, D. Carboni, N. Senes, P. Innocenzi, Highly durable graphene-mediated surface enhanced raman scattering (G-SERS) nanocomposites for molecular detection, Appl. Surf. Sci. 450 (2018) 451–460.
[120] Y. Ma, Y. Wang, Y. Luo, H. Duan, D. Li, H. Xu, E.K. Fodjo, Rapid and sensitive on-site detection of pesticide residues in fruits and vegetables using screen-printed paper-based SERS swabs, Anal. Methods 10 (2018) 4655–4664.
[121] L. Zhao, C. Deng, S. Xue, H. Liu, L. Hao, M. Zhu, Multifunctional g-C_3N_4/Ag NPs intercalated GO composite membrane for SERS detection and photocatalytic degradation of paraoxon-ethyl, Chem. Eng. J. 402 (2020) 126223.
[122] C. Zhu, Q. Zhao, X. Wang, Z. Li, X. Hu, Ag-Nanocubes/Graphene-Oxide/Au-nanoparticles composite film with highly dense plasmonic hotspots for surface-enhanced raman scattering detection of pesticide, Microchem. J. 165 (2021) 106090.
[123] X. Wang, C. Zhu, X. Hu, Q. Xu, H. Zhao, G. Meng, Y. Lei, Highly sensitive surface-enhanced raman scattering detection of organic pesticides based on Ag-nanoplate decorated graphene-sheets, Appl. Surf. Sci. 486 (2019) 405–410.
[124] T.H. Nguyen, Z. Zhang, A. Mustapha, H. Li, M. Lin, Use of graphene and gold nanorods as substrates for the detection of pesticides by surface enhanced raman spectroscopy, J. Agric. Food Chem. 62 (2014) 10445–10451.
[125] L. Zhang, C. Jiang, Z. Zhang, Graphene oxide embedded sandwich nanostructures for enhanced raman readout and their applications in pesticide monitoring, Nanoscale 5 (2013) 3773–3779.
[126] L. Ouyang, L. Yao, T. Zhou, L. Zhu, Accurate SERS detection of malachite green in aquatic products on basis of graphene wrapped flexible sensor, Anal. Chim. Acta 1027 (2018) 83–91.
[127] H. Sun, H. Liu, Y. Wu, A green, reusable SERS film with high sensitivity for *in-situ* detection of thiram in apple juice, Appl. Surf. Sci. 416 (2017) 704–709.
[128] C. Zhu, X. Hu, X. Wang, Silver nanocubes/graphene oxide hybrid film on a hydrophobic surface for effective molecule concentration and sensitive SERS detection, Appl. Surf. Sci. 470 (2019) 423–429.
[129] Q. He, Y. Han, Y. Huang, J. Gao, Y. Gao, L. Han, Y. Zhang, Reusable dual-enhancement SERS sensor based on graphene and hybrid nanostructures for ultrasensitive lead (II) detection, Sens. Actuators B: Chem. 341 (2021) 130031.
[130] C. Awada, H.H. Hammud, H.A. Bukhamsin, D.E. Al-Hudairi, F. Ruffino, Development of ultrasensitive new sensors based on thio-functionalized heterogenous layers of gold/graphene/copper for glucose detection, Appl. Surf. Sci. 638 (2023) 158012.
[131] L. Wang, H. Chen, S. Ma, M. Chang, X. Zhang, Ultra-sensitive SERS detection of Aβ 1-42 for Alzheimer's disease using graphene oxide/gold nanohybrids, Vib. Spectrosc. 129 (2023) 103614.
[132] X. Liu, T. Li, Y. Han, Y. Sun, A. Zada, Y. Liu, J. Chen, A. Dang, Large-scale fabrication of flexible macroscopic SERS substrates with high sensitivity and long-term stability by wet-spinning technique: uniform encapsulation of plasmon in graphene oxide fibers, Appl. Surf. Sci. 654 (2024) 159513.
[133] N. Nasr, M. Shafi, T. Zhao, R. Ali, I. Ahmad, M. Khan, A. Deifalla, A.E. Ragab, M. Z. Ansari, A two-fold SPR-SERS sensor utilizing gold nanoparticles and graphene thin membrane as a spacer in a 3D composite structure, Spectrochim. Acta A Mol. Biomol. Spectrosc. 304 (2024) 123331.
[134] S. Li, Z. Li, Q. Hao, S. Wang, Y. Yang, J. Xu, Z. Yin, L. Zhang, Z. Chen, Ultrastable graphene isolated AuAg nanoalloy for SERS biosensing and photothermal therapy of bacterial infection, Chin. Chem. Lett. 35 (2024) 108636.
[135] M. Xian, H. Luo, X. Xia, C. Fares, P.H. Carey, C.W. Chiu, F. Ren, S.S. Shan, Y. T. Liao, S.M. Hsu, J.F.E. Upshaw, C.W. Chang, J. Lin, S.C. Ghivizzani, S.J. Pearton, Fast SARS-CoV-2 virus detection using disposable cartridge strips and a semiconductor-based biosensor Platform, J. Vac. Sci. Technol. B 39 (2021) 033202.
[136] Y. Yu, Y.T. Li, D. Jin, F. Yang, D. Wu, M.M. Xiao, H. Zhang, Z.Y. Zhang, G. J. Zhang, Electrical and label-free quantification of exosomes with a reduced graphene oxide field effect transistor biosensor, Anal. Chem. 91 (2019) 10679–10686.
[137] D. Li, H. Chen, K. Fan, V. Labunov, S. Lazarouk, X. Yue, C. Liu, X. Yang, L. Dong, G. Wang, A supersensitive silicon nanowire array biosensor for quantitating tumor marker ctDNA, Biosens. Bioelectron. 181 (2021) 113147.

[138] H. Qiu, S. Ippolito, A. Galanti, Z. Liu, P. Samori, Asymmetric dressing of WSe_2 with (Macro)molecular switches: fabrication of quaternary-responsive transistors, ACS Nano 15 (2021) 10668–10677.

[139] K.S. Bhat, R. Ahmad, T. Mahmoudi, Y.B. Hahn, High performance chemical sensor with field-effect transistors array for selective detection of multiple ions, Chem. Eng. J. 417 (2021) 128064.

[140] G.V. Presnova, I.I. Tciniaikin, I.V. Bozhev, M.Y. Rubtsova, V.V. Shorokhov, A.S. Trifonov, M.M. Ulyashova, V.A. Krupenin, D.E. Presnov, Thyroglobulin detection by biosensor based on two independent Si NW FETs, Int. Conf. on Micro- and Nano-Electronics 2018 (Proc. SPIE) 2019, ed Lukichev, V. F.; Rudenko, K. V. vol 110222019.

[141] L. Qi, Q. Hu, Q. Kang, Y. Bi, Y. Jiang, L. Yu, Detection of biomarkers in blood using Liquid crystals assisted with aptamer-target recognition triggered *in situ* rolling circle amplification on magnetic beads, Anal. Chem. 91 (2019) 11653–11660.

[142] W. Li, Y. Gao, J. Zhang, X. Wang, F. Yin, Z. Li, M. Zhang, Universal DNA detection realized by peptide based carbon nanotube biosensors, Nanoscale Adv. 2 (2020) 717–723.

[143] T. Chalklen, Q. Jing, S.K. Narayan, Biosensors based on mechanical and electrical detection techniques, Sensors 20 (19) (2020) 5605.

[144] T. Bungon, C. Haslam, S. Damiati, B. ODriscoll, T. Whitley, P. Davey, G. Siligardi, J. Charmet, S.A. Awan, Graphene FET sensors for alzheimers disease protein biomarker clusterin detection, Front. Mol. Biosci. 8 (2021) 651232.

[145] S.I. Zida, C.C. Yang, Y.L. Khung, Y.D. Lin, Fabrication and characterization of an aptamer-based N-type silicon nanowire FET biosensor for VEGF detection, J. Med. Biol. Eng. 40 (2020) 601–609.

[146] I. Novodchuk, M. Bajcsy, M. Yavuz, Graphene-based Field effect transistor biosensors for breast cancer detection: a review on biosensing strategies, Carbon 172 (2021) 431–453.

[147] T. Chalklen, Q. Jing, K.S. Narayan, Biosensors based on mechanical and electrical detection techniques, Sensors 20 (2020) 5605.

[148] T. Bungon, C. Haslam, S. Damiati, B. O'Driscoll, T. Whitley, P. Davey, G. Siligardi, J. Charmet, S.A. Awan, Graphene FET sensors for alzheimer's disease protein biomarker clusterin detection, Front. Mol. Biosci. 8 (2021) 651232.

[149] J. Oh, G. Yoo, Y.W. Chang, H.J. Kim, J. Jose, E. Kim, J.C. Pyun, K.H. Yoo, A carbon nanotube metal semiconductor field effect transistor-Based biosensor for detection of myloid-beta in human serum, Biosens. Bioelectron. 50 (2013) 345–350.

[150] D.R. Dreyer, S. Park, C.W. Bielawski, R.S. Ruoff, The chemistry of graphene oxide, Chem. Soc. Rev. 39 (2010) 228–240.

[151] K.M. Cheung, J.M. Abendroth, N. Nakatsuka, B. Zhu, Y. Yang, A.M. Andrews, P. S. Weiss, Detecting DNA and RNA and differentiating single-nucleotide variations via field-effect transistors, Nano Lett. 20 (2020) 5982–5990.

[152] L. Zhou, K. Wang, H. Sun, S. Zhao, X. Chen, D. Qian, H. Mao, J. Zhao, Novel graphene biosensor based on the functionalization of multifunctional nano-bovine serum albumin for the highly sensitive detection of cancer biomarkers, Nano-Micro Lett. 11 (2019) 20.

[153] F. Santos, N.C.S. Vieira, N.A. Zambianco, B.C. Janegitz, V. Zucolotto, The layer-by-layer assembly of reduced graphene oxide films and their application as solution-gated field-effect transistors, Appl. Surf. Sci. 543 (2021) 148698.

[154] I. Zeimpekis, K. Sun, C. Hu, N.M. Ditshego, O. Thomas, M.R. de Planque, H. M. Chong, H. Morgan, P. Ashburn, Dual-gate polysilicon nanoribbon biosensors enable high sensitivity detection of proteins, Nanotechnology 27 (2016) 165502.

[155] D. Han, R. Chand, Y.S. Kim, Microscale loop-mediated isothermal amplification of viral DNA with real-time monitoring on solution-gated graphene FET microchip, Biosens. Bioelectron. 93 (2017) 220–225.

[156] I. Heller, S. Chatoor, J. Mannik, M.A. Zevenbergen, C. Dekker, S.G. Lemay, Influence of electrolyte composition of liquid-gated carbon nanotube and graphene transistors, J. Am. Chem. Soc. 132 (2010) 17149–17156.

[157] W. Fu, C. Nef, O. Knopfmacher, A. Tarasov, M. Weiss, M. Calame, C. Schonenberger, Graphene transistors are insensitive to pH changes in solution, Nano Lett. 11 (2011) 3597–3600.

[158] P.K. Ang, W. Chen, A.T. Wee, K.P. Loh, Solution-gated epitaxial graphene as pH Sensor, J. Am. Chem. Soc. 130 (2008) 14392–14393.

[159] J. Ristein, W. Zhang, F. Speck, M. Ostler, L. Ley, T. Seyller, Characteristics of solution gated field effect transistors on the basis of epitaxial graphene on silicon carbide, J. Phys. D: Appl. Phys. 43 (2010) 345303.

[160] X. Lin, J. Shi, J. Pang, W. Liu, H. Liu, X. Wang, Graphene channel liquid container field effect transistor as pH Sensor, J. Nanomater. 2014 (2014) 547139.

[161] M.H. Lee, B.J. Kim, K.H. Lee, I.S. Shin, W. Huh, J.H. Cho, M.S. Kang, Apparent pH sensitivity of solution-gated graphene transistors, Nanoscale 7 (2015) 7540–7544.

[162] S.S. Kwon, J. Yi, W.W. Lee, J.H. Shin, S.H. Kim, S.H. Cho, S. Nam, W. Park, Reversible and irreversible responses of defect-engineered graphene-based electrolyte-gated pH sensors, ACS Appl. Mater. Interfaces 8 (2016) 834–839.

[163] X. Tan, H.J. Chuang, M.W. Lin, Z. Zhou, M.M.C. Cheng, Edge effects on the pH response of graphene nanoribbon field effect transistors, J. Phys. Chem. C. 117 (2013) 27155–27160.

[164] K.B. Parizi, X. Xu, A. Pal, X. Hu, H.S.P. Wong, ISFET pH sensitivity: counter-ions play a key role, Sci. Rep. 7 (2017) 41305.

[165] B.N. Yawson, G.D. Tabi, Y.Y. Noh, Polymer electrolyte blend gate dielectrics for high-performance ultrathin organic transistors: toward favorable polymer blend miscibility and reliability, ACS Appl. Mater. Interfaces 19 (2019) 17610–17616.

[166] M. Awais, H. Mousa, K. Teker, Effect of pH on transport characteristics of silicon carbide nanowire field-effect transistor (SiCNW-FET), J. Mater. Sci. Mater. Electron 32 (2021) 3431–3436.

[167] R. Ranjan, N. Kashyap, A. Raman, Design and analytical assessment of non-ideal ion- sensitive β-MIS-$(AlGa)_2O_3/Ga_2O_3$ high electron mobility transistor, IEEE Trans. Nanotechnol. 22 (2023) 84–90.

[168] B. Zhang, T. Cui, Suspended graphene nanoribbon ion-sensitive field-effect transistors formed by shrink lithography for pH/Cancer biomarker sensing, J. Micro Syst. 22 (5) (2013) 1140–1146.

[169] C.Y. Lee, K.F. Lei, S.W. Tsai, N.M. Tsang, Development of graphene-based sensors on paper substrate for the measurement of pH value of analyte, BioChip J. 10 (2016) 182–188.

[170] C. Mattevi, H. Kim, M. Chhowalla, A Review of chemical vapour deposition of graphene on copper, J. Mater. Chem. 21 (2011) 3324–3334.

[171] R. Munoz, C. Gómez-Aleixandre, Review of CVD synthesis of graphene, Chem. Vap. Depos. 19 (2013) 297–322.

[172] M. Wang, S.K. Jang, W.J. Jang, M. Kim, S.Y. Park, S.W. Kim, S.J. Kahng, J.Y. Choi, R.S. Ruoff, Y.J. Song, S. Lee, A platform for large-scale graphene electronics - CVD growth of single-layer graphene on CVD-grown hexagonal boron nitride, Adv. Mater. 25 (2013) 2746–2752.

[173] Y. Si, E.T. Samulski, Exfoliated graphene separated by platinum nanoparticles, Chem. Mater. 20 (2008) 6792–6797.

[174] A.N. Obraztsov, Chemical vapour deposition: making graphene on a large scale, Nat. Nanotechnol. 4 (2009) 212–213.

[175] P. Salvo, B. Melai, N. Calisi, C. Paoletti, F. Bellagambi, A. Kirchain, M.G. Trivella, R. Fuoco, F.D. Francesco, Graphene-based devices for measuring pH, Sens. Actuators B Chem. 256 (2018) 976–991.

[176] P.K. Ang, W. Chen, A.T. Wee, K.P. Loh, Solution-gated epitaxial graphene as pH sensor, J. Am. Chem. Soc. 130 (2008) 14392–14393.

[177] Y. Ohno, K. Maehashi, Y. Yamashiro, K. Matsumoto, Electrolyte-gated graphene field-effect transistors for detecting pH and protein adsorption, Nano Lett. 9 (2009) 3318–3322.

[178] Z. Cheng, Q. Li, Z. Li, Q. Zhou, Y. Fang, Suspended graphene sensors with improved signal and reduced noise, Nano Lett. 10 (2010) 1864–1868.

[179] N. Lei, P. Li, W. Xue, J. Xu, Simple graphene chemiresistors as pH sensors: fabrication and characterization, Meas. Sci. Technol. 22 (2011) 107002.

[180] Z. Yang, S. Xu, L. Zhao, J. Zhang, Z. Wang, X. Chen, X. Cheng, F. Yu, X. Zhao, A new direct growth method of graphene on Si-face of 6H-SiC by synergy of the inner and external carbon sources, Appl. Surf. Sci. 436 (2018) 511–518.

[181] I.S. Kotousova, S.P. Lebedev, A.A. Lebedev, P.V. Bulat, Electron diffraction study of epitaxial graphene structure grown upon SiC(0001) thermal destruction in Ar atmosphere and in high vacuum, Phy. Solid State 61 (2019) 1940–1946.

[182] B. Yang, H. Yang, T. Li, J. Yang, P. Yang, Thermal transport at 6H-SiC/graphene buffer layer/GaN heterogenous interface, Appl. Surf. Sci. 536 (2021) 147828.

[183] A.A. Lebedev, S.Y. Davydov, I.A. Eliseyev, A.D. Roenkov, O. Avdeev, S. P. Lebedev, Y. Makarov, M. Puzyk, S. Klotchenko, A.S. Usikov, Materials 14 (3) (2021) 590.

[184] S. Chattopadhyay, V. Munya, R. Kumar, D. Pal, S. Bandyopadhyay, A. Ghosh, P. Yogi, J. Koch, H. Pfnur, F4-TCNQ on epitaxial bi-layer graphene: concentration and orientation-dependent charge transfer at the interface, Langmuir 38 (2022) 16067–16072.

[185] H. Ichou, M. Alchaar, B. Baris, A. Michon, R. Dagher, E. Dujardin, D. Martrou, Structural identification of graphene films and nanoislands on 6H-SiC(0001) by direct height measurement, Nanotechnology 34 (2023) 165703.

[186] S. Stankovich, D.A. Dikin, G.H. Dommett, K.M. Kohlhaas, E.J. Zimney, E.A. Stach, R.D. Piner, S.T. Nguyen, R.S. Ruoff, Graphene-based composite materials, Nature 442 (2006) 282–286.

[187] A. Lerf, H. He, M. Forster, J. Klinowski, Structure of graphite oxide revisited, J. Phys. Chem. B 102 (1998) 4477–4482.

[188] H.Y. He, J. Klinowski, M. Forster, A. Lerf, A New structural model for graphite Oxide, Chem. Phys. Lett. 287 (1998) 53–56.

[189] H. Wu, J.J. Shao, C. Zhang, M.B. Wu, B.H. Li, Q.H. Yang, pH-dependent size, Surface chemistry and electrochemical properties of graphene oxide, N. Carbon Mater. 28 (2013) 327–335.

[190] H. Bai, C. Li, X. Wang, A pH-sensitive graphene oxide composite hydrogel, Chem. Commun. 46 (2010) 2376–2378.

[191] C. Shih, S. Lin, R. Sharma, M.S. Strano, D. Blankschtein, Understanding the pH-dependent behavior of graphene oxide aqueous solutions: a comparative experimental and molecular dynamics simulation study, Langmuir 28 (2012) 235–241.

[192] S. Sun, P. Wu, A One-Step Strategy for Thermal- and pH-responsive graphene oxide interpenetrating polymer hydrogel networks, J. Mater. Chem. 21 (2011) 4095–4097.

[193] S. Qin, X.L. Liu, R.X. Zhuo, X.Z. Zhang, Microstructure-controllable graphene oxide hydrogel film based on a pH-responsive graphene oxide hydrogel, Macromol. Chem. Phys. 213 (2012) 2044–2051.

[194] W.S. Hummers Jr., R.E. Offeman, Preparation of graphitic oxide, J. Am. Chem. Soc. 80 (1958) 1339.

[195] G. Wang, L.T. Jia, B. Hou, D.B. Li, J.G. Wang, Y.H. Sun, Self-assembled graphene monoliths: Properties, structures and their pH-dependent self-assembly behaviour, N. Carbon Mater. 30 (2015) 30–40.

[196] H. Hosseinzadeh, S. Ramin, Magnetic and pH-responsive Starch-g-poly(acrylic acid-coacrylamide)/graphene oxide superabsorbent nanocomposites: one-Pot synthesis, characterization, and swelling behaviour, Starch/Starke 68 (2016) 200–212.

[197] B. Melai, P. Salvo, N. Calisi, L. Moni, A. Bonini, C. Paoletti, T. Lomonaco, V. Mollica, R. Fuoco, F.D. FrancescoA Graphene oxide pH sensor for wound monitoring Proc. of 38th Annual International Conference of the IEEE Engineering in Medicine and Biology Society (EMBC) , 1901, , 1898–1901.

[198] P. Salvo, V. Dini, F.D. Francesco, M. Romanelli, The role of biomedical sensors in wound healing, Wound Med 8 (2015) 15–18.
[199] L. Liu, Y. Huang, J. Zhao, Z. Zhu, H. Zhang, C. Wang, All-solid-Sate pH sensing material based on cysteic acid/graphene oxide nanocomposites. in: Proc. Of the 3rd International Conference on Industrial Application Engineering, Kitakyushu (Japan) (2015) 144-148.
[200] P. Salvo, N. Calisi, B. Melai, V. Dini, C. Paoletti, T. Lomonaco, A. Pucci, F. D. Francesco, A. Piaggesi, M. Romanelli, Temperature and pH sensitive wearable materials for monitoring foot ulcers, Int. J. Nanomed. 12 (2017) 949–954.
[201] P. Salvo, N. Calisi, B. Melai, B. Cortigiani, M. Mannini, A. Caneschi, Temperature and pH sensors based on graphenic materials, Biosens. Bioelectron. 91 (2017) 870–877.
[202] Y. Seekaew, C. Wongchoosuk, A novel graphene-based electroluminescent gas sensor for carbon dioxide detection, Appl. Surf. Sci. 479 (2019) 525–531.
[203] L. Zhang, X. Hu, C. Wang, Y. Tai, Water-dispersible and recyclable magnetic TiO_2/graphene nanocomposites in wastewater treatment, Mater. Lett. 231 (2018) 80–83.
[204] H. Xu, H. Dai, G. Chen, Direct electrochemistry and electrocatalyst of hemoglobin protein entrapped in graphene and chitosan composite film, Talanta 81 (1) (2010) 334–338.
[205] K. Yuan, P.G. Wang, T. Hu, L. Shi, R. Zong, M. Forster, T. Pichler, Y. Chen, U. Scherf, Nanofibrous and graphene-templated conjugated microporous polymer materials for flexible chemosensors and supercapatiors, Chem. Mater. 27 (21) (2015) 7403–7411.
[206] J.H. An, S.J. Park, O.S. Kwon, J. Bae, J. Jang, High-performance flexible graphene aptasensors for mercury detection in mussels, ACS Nano 7 (12) (2013) 10563–10571.
[207] J. Park, J. Kim, K. Kim, S.Y. Kim, W.H. Cheong, K. Park, J.H. Song, G. Namgong, J.J. Kim, J. Heo, F. Bien, J.U. Park, Wearable, wireless gas sensors using highly stretchable and transparent structures of nanowires and graphene, Nanoscale 8 (20) (2016) 10591–10597.
[208] F. Meng, H. Zheng, Y. Chang, Y. Zhao, M. Li, C. Wang, Y. Sun, J. Liu, On-step synthesis of Au/SnO_2/RGO Nanocomposites and their VOC sensing properties, IEEE Trans. Nanotechnol 17 (2) (2018) 212–219.
[209] M. Pumera, Graphene in biosensing, Mater. Today 14 (7) (2011) 308–315.
[210] F. Yan, M. Zhang, J. Li, Solution-gated graphene transistors for chemical and biological sensors, Adv. Healthc. Mater. 3 (3) (2014) 313–331.
[211] H. Huang, S. Su, N. Wu, H. Wan, S. Wan, H. Bi, L. Sun, Graphene-based sensors for human health monitoring, Front. Chem. 7 (2019) 399.
[212] N.K. Swamy, K.N.S. Mohana, A.M. Madhusudana, J.G. Manjunatha, H. M. Manukumar, Graphene nanoribbon derived from multi-walled carbon nanotube: an efficient viral gene hosting and biosensing molecular platform for the electroanalysis of HIV-1 gene, Results Chem. 7 (2024) 101393.
[213] R. Hasler, G.E. Fenoy, A. Gotz, V. Montes-Garcia, C. Valentini, Z. Qiu, C. Kleber, P. Samori, K. Mullen, W. Knoll, "Clickable" graphene nanoribbons for biosensor interfaces, Nanoscale Horiz. (2024), https://doi.org/10.1039/D3NH00590A).
[214] N. Gholamalizadeh, S. Mazinani, M. Abdouss, A.M. Bazargan, F. Fatemi, A precise flexible printed biosensor based on graphene ink decorated with N-doped graphene quantum dots, J. Mol. Struct. 1304 (2024) 137700.
[215] Q. Li, J. Fu, W. Chen, F. Zhang, J. Cao, X. Liu, Synthesis of graphene quantum dots from organic dye for the biosensor application, Carbon Lett. 33 (2023) 1189–1196.
[216] C.H. Lu, H.H. Yang, C.L. Zhu, X. Chen, G.N. Chen, A Graphene platform for sensing biomolecules, Angew. Chem. 121 (26) (2009) 4879–4881.
[217] X. Dong, Y. Shi, W. Huang, P. Chen, L.J. Li, Electrical detection of DNA hybridization with single-base specificity using transistors based on CVD-Grown graphene sheets, Adv. Mater. 22 (14) (2010) 1649–1653.
[218] X. Kang, J. Wang, H. Wu, I.A. Aksay, J. Liu, Y. Lin, Glucose oxidase-graphene-chitosan modified electrode for direct electrochemistry and glucose sensing, Biosens. Bioelectron. 25 (4) (2009) 901–905.
[219] Y. Wang, L. Zhang, R.P. Liang, J.M. Bai, J.D. Qiu, Using graphene quantum dots as photoluminescent probes for protein kinase sensing, Anal. Chem. 85 (19) (2013) 9148–9155.
[220] M.B. Lerner, D. Pan, Y. Gao, L.E. Locascio, K.Y. Lee, J. Nokes, S. Afsahi, J. D. Lerner, A. Walker, P.G. Collins, K. Oegema, F. Barron, B.R. Goldsmith, Large scale commercial fabrication of high-quality graphene-based assays for biomolecule detection, Sens. Actuators B Chem. 239 (2017) 1261–1267.
[221] X. Pan, L. Li, H. Lin, J. Tan, H. Wang, M. Liao, C. Chen, B. Shan, Y. Chen, M. Li, A graphene oxide-gold nanostar hybrid based-paper biosensor for label-free SERS detection of serum bilirubin for diagnosis of jaundice, Biosens. Bioelectron. 145 (2019) 111713.
[222] Z. Sadeghi, N. Shojaeihagh, H. Shirkani, Multiple-step graphene grating optical sensors based on surface plasmons in IR range for ultra-sensing biomolecules, Mater. Sci. Eng. B 265 (2021) 114988.
[223] C. Gu, Z. Yu, X. Li, X. Zhu, C. Jin, Z. Cao, S. Dong, J. Luo, Z. Ye, Y. Liu, Experimental study on single biomolecules sensing using MoS_2-graphene heterostructure nanopores, Nanoscale 15 (2023) 266–274.



Dr. Ramaswamy Sandeep Perala is working as a Postdoctoral Research Associate under the supervision of Prof. Michael Taeyoung Hwang in the Department of BioNanotechnology, Gachon University, 1342 Seongnam-daero, Sujeong-gu, Seongnam-si, Gyeonggi-do, Republic of Korea. He earned his B. Sc and M.Sc (Integrated M.Sc Chemistry) from Kakatiya University, Telangana, India. His master's dissertation work on "Solvatochromic Studies of Novel Boron Di-Pyrrin Dyes" is completed in Indian Institute of Technology Gandhinagar (IIT-GN), India. He had an opportunity to work in Bhabha Atomic Research Centre (BARC), Mumbai, and GITAM University, Hyderabad, India for his dissertation work in Chemistry on "Synthesis, Characterization and Applications of Lanthanide Doped Nanophosphor Materials" and earned his Ph.D in 2022. His research focuses on luminescent nanomaterials (dual conversion properties) for LEDs, Anti-counterfeiting, Hyperthermia, Adsorption and Biomedical devices for superior sensitive detection using multiple techniques.



Dr. Narendhar Chandrasekar is a Post-Doctoral Researcher in the Department of BioNanotechnology, Gachon University, South Korea in Prof. Michael Taeyoung Hwang's lab. His Masters in Nanotechnology was from SASTRA University, India and PhD work was to develop a "Targeted drug delivery system for cancer therapy" from Anna University, India. His research interests include Biomaterials, Biosensors, Drug delivery systems and Environmental Monitoring and Remediation. He has secured an Industry grant to develop a biofouling prevention nanocomposite paint from Cameron Schlumberger, USA and from DST India for developing a Rapid wound healing nanofiber composite.



Dr. Ramachandran Balaji earned his Master's in Nanoscience and Technology in 2016 at Anna University, India and his Ph. D. in Chemical Engineering in 2022 at National Taipei University of Technology, Taiwan. He was a post-doctoral researcher at National Taiwan University, Taiwan. He currently holds an assistant professor position at K. L. Deemed to be University, India. His research focuses on Optical biosensors, SERS and Electrochemical sensors.



Dr. Pinky Steffi Alexander obtained her Master's degree from Bharathiar University, Tamil Nadu, India in Physics and PhD in Science and Humanities (Nanoscience and Technology) from Anna University, Tamil Nadu, India. Her research focuses on Nanomaterials, Nanocomposites, two dimensional materials for environmental remediation and sensing applications.



Mr. Nik Humaidi Nik Zulkarnine, is an undergraduate student in Bachelor of Science (pure chemistry) at department of chemistry, University of Malaya, Malaysia. His major part of the research is done under the supervision of Prof. Michael Taeyoung Hwang in the Department of BioNano Technology, Gachon University, Republic of Korea. His research interests include developing biosensors that involve 2-dimensional materials for enabling multiple modes of detection (electrical, electrochemical, and enhanced Raman signal) for superior sensitive sensor for molecular diagnostic specifically detection of Nucleic acid. He is also featured in some computational works of plasmonic based devices involving 3-dimensional crested pristine graphene.



Dr. Michael Taeyoung Hwang, Assistant Professor at Department of BioNano Technology, Gachon University, 1342 Seongnam-daero, Sujeong-gu, Seongnam-si, Gyeonggi-do, Republic of Korea. He received B.S and M.S in Materials Science and Engineering from Seoul National University (SNU), from Korea. He earned a Ph.D in Materials Science and Engineering under the guidance of Prof. Ratnesh Lal on "Gene-Chip Diagnostics for Personalized Global Medicine" at University of California, San Diego, USA. He had an opportunity to work with Prof. Rashid Bashir, University of Illinois Urbana Champaign, USA. His research expertise is in the Biomedical devices, nanobiotechnology, electrical biosensor, mechanical engineering of 2D materials, Bioelectronics. His research was published in Nature Communications, Advanced Materials, Advanced Functional Materials, PNAS, Nano Letters, ACS Applied Materials & Interface, ACS Sensors, Langmuir, etc.

Update

Materials Science & Engineering R
Volume 160, Issue , September 2024, Page

DOI: https://doi.org/10.1016/j.mser.2024.100816

Materials Science & Engineering R 160 (2024) 100816

Contents lists available at ScienceDirect

Materials Science & Engineering R

journal homepage: www.elsevier.com/locate/mser

Corrigendum

Corrigendum to "A comprehensive review on graphene-based materials: From synthesis to contemporary sensor applications" [Mater. Sci. Eng. R 159 (2024) 100805]

Ramaswamy Sandeep Perala [a,*], Narendhar Chandrasekar [a], Ramachandran Balaji [b], Pinky Steffi Alexander [c], Nik Zulkarnine Nik Humaidi [a], Michael Taeyoung Hwang [a]

[a] Department of BioNanotechnology, Gachon University, 1342 Seongnam-Daero, Sujeong-Gu, Seongnam-si, Gyeonggi-do 13120, Republic of Korea
[b] Department of Electronics and Communication Engineering, Koneru Lakshmaiah Education Foundation, Andhra Pradesh 522302, India
[c] Department of Physics, Bharthiar University, Coimbatore 641046, India

The authors regret It is our sincere request to rectify the double printing of Fig. 8 (in Fig. 7 as well) in the published version and please go through the Fig. 7 and Fig. 8 in the following page for your reference.

The authors would like to apologise for any inconvenience caused.

DOI of original article: < https://doi.org/10.1016/j.mser.2024.100805 >

DOI of original article: https://doi.org/10.1016/j.mser.2024.100805.
* Corresponding author.
E-mail addresses: ramaswamysandeep@gmail.com (R.S. Perala), anol81@gachon.ac.kr (M.T. Hwang).

https://doi.org/10.1016/j.mser.2024.100816

Available online 14 June 2024
0927-796X/© 2024 Elsevier B.V. All rights are reserved, including those for text and data mining, AI training, and similar technologies.

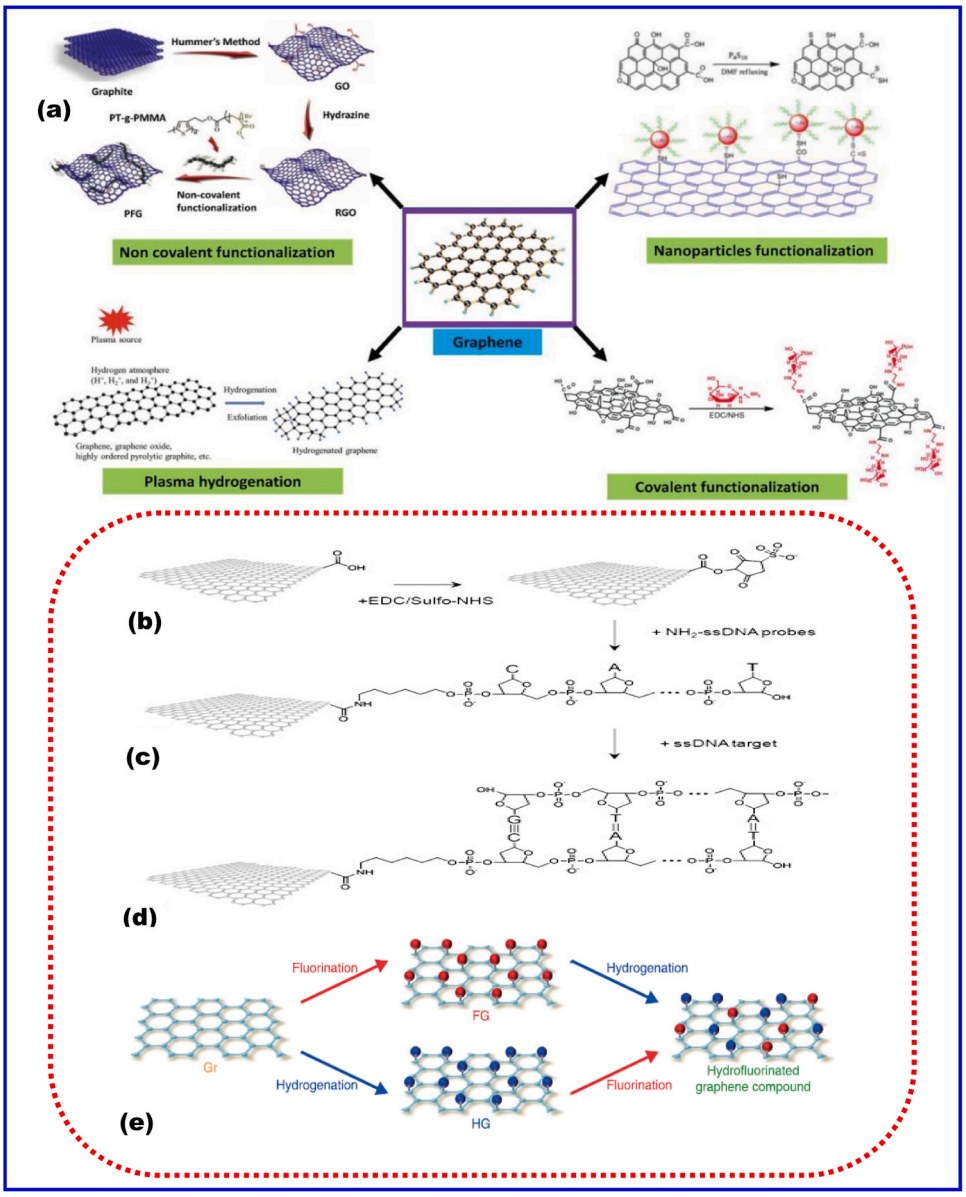


Fig. 7. (a) Types of functionalization possibilities and ssDNA functionalization of graphene, (b) Suo-NHS esters on carboxylated graphene form an amide bond with amine-terminated ssDNA probes, resulting in (c) ssDNA functionalized graphene and (d) hybrid formation after incubation with cDNA. A:G:C:T [53] and (e) hydrofluorinated graphene synthesis [69].

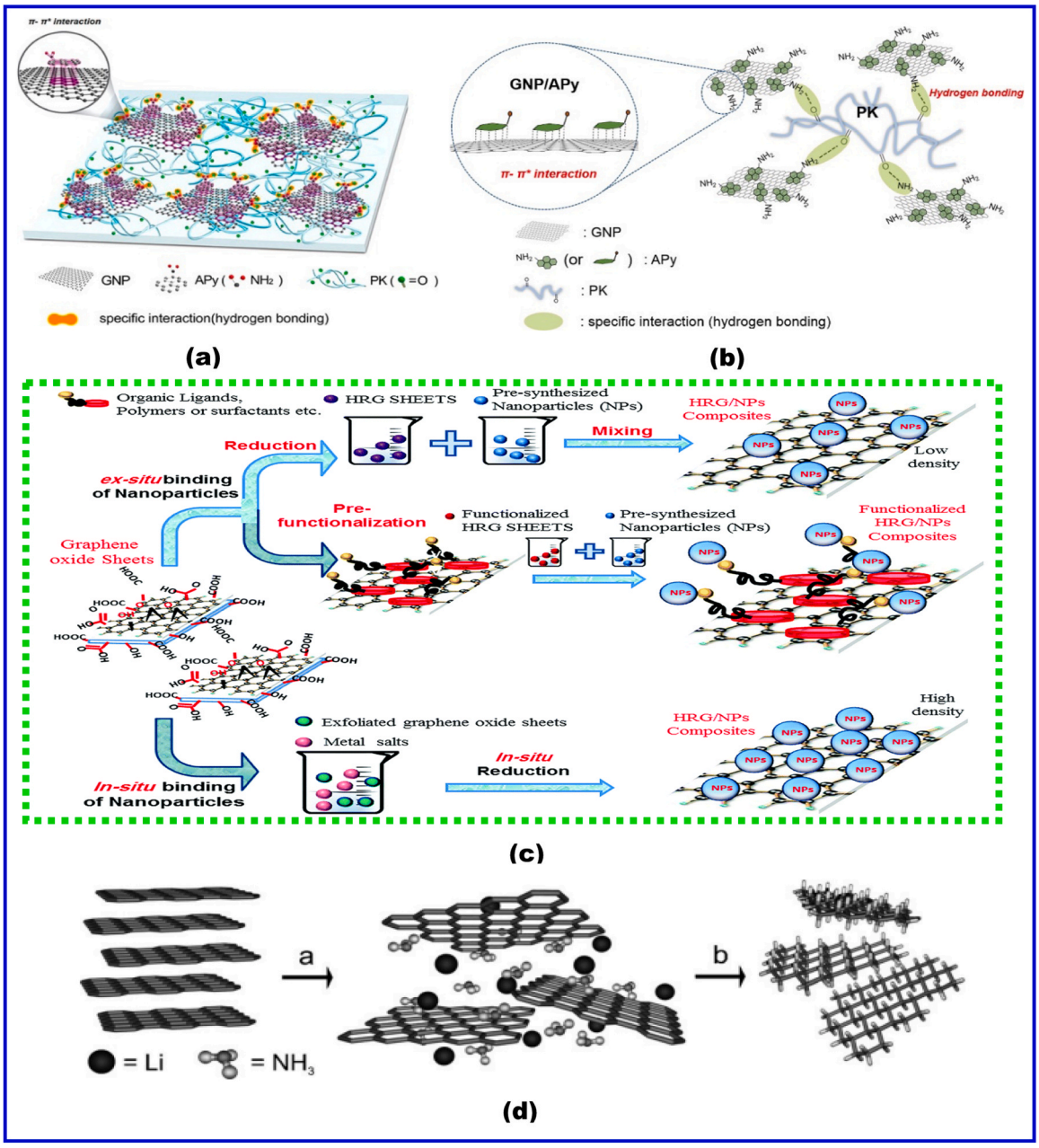


Fig. 8. (a) Hydrogen-based functionalization and the (b) interaction mechanism with the polyketone matrix [73], (c) nanoparticle functionalization with graphene via π–π stacking or C-C covalent coupling [103], and (d) Birch-type wet-chemical hydrogenation of graphene [108].